

A Dynamic Model of Vortex-Type

Fluid Amplifiers

by

Wallace W. Anderson

B.S., Iowa State University
(1966)

S.M., Massachusetts Institute of Technology
(1968)

Submitted in Partial Fulfillment of the Requirements
for the Degree of Doctor of Science
at the
Massachusetts Institute of Technology

October, 1971 (i.e. Feb. 1972)

Signature of Author
Department of Mechanical Engineering, October, 1971

Certified by...
Thesis Supervisor

Accepted by
Chairman, Departmental Committee on Graduate Students



A Dynamic Model of Vortex-type

Fluid Amplifiers

Wallace W. Anderson

Submitted to the Department of Mechanical Engineering on October 12, 1971, in partial fulfillment of the requirements for the degree of Doctor of Science.

Abstract

A lumped, linearized analytical dynamic model of a vortex-type fluid amplifier was developed and the dynamic response for a range of valve operating conditions was experimentally verified. The lumped parameter model for the proportional small signal behavior of a vortex amplifier was developed from a distributed system analysis of the basic flow field in the vortex chamber, assuming the flow to be incompressible. The model was developed for conditions of high swirl in the vortex chamber for which viscous effects are important. The two dynamic time parameters used in the model are a pure transportation delay associated with the flow propagation of control signals through the boundary layers, and a first order lag time constant associated with the changes due to viscous friction in the region of zero radial flow. The lumped model response was compared with experimental data taken for a range of valve operating conditions, and was found to agree quite well. A Fortran computer program was developed to provide a designer with an initial estimate of a prototype vortex amplifier dynamic characteristic.

Thesis Supervisor: David N. Wormley

Title: Associate Professor of Mechanical Engineering

ACKNOWLEDGMENTS

I would like to thank the many people who have contributed to my educational experience while at M.I.T. Professor D.N. Wormley, as thesis advisor, has especially contributed to the completion of this thesis through his suggestions and supervision. Professor L.R. Glicksman, S.Y. Lee, and R.F. Salant, as thesis committee members, have provided generous encouragement and helpful advice.

I would also like to express my gratitude to the members of the Engineering Projects Laboratory who have made my time at M.I.T. enjoyable, and especially to Don Margolis for the many stimulating discussions and suggestions he has provided.

I would also like to thank Mrs. Sandy Williams for her patience while providing an excellent typing job on this thesis.

Special appreciation goes to my wife Dotti, whose encouragement and understanding have made this thesis possible.

This thesis was supported in part by the Harry Diamond Laboratory under contract DAAG 39-67-C-0019 and by the U.S. Department of Transportation under contract DOT-FR-10007, and sponsored by the Division of Sponsored Research of M.I.T.

TABLE OF CONTENTS

| | <u>Page</u> |
|--|-------------|
| Abstract | 2 |
| Acknowledgments | 3 |
| Table of Contents | 4 |
| List of Figures | 6 |
| List of Tables | 8 |
| Nomenclature | 9 |
| Chapter 1. The Problem | 12 |
| 1.1 Introduction | 12 |
| 1.2 Vortex Amplifier Literature | 16 |
| 1.3 Scope of This Thesis | 19 |
| Chapter 2. Distributed System Vortex Dynamic Response | 21 |
| 2.1 Introduction | 21 |
| 2.2 Inviscid Model | 23 |
| 2.3 Viscous Model | 29 |
| 2.3.1 Steady State Viscous Model | 31 |
| 2.3.2 Dynamic Viscous Model | 39 |
| Chapter 3. Lumped Model | 61 |
| 3.1 Introduction | 61 |
| 3.2 Inlet Ports | 65 |
| 3.3 Mixing Region | 66 |
| 3.4 Main Vortex Region | 69 |
| 3.5 Exit Port | 74 |
| 3.6 Total Lumped Model | 74 |
| 3.7 Calculation of k_1 , k_2 and R_e | 79 |
| Chapter 4. Experimental Results | 83 |
| 4.1 Objectives of the Experiments | 83 |
| 4.2 Apparatus | 83 |
| 4.3 Experimental Valve Configurations | 89 |
| 4.4 Calculation of Theoretical Responses | 90 |
| 4.5 Step Response | 93 |
| 4.6 Frequency Response | 97 |
| 4.7 Choice of Friction Constant k | 108 |
| 4.8 Large Signal Step Response | 108 |
| 4.9 Frequency Response Sensitivity to Gain and Time Constant Changes | 111 |

| | <u>Page</u> |
|---|-------------|
| Chapter 5. Dynamic Vortex Valve Design | 113 |
| 5.1 General Dynamic Design | 113 |
| 5.2 Example Design | 114 |
| Chapter 6. Conclusions and Recommendations | 120 |
| 6.1 Conclusions | 120 |
| 6.2 Recommendations | 120 |
| Appendix A - Distributed Dynamic Response Computer Program | 123 |
| Bibliography | 141 |
| Biography | 145 |

LIST OF FIGURES

| | <u>Page</u> |
|--|-------------|
| 1.1 Schematic of Vortex Amplifier | 13 |
| 1.2 Typical Steady State Flow Characteristic | 15 |
| 2.1 Schematic of Main Vortex Region | 22 |
| 2.2 Inviscid Circulation Distribution Step Response | 27 |
| 2.3 Inviscid Vortex Chamber Pressure Step Response | 28 |
| 2.4 Division of Valve Regions for Steady State Calculations | 32 |
| 2.5 Typical Steady State Flow Distribution Variables | 40 |
| 2.6 Dynamic Flow Visualization | 42 |
| 2.7 Valve Region Conditions for Dynamic Calculations | 43 |
| 2.8 Conceptual Dynamic Response | 45 |
| 2.9 Important Effects for Viscous Dynamic Response, by Region | 48 |
| 2.10 Single Finite Element for Dynamic Response Calculation | 49 |
| 2.11 Dynamic Tangential Velocity Axial Distribution | 50 |
| 2.12 Viscous Vortex Chamber Pressure Step Response | 58 |
| 2.13 Viscous Circulation Distribution Step Response | 59 |
| 3.1 Regions of Dynamic Operation | 63 |
| 3.2 Schematic of Vortex Valve with Definition of Variables | 64 |
| 3.3 Jet Recovery Factor ϵ | 68 |
| 3.4 Distributed Response with Lumped Model Response Approximation | 70 |
| 3.5 Change in Circulation Distribution for Change in u_0 | 73 |
| 3.6 Lumped Model Block Diagram | 77 |
| 3.7 Typical Lumped Model Frequency Response | 78 |
| 3.8 Plot of P/λ^2 vs. BLC^* | 80 |
| 4.1 Disassembled Vortex Valve | 84 |
| 4.2 Schematic of Experimental Apparatus | 86 |
| 4.3 Schematic of Signal Generator | 87 |
| 4.4 Signal Generating Apparatus | 88 |

| | <u>Page</u> |
|--|-------------|
| 4.5 Experimental Steady State Characteristics | 91 |
| 4.6 Experimental Small Signal Step Response | 95 |
| 4.7 Comparison of Theoretical and Experimental Step Responses | 96 |
| 4.8 Block Diagram of Frequency Response Fourier Decomposition | 98 |
| 4.9 Butterworth Filter for Pressure Signal | 100 |
| 4.10 Theoretical and Experimental Frequency Responses - Case A | 102 |
| 4.11 Theoretical and Experimental Frequency Responses - Case B | 103 |
| 4.12 Theoretical and Experimental Frequency Responses - Case C | 104 |
| 4.13 Theoretical and Experimental Frequency Responses - Case D | 105 |
| 4.14 Experimental Large Signal Step Responses | 110 |
| 4.15 Frequency Responses with Gain and Time Constant Changes | 112 |
| 5.1 Changes in T_1 and T_2 Due to Swirl and Height Changes | 115 |
| 5.2 Estimated Steady State Characteristic for Example Design | 116 |
| 5.3 Comparison of Step Responses for Example Design | 119 |

LIST OF TABLES

| | <u>Page</u> |
|---|-------------|
| 3.1 Lumped Model Transfer Functions | 76 |
| 3.2 Calculation of Gains k_1 , k_2 and R_e | 82 |
| 4.1 Lumped Model Parameters for Experimental Configurations | 94 |
| 4.2 Effects of Friction Constant K on Time Constants | 109 |
| 5.1 Operating Conditions for Example Design | 118 |

NOMENCLATURE

| | |
|-------------|---|
| A_c | total tangential control port area |
| A_e | total exit port |
| A_o | chamber outer periphery area |
| A_s | total radial supply port area |
| BLC | boundary layer coefficient, $\frac{2r_o}{h} \frac{f}{\left(\frac{\rho u_o h}{2\mu}\right)^{1/4}}$ |
| BLC* | modified boundary layer coefficient, $\lambda \cdot \text{BLC}$ |
| C_d | orifice discharge coefficient |
| $f(\eta)$ | velocity profile function |
| $g(\eta)$ | velocity profile function |
| h | chamber height |
| $k_1, k_2,$ | lumped parameter model gains |
| k_u, k_e | |
| R_c | linearized control port resistance |
| R_e | linearized exit port resistance |
| R_s | linearized supply port resistance |
| p_a | ambient pressure |
| p_c | control pressure |
| p_e | chamber exit pressure at $r = r_e$ |
| p_o | chamber outer periphery pressure at $r = r_o$ |
| p_s | supply pressure |
| P | non-dimensional chamber pressure |
| Q_c | total control port flow |
| Q_e | total exit port flow |

| | |
|--------------------|---|
| Q_s | total supply port flow |
| r | radius |
| r_e | exit port radius |
| r_o | outer periphery radius |
| r^* | radius at which radial flow in core region goes to zero |
| s | Laplace operator |
| T_1 | transport delay time |
| T_2 | first order lag time constant |
| t | time |
| $T'_1, T'_2,$ | non-dimensional times |
| t' | |
| u | radial velocity |
| u_o | outer periphery radial velocity |
| U, U_s | non-dimensional radial velocities |
| v | tangential velocity |
| v_o | outer periphery tangential velocity |
| w | axial velocity |
| x | non-dimensional radial coordinate |
| y | axial coordinate |
| v | non-dimensional volume |
| $\alpha_1, \dots,$ | non-dimensional velocity integrals in boundary layer |
| α_5 | |
| β | proportionality constant for dynamic changes |
| Γ | non-dimensional circulation $vr/v_o r_o$ |

| | |
|---------------------|---|
| γ | dimensional circulation $v r$ |
| Δ | difference operator |
| δ | boundary layer height |
| $\bar{\delta}$ | non-dimensional boundary layer height |
| $\bar{\delta}_\tau$ | non-dimensional boundary layer shear height |
| ϵ | jet mixing coefficient |
| η | non-dimensional axial coordinate |
| θ | tangential coordinate |
| λ | swirl number v_o/u_o |
| μ | fluid viscosity |
| ρ | fluid density |
| τ | viscous shear |
| $\bar{\tau}$ | non-dimensional viscous shear |
| ω | circular frequency |

Chapter 1

THE PROBLEM

1.1 Introduction

Pure fluid amplifiers, in which one fluid stream is used to control one or more other fluid streams with no moving parts, have been the subject of considerable recent interest (6, 10). They are inherently insensitive to radiation, and have a good potential for operating in environments with vibration or high temperature without degradation of performance. They may operate effectively in explosive atmospheres where there would be danger of sparking from equivalent electrical components. Their potential reliability is high due to their simplicity.

In the past few years a number of basic fluid amplifiers have been developed, including turbulence amplifiers, digital and proportional beam deflection amplifiers, impact modulators, and vortex amplifiers (6, 10).

For applications in which it is important to modulate power level flows, the vortex amplifier is especially attractive because it is the only fluid amplifier in which total power flow is modulated. A simple schematic drawing of a vortex valve is shown in Fig. 1.1. The amplifier contains three fluid ports:

- 1) A radial supply port which supplies the main portion of the flow through the valve.

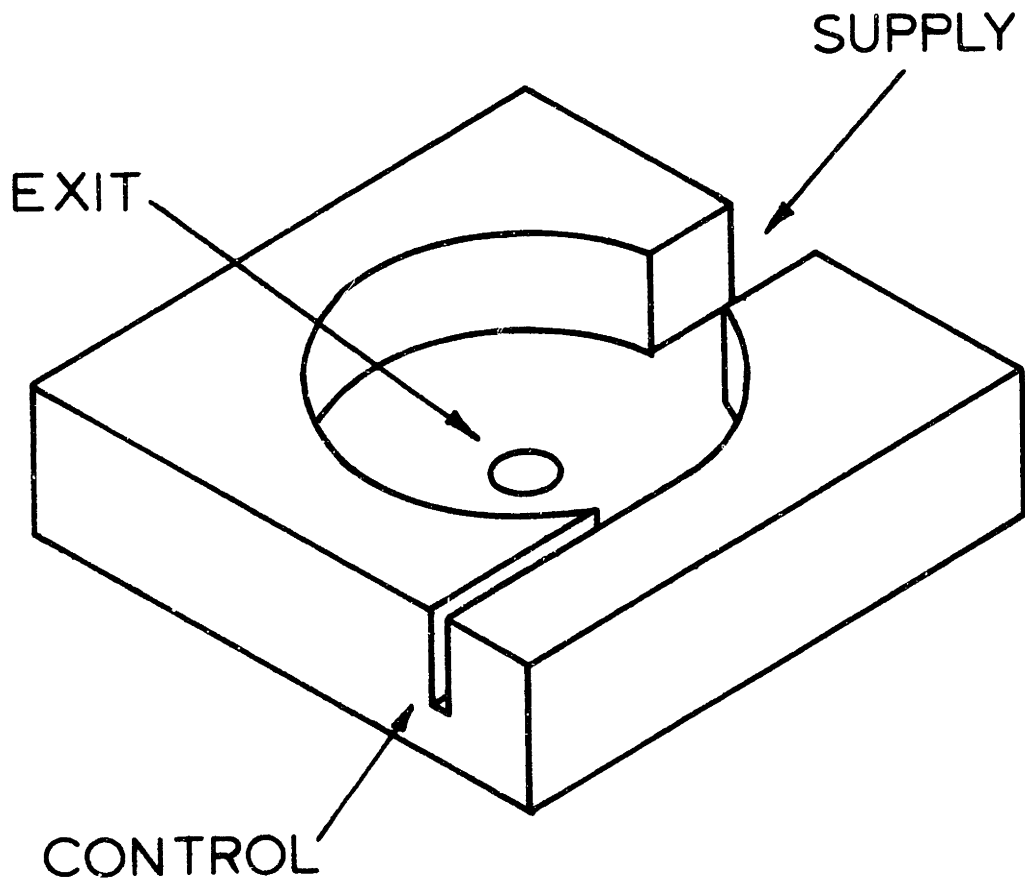


Fig. 1.1 Schematic of Vortex Amplifier

- 2) A tangential control port which supplies the flow which drives the vortex.
- 3) An axial exit port through which all of the flow leaves the valve.

When there is no tangential control flow, the supply flow streams across the chamber and out the exit, with the main restriction to flow provided by the exit port itself. With the addition of tangential control flow, a vortex is formed in the chamber, causing a pressure drop due to the centrifugal flow field. This centrifugally induced pressure drop further restricts the flow, and at some value of control flow, the pressure drop across the chamber is sufficient to completely shut off the supply flow; then, the only flow through the amplifier is the control flow necessary to maintain the vortex, which is on the order of five to ten percent of the maximum supply flow with no control flow. A typical steady state characteristic of the amplifier is shown in Fig. 1.2.

This characteristic shows the total output flow as a function of the tangential control flow, with both flows normalized by the maximum output flow which occurs with no tangential flow. As the tangential flow is increased, there is initially little change in the outlet flow, since the resistance due to the centrifugal flow field is small compared to the exit port resistance. Then, there is a sharp drop in the exit flow, as the centrifugal flow field resistance becomes significant, followed by a region of less change as the losses due to the high tangential velocities decrease the effect of increased

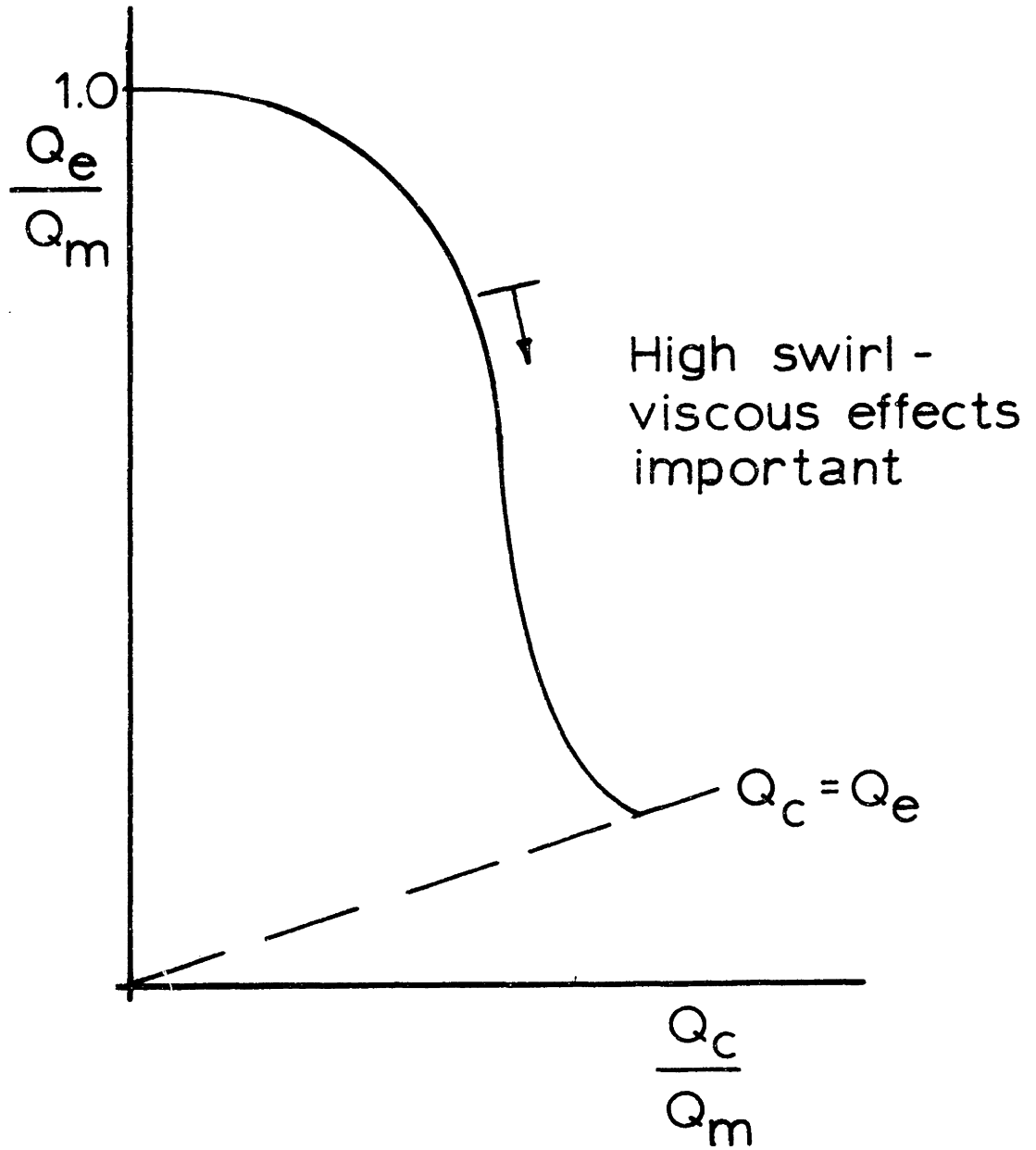


Fig. 1.2 Typical Steady State Flow Characteristic

tangential flow. At the cutoff point, the total output flow is equal to the control flow.

Because of its ability to modulate the total flow, the vortex amplifier is useful as a controller for power level fluid control devices, as well as a signal level device, and is often referred to as a vortex valve as well as a vortex amplifier.

Some of its applications have included use as a hydraulic servovalve stage (17), as a rate gyro (22), and as a rocket thrust vector controller (19). Several small vortex valves are commercially available, and have been used as fluid level controllers (13). In many of the referenced applications above and in future applications, both the steady state and dynamic (transient) characteristics are important in determining the performance of the total system in which a valve operates.

1.2 Vortex Amplifier Literature

This section reviews the information available concerning both steady state and dynamic design of vortex amplifiers.

General vortex flow devices have been of some interest for some time (9,27), while the study of vortex amplifiers has been more recent (14,16). Progress has been made on the analytical understanding and prediction of the steady state flow conditions and behavior, so that published information is available to aid in the design of vortex amplifiers to meet steady state requirements. Wormley (28) has presented a vortex flow fluid analysis and a method of predicting part of a steady state response. He provides an inviscid analysis which agrees well with experimental results for

the upper portion of the steady state characteristic (see Fig. 1.2) and also provides an empirical method for predicting the cutoff point. Because he does not provide a model of the swirling flow through the exit port, the prediction of the intermediate portion of the characteristic amounts to an estimate based on intuition and past experience. However, he has shown that an intuitive smooth curve will generally be within 10 - 15% of the experimental curve, on the same order of accuracy as points explicitly predicted.

Bichara and Orner (2) have presented a method for the approximate prediction of an entire steady state valve characteristic. By varying the discharge coefficient of the exit and a friction coefficient to represent the effect of the viscous shear on the end walls, they were able to match the experimental results of Ref. (28). However, their empirical correlation of the friction coefficient differed by as much as 30% from the friction coefficients actually used to match the data, and the correlation was based on the flow conditions at cutoff, which may only be approximately predicted from Ref. (28). They did not present a comparison of the experimental data and the theory using the empirical correlation.

Thus, although it must be recognized as an estimate with limited accuracy, Ref. (28) provides a simple and reasonable method of predicting the steady state characteristic and is preferable to Ref. (2).

Less information is available concerning the dynamic characteristics, but some work has been done. Duff, Foster and Mitchell (5) have presented one step response trace of a dynamic vortex response. The vortex valve had only one supply and one control

port, rather than an axisymmetric vortex configuration. Flow visualization of a step change, starting from a condition with no swirl, indicated that the response was associated with the change in size of the two vortices on each side of the supply jet. However, no general model was proposed for the valve to explain the response.

Knapp (11) has presented both frequency response and step response data for a specific valve, but did not specify the dimensions or flow conditions of the valve, or present a general model for other conditions.

Several researchers have investigated the dynamics of the vortex rate sensor (18), which are mainly concerned with low swirl flow conditions, since the steady state condition is one with no swirl.

Taplin (25,26) has presented an equivalent electrical circuit for a vortex valve in several papers. He has also presented experimental results which indicate the valve may be modelled as a pure delay and a first order lag, each equal to one-fourth of the fill time of the valve, where the fill time is defined to be the volume of the valve chamber divided by the volume flow rate through the valve. However, he did not give the details of the valve construction or the flow conditions, and did not indicate if these results had been verified for extensive ranges of valve geometry or flow conditions. Also, he did not relate the parameters of his equivalent electrical circuit to the geometry of the valve or the properties of the fluid. The inadequacy of modelling the valve dynamics with fixed fractions of the fill time will be demonstrated in this thesis.

Bell (1) has given a more complete description of valve geometry and flow conditions for a vortex valve responding to a step change in control flow. He measured the flow out of the valve for a change in flow conditions from essentially maximum supply flow to minimum supply flow. A model consisting of a delay of one-half the fill time and a first order log of 1.3 fill times was proposed. Since the consideration of this large signal response is beyond the scope of this thesis, Bell's model will not be considered further.

1.3 Scope of this Thesis

Since the vortex amplifier has the capability to modulate power flow, it is potentially useful in fluid power control systems. However, this control implies that the flow is to be changed to meet changing requirements, and for the amplifier to be used to its full potential, an understanding of the behavior and speed of the amplifier in meeting changing requirements is necessary.

For a fluid power control system designer, the most convenient method of gaining an initial estimate of the behavior of several individual elements connected to provide a complete system is to combine the lumped, linear transfer functions of the elements. Therefore, in order to provide a useful tool for fluid circuit design, this thesis presents a lumped linearized analytical model of a vortex valve and experimental verification of the dynamic response.

In the work that follows, a lumped parameter model for the proportional small signal behavior of a vortex amplifier is developed from an analysis of the basic flow field in the vortex chamber. In the flow field analysis, the flow in the amplifier is assumed

incompressible and turbulent. The analysis concentrates on the proportional region of the amplifier operation and in particular is developed for conditions of high swirl in the vortex chamber in which viscous effects are important. The lumped parameter model is specifically developed for an amplifier operating nominally at constant supply and exhaust pressures and with changing control pressure and changing control, supply, and exit flows. The basic analysis is compared with experimental data taken for a range of valve operating conditions. A Fortran computer program is provided so that a designer may gain an initial estimate of a prototype vortex amplifier dynamic characteristic.

For some applications, the vortex valve will be used as a bistable "on-off" valve rather than as a proportional valve. The prediction of the dynamic response in this type of application is beyond the scope of this thesis.

Chapter 2

DISTRIBUTED SYSTEM VORTEX DYNAMIC RESPONSE

2.1 Introduction

In this chapter, the development of an analytical model for the main region of a vortex amplifier is considered, starting with a simple inviscid model and then extending consideration to the complex viscous flow field. This main region of the vortex amplifier plays a dominant role in the dynamic behavior of a vortex amplifier and therefore is considered in detail in this chapter.

A schematic drawing of the region under consideration is shown in Fig. 2.1. The general radial and tangential velocities are assumed to be axisymmetric, and thus are designated as $u(r,y,t)$ and $v(r,y,t)$. The axial velocity is designated by $w(r,y,t)$ and is considered to be small with respect to u and v , as discussed by several investigators (15,28).

It is assumed that at the chamber outer periphery the radial and tangential velocities are uniform and are designated by $u_o(t)$ and $v_o(t)$. Since u is defined positive outward and u_o is inward, u at the outer periphery is equal to $-u_o$.

The ratio of the outer periphery velocities is designated by $\lambda = v_o/u_o$, and is called the swirl parameter. For $\lambda < 1$, the swirl is small and the vortex chamber flow may be characterized as nearly inviscid, while for large swirl $\lambda \gg 1$, the flow in the chamber depends very strongly on viscous effects (29).

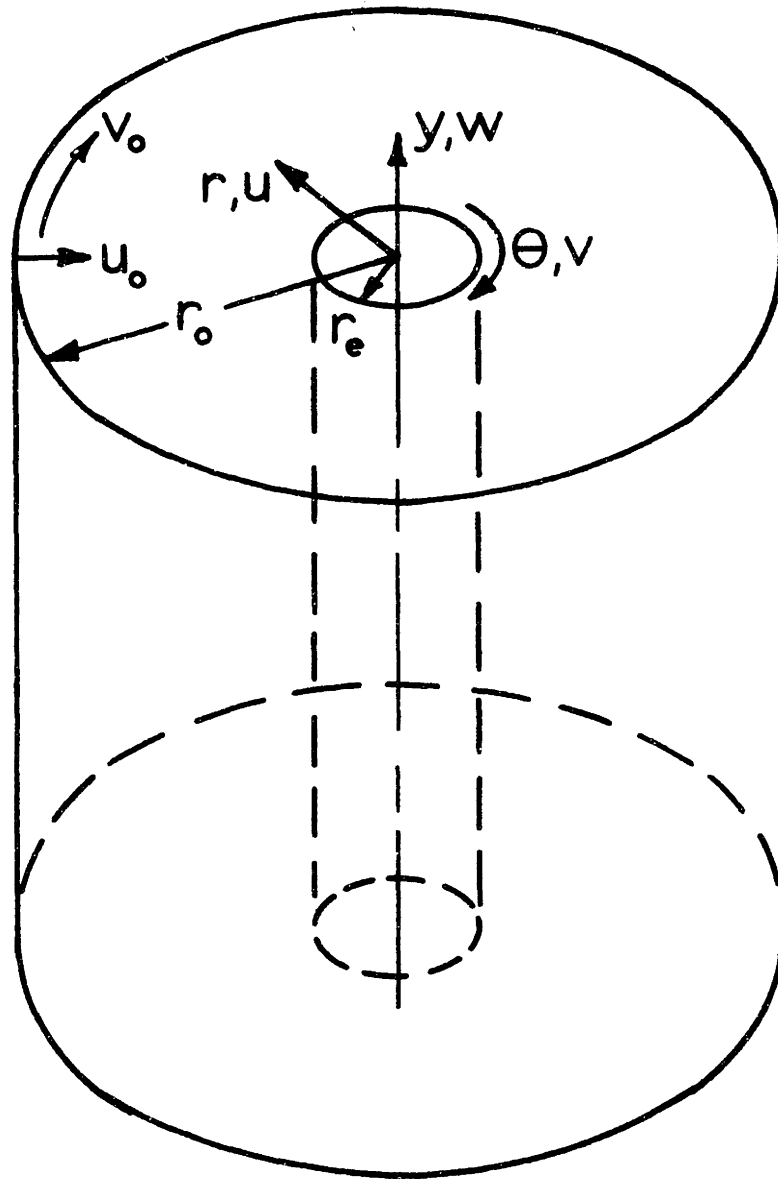


Fig. 2.1 Schematic of Main Vortex Region

In the past, several studies of the flow fields in vortex devices have been made. Savino and Keshock (23) performed an experimental study of the steady state velocity distributions in a 12 inch diameter vortex chamber operating on air. Wormley (29) developed a model for the steady state flows in the chamber, using the momentum integral method, which predicted pressure distributions quite accurately. Rosenweig, Lewellen, and Ross (20) included an approximation of the effects of the exit region on the main vortex chamber in a steady state model.

While these studies have provided useful information, they have considered only steady state behavior and not the dynamic behavior which is of interest here. Deissler (4) completed a numerical study of a dynamic model, but he assumed that the effects of the boundary layers on the end walls were eliminated by suitably rotating end walls. The important effects of the end wall boundary layers are included in the following analysis to provide an improved dynamic model.

2.2 Inviscid Model

Consideration of the inviscid potential vortex can provide some insight into the vortex flow field, and can furnish a preliminary basis for the study of the full viscous model.

For inviscid, incompressible flow in the main vortex region, the radial and tangential velocities reduce to functions only of the radius and time, $u(r,t)$ and $v(r,t)$ and the axial velocity w is

zero everywhere. Thus, the axisymmetric, unsteady radial and tangential momentum equations are:

$$\frac{\partial u}{\partial t} + u \frac{\partial u}{\partial r} - \frac{v^2}{r} = -\frac{1}{\rho} \frac{\partial p}{\partial r} \quad (2.1)$$

$$\frac{\partial v}{\partial t} + u \frac{\partial v}{\partial r} + \frac{uv}{r} = 0 \quad (2.2)$$

The continuity equation is:

$$\frac{\partial u}{\partial r} + \frac{u}{r} = 0 \quad (2.3)$$

In the case of steady flow, the radial and tangential velocities become functions only of r , and the continuity and tangential momentum equations may be solved to give:

$$u = -\frac{u_0 r_0}{r} \quad (2.4)$$

$$v = \frac{v_0 r_0}{r} \quad (2.5)$$

Substituting these velocity equations into the radial momentum equation gives the pressure gradient as a function of r :

$$\begin{aligned} \frac{dp}{dr} &= \rho \left(\frac{v^2}{r} - u \frac{du}{dr} \right) \\ &= \rho \left(\frac{v_0^2}{r} - \frac{u^2}{r} \right) \\ &= \rho \left(\frac{r_0^2 v_0^2}{r^3} + \frac{r_0^2 u_0^2}{r^3} \right) \end{aligned} \quad (2.6)$$

Equation (2.6) may be integrated to give

$$p_o - p_e = \frac{\rho(v_o^2 + u_o^2)r_o^2}{2} \left[\frac{1}{r_e} - \frac{1}{r_o} \right] \quad (2.7)$$

This equation shows that for a given fluid, the steady state pressure drop is a function of u_o , v_o , the radius ratio r_o/r_e , and the fluid density ρ .

The transient changes in pressure drop across the valve due to changes in v_o for the case of a constant radial velocity distribution may be found by solving Eq. (2.2). Letting $\gamma = vr$, Eq. (2.2) may be written as

$$\frac{\partial \gamma}{\partial t} + u \frac{\partial \gamma}{\partial r} = 0 \quad (2.8)$$

Combining Eqs. (2.4) and (2.8) and using the Laplace operator s to represent time differentiation, the differential equation becomes:

$$s\gamma = \frac{u_o r_o}{r} \frac{d\gamma}{dr} \quad (2.9)$$

This equation may be solved by separation of variables to give the Laplace transform equation:

$$\frac{\gamma}{\gamma_o} = e^{-\frac{r_o^2 - r^2}{2u_o r_o} s} \quad (2.10)$$

Taking the inverse Laplace transform gives the circulation γ as a function of radius and time:

$$\gamma(r,t) = \gamma_0 \left(t - \frac{r_o^2 - r^2}{2u_o r_o} \right) \quad (2.11)$$

This expression for $\gamma(r,t)$ may be interpreted to mean that the circulation γ at any radius is related to the outer periphery circulation γ_0 by a pure transportation delay. That is, the circulation at any radius r is simply the same as γ_0 was $\frac{r_o^2 - r^2}{2u_o r_o}$ seconds earlier. The response to a step change in v_o at $t=0$ is shown in Fig. 2.2.

Thus the vortex chamber consists of two regions, one containing the "old" and one the "new" conditions. The total pressure drop is the sum of the pressure drops in these two regions, which may be written as

$$p_o - p_e = \frac{\rho}{2} \left[\gamma_{02}^2 \left(\frac{1}{r_d^2} - \frac{1}{r_o^2} \right) + \gamma_{01}^2 \left(\frac{1}{r_e^2} - \frac{1}{r_d^2} \right) \right] + \frac{\rho u_o^2 r_o^2}{2} \left[\frac{1}{r_e^2} - \frac{1}{r_o^2} \right] \quad (2.12)$$

where γ_{02} and γ_{01} are the new and old outer periphery circulation values and r_d is the outer radius of the "old" region. For cases of interest in this study, $v_o \gg u_o$ and the second term on the right side is negligible.

The time response of the change in pressure drop is shown in Fig. 2.3 for a radius ratio $r_e/r_o = 0.1$. As can be seen, this response can very nearly be represented by the transportation delay to the exit radius, $T_1 = \frac{r_o^2 - r_e^2}{2u_o r_o}$.

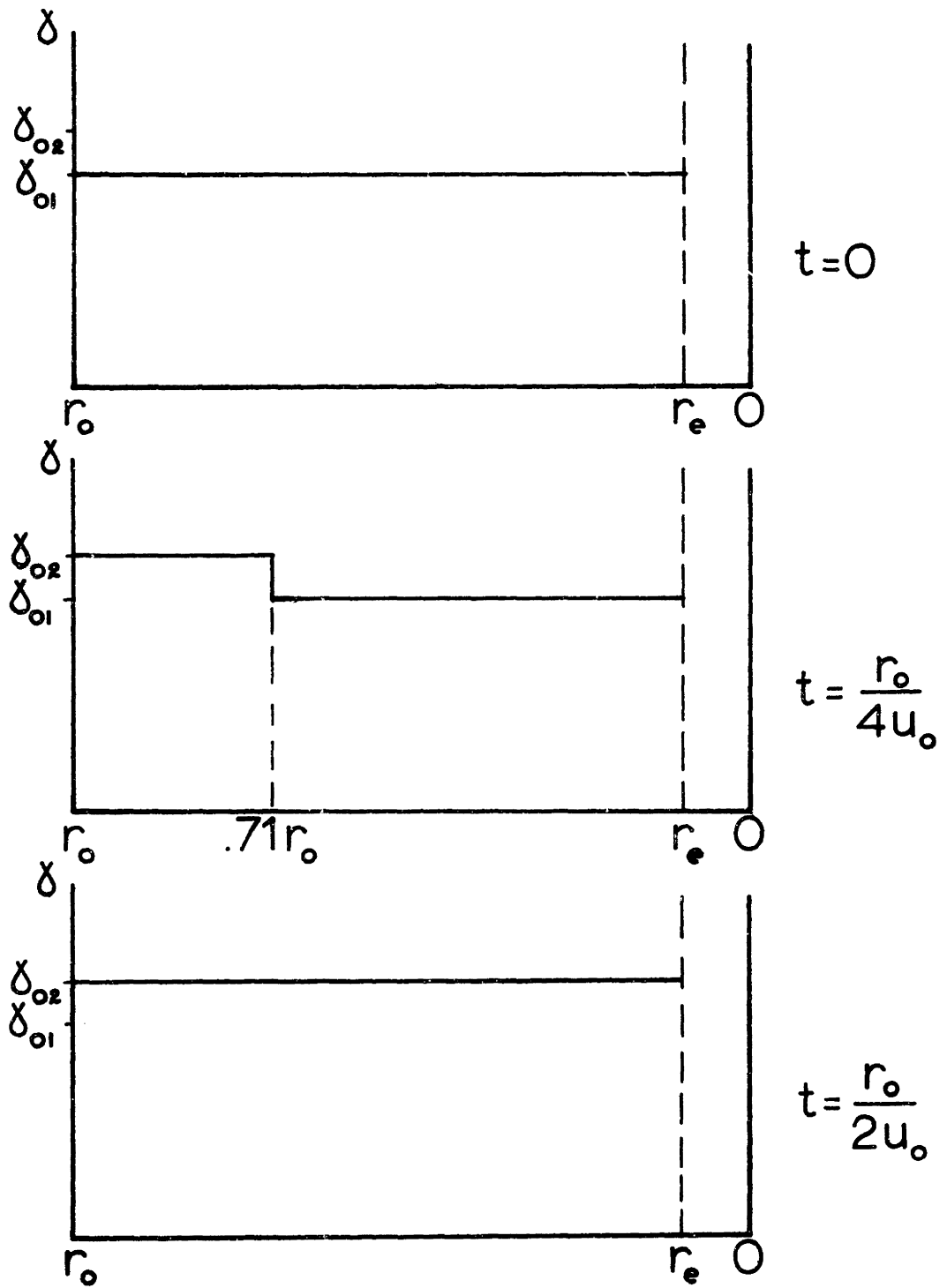


Fig. 2.2 Inviscid Circulation Distribution Step Response

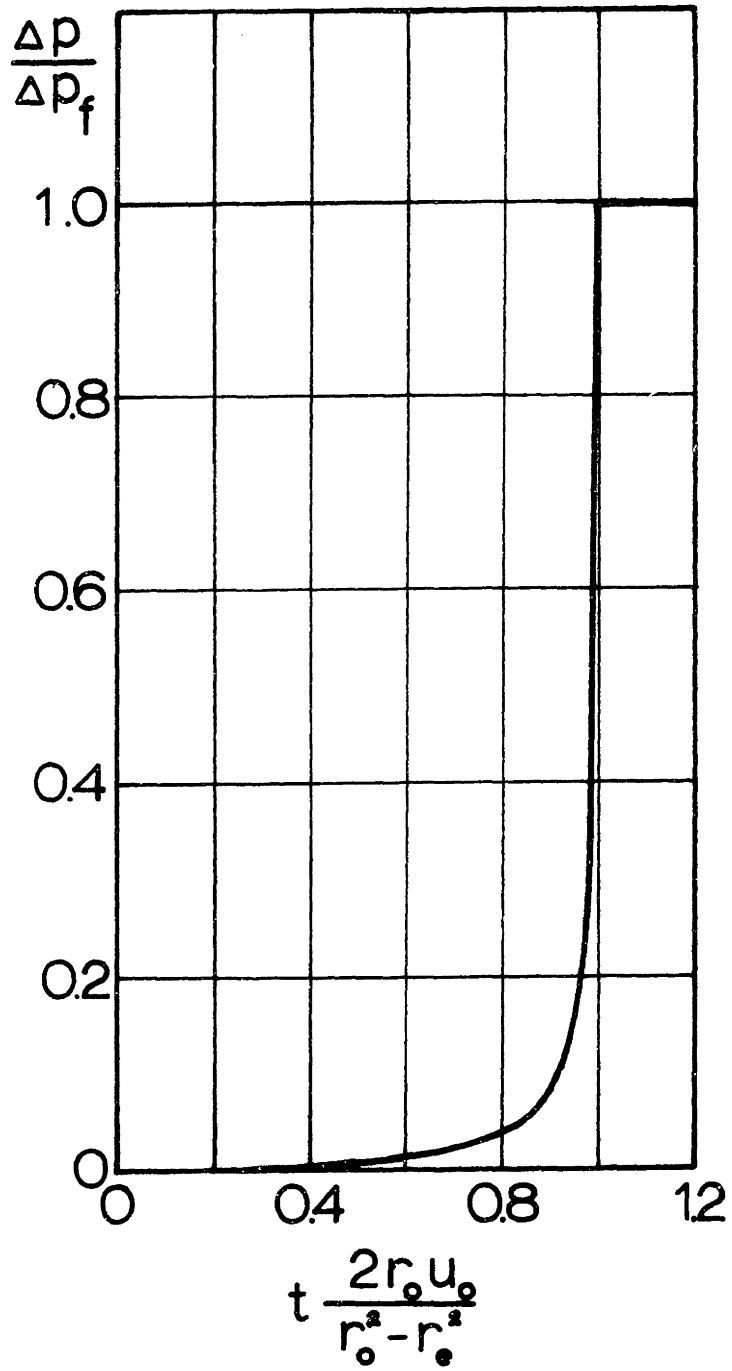


Fig. 2.3 Inviscid Vortex Chamber Pressure Step Response

The conceptual explanation for the concentration of the response near $t = T_1$ is due to two reinforcing effects. First, since most of the pressure drop occurs near the exit, the change is small until the new momentum effects reach this region. Secondly, since the radial velocity is low in the outer portion and becomes higher near the exit, the change is transported quickly across the region of the highest pressure drop. Thus, little change in the pressure drop occurs initially as the change in momentum slowly propagates across the low-pressure-drop region. The large change in pressure drop occurs as the change in momentum quickly crosses the high-pressure-drop region.

This time delay is simply the fill time of the chamber obtained by dividing the volume of the chamber by the volume flow rate through it. The fill time has been used in a number of investigations to characterize the dynamics of the vortex chamber, as discussed in Section 1.2. The usefulness of this characterization is discussed after the development of the viscous model for the chamber and after experimental results have been presented.

2.3 Viscous Model

In vortex chambers of interest in the present study where operation under high swirl conditions is considered the effects of viscosity become important. Near the end walls, the decreased tangential velocities in the boundary layers reduce the centrifugal force and fluid is accelerated inward by the pressure gradient. By

continuity, the increase in the boundary layer radial velocity above the core velocity is balanced by a decrease in the core radial velocity. Depending upon the valve configuration and the operating conditions, the radial velocity in a portion of the core region may go to zero, with all of the radial flow occurring in the boundary layers.

Previous experimental work (28) and the dynamic flow visualization discussed in Chapt. 4 have shown that once this core velocity reaches zero at a given radius r^* , it remains essentially zero for all r such that $r^* > r > r_e$ and all of the radial flow remains in the boundary layers for $r^* > r > r_e$ until the exit is reached at r_e .

With this physical concept as a guide, a dynamic analysis of the main vortex region may be made. In the viscous, turbulent, incompressible case, the radial and tangential velocities are functions of r , y , and t in the boundary layer, but remain functions only of r and t in the core region. The axial velocity can be shown to be small (15), but not zero or constant, as there must be axial flow into the boundary layers.

The viscous effects due to radial circulation gradients are neglected since the radial circulation gradient is very small compared with the high velocity gradients in the boundary layers. This assumption is discussed further below. Thus, all the viscous effects occur in the boundary layers at the wall.

The radial and tangential boundary layers are assumed to be equal, since the main factor in the development of the radial boundary layer is the decreased velocity in the boundary layer.

The boundary layers are assumed to start from zero at the outer periphery, and are assumed to be identical on both end plates so that the flow is symmetric about the midplane of the chamber. These conditions are illustrated in Fig. 2.4 for the four regions of the valve main chamber.

2.3.1 Steady State Viscous Model

First the steady state flow conditions in the chamber are considered. Under the assumptions outlined above, the equations describing the steady state flow conditions may be derived for each of the regions identified in Fig. 2.4.

In Region I, the radial and tangential steady state momentum equations become:

$$u \frac{\partial u}{\partial r} - \frac{v^2}{r} + w \frac{\partial u}{\partial y} = - \frac{1}{\rho} \frac{\partial p}{\partial r} \quad (2.13)$$

$$u \frac{\partial v}{\partial r} + \frac{uv}{r} + w \frac{\partial v}{\partial y} = 0 \quad (2.14)$$

while the boundary layer radial and tangential steady state momentum equations for Region II become:

$$u \frac{\partial u}{\partial r} - \frac{v^2}{r} + w \frac{\partial u}{\partial y} = - \frac{1}{\rho} \frac{\partial p}{\partial r} + \frac{1}{\rho} \frac{\partial \tau_r}{\partial y} \quad (2.15)$$

$$u \frac{\partial v}{\partial r} + \frac{uv}{r} + w \frac{\partial v}{\partial y} = \frac{1}{\rho} \frac{\partial \tau_t}{\partial y} \quad (2.16)$$

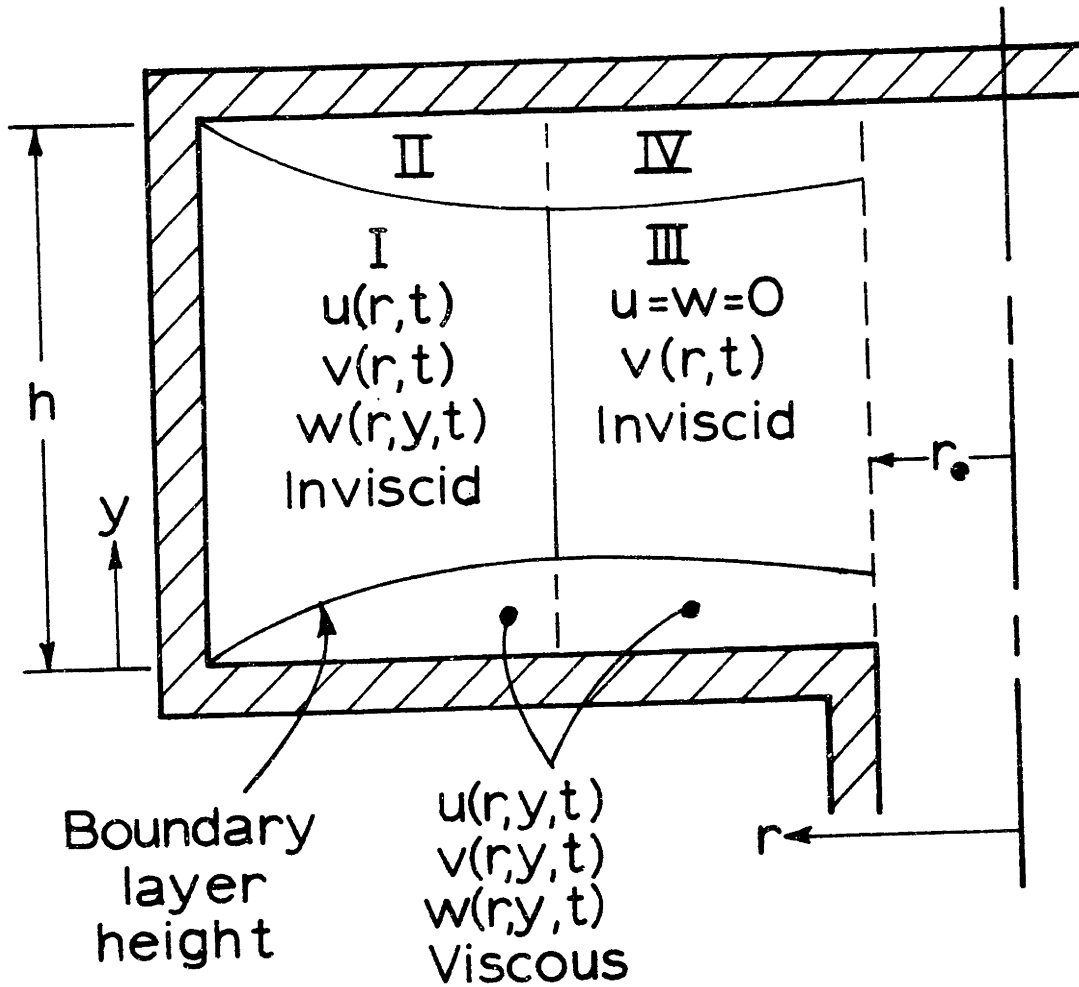


Fig. 2.4 Division of Valve Regions for Steady State Calculations

The continuity equation is:

$$\frac{\partial u}{\partial r} + \frac{u}{r} + \frac{\partial w}{\partial y} = 0 \quad (2.17)$$

The boundary conditions are:

$$\text{at } y = 0; \quad u = v = w = 0 \quad (2.18)$$

$$\text{at } y = \frac{h}{2}; \quad w = \frac{\partial u}{\partial y} = \frac{\partial v}{\partial y} = 0 \quad (2.19)$$

$$\text{at } r = r_0; \quad u = -u_0, v = v_0, w = 0, p = p_0 \quad (2.20)$$

These equations have been solved in Reference 29 using the momentum integral method (24). The forms of the velocity profiles utilized in the solution are as follows:

$$0 \leq y \leq \delta; \quad u = u_\delta f(\eta) + u_g g(\eta), \quad v = v_\delta f(\eta) \quad (2.21)$$

$$\delta \leq y \leq \frac{h}{2}; \quad u = u_\delta, \quad v = v_\delta$$

where δ is the boundary layer height and:

$$\eta = \frac{y}{\delta}$$

$$g(0) = 0 \quad g(1) = 0$$

$$f(0) = 0 \quad f(1) = 1.0$$

The integrals of these velocity profiles are represented by α 's as follows:

$$\begin{aligned}\alpha_1 &= \int_0^1 f^2(\eta) d\eta \\ \alpha_2 &= \int_0^1 f(\eta)g(\eta) d\eta \\ \alpha_3 &= \int_0^1 g^2(\eta) d\eta \\ \alpha_4 &= \int_0^1 g(\eta) d\eta \\ \alpha_5 &= \int_0^1 f(\eta) d\eta\end{aligned}\tag{2.22}$$

For simplicity, the equations are non-dimensionalized as follows:

$$\begin{aligned}\Gamma &= \frac{v_\delta r}{v_o r_o} & u &= -\frac{u_\delta}{u} & u_s &= -\frac{u_s}{u_o} \\ \bar{\delta} &= \frac{\delta}{h/2} & \lambda &= \frac{v_o}{u_o} & x &= 1 - \frac{r}{r_o} \\ \bar{\tau}_{tw} &= \left. \frac{\tau_t}{\rho u_o^2} \right|_{y=0} & \bar{\tau}_{rw} &= \left. \frac{\tau_r}{u_o^2} \right|_{y=0} & \bar{p} &= \frac{p}{\rho u_o^2}\end{aligned}\tag{2.23}$$

The velocity profiles used, based on the experimental data of Reference 23, are:

$$f(\eta) = \eta^{1/7} \quad (2.24)$$

$$g(\eta) = 1.69\eta^{1/7}(1-\eta)^2 \quad (2.25)$$

Using the non-dimensional variables of Eq. (2.23) the non-dimensional differential equations describing the steady state viscous flow in the chamber are as follows:

Continuity equation:

$$\begin{aligned} & [\alpha_5 U + \alpha_4 U_s - U] \frac{d\Gamma}{dx} + [\alpha_5 \bar{\delta} + (1 - \bar{\delta})] \frac{dU}{dx} + \alpha_4 \bar{\delta} \frac{dU_s}{dx} \\ & = \frac{1}{(1-x)} [\alpha_5 \bar{\delta} U + \alpha_4 \bar{\delta} U_s + (1-\bar{\delta})U] \end{aligned} \quad (2.26)$$

Boundary layer radial momentum equation:

$$\begin{aligned} & -[\alpha_1 U^2 + 2\alpha_2 U U_s - \alpha_5 U^2 - \alpha_4 U U_s + \alpha_3 U_s^2] \frac{d\bar{\delta}}{dx} \\ & - [2\alpha_1 \bar{\delta} U + 2\alpha_2 \bar{\delta} U_s - \alpha_5 \bar{\delta} U] \frac{dU}{dx} - [2\alpha_2 \bar{\delta} U - \alpha_4 \bar{\delta} U + 2\alpha_3 \bar{\delta} U_s] \frac{dU_s}{dx} \\ & = \frac{1}{(1-x)} \left[\frac{\alpha_1 \bar{\delta} \lambda^2 \Gamma^2}{(1-x)^2} - \alpha_1 \bar{\delta} U^2 - 2\alpha_2 \bar{\delta} U U_s - \alpha_3 \bar{\delta} U_s^2 + \alpha_5 \bar{\delta} U^2 \right. \\ & \left. + \alpha_4 \bar{\delta} U U_s \right] + \bar{\delta} \frac{dP}{dx} + \frac{2r_0}{h} \bar{\tau}_{rw} \end{aligned} \quad (2.27)$$

Boundary layer tangential momentum equation:

$$\begin{aligned}
 & [\alpha_1 U + \alpha_2 U_s - \alpha_5 U - \alpha_4 U_s] \frac{d\bar{\delta}}{dx} + [\alpha_1 \bar{\delta} - \alpha_5 \bar{\delta}] \frac{dU}{dx} + [\alpha_2 \bar{\delta} - \alpha_4 \bar{\delta}] \frac{dU_s}{dx} \\
 & = - \frac{[\alpha_1 \bar{\delta} U + \alpha_2 \bar{\delta} U_s]}{\Gamma} \frac{d\Gamma}{dx} - \frac{[-\alpha_1 \bar{\delta} U - \alpha_2 \bar{\delta} U_s + \alpha_5 \bar{\delta} U + \alpha_4 \bar{\delta} U_s]}{(1-x)} \\
 & \quad - \frac{(1-x) 2r_o}{\Gamma \lambda h} \bar{\tau}_{tw}
 \end{aligned} \tag{2.28}$$

Inviscid core radial momentum equation:

$$-U \frac{dU}{dx} - \frac{\Gamma^2 \lambda^2}{(1-x)^3} = \frac{dP}{dx} \tag{2.29}$$

Inviscid core tangential momentum equation:

$$U \frac{d\Gamma}{dx} = 0 \tag{2.30}$$

To reiterate, the five non-dimensional variables of interest and their definitions are as follows, and as defined in Eq. 2.23:

1. U - the non-dimensional core radial velocity, $-u_s/u_o$
2. U_s - the non-dimensional boundary layer secondary velocity peak, $-u_s/u_o$
3. Γ - the non-dimensional circulation associated with the core tangential velocity, $v_s r/v_o r_o$
4. $\bar{\delta}$ - the non-dimensional boundary layer height, $s/h/2$
5. P - the non-dimensional pressure P/u_o^2

In the developed flow regions, III and IV, where all of the flow is in the boundary layers, the equations are simplified by setting U equal to zero. In this case, the continuity and tangential

momentum equations may be combined to give the circulation gradient:

$$\frac{d\Gamma}{dx} = - \frac{2r_o \alpha_4 (1-x)^2}{h \alpha_2 \lambda} \bar{\tau}_{tw} \quad (2.31)$$

The shear law used is similar to the shear law used by Prandtl for flow over a flat plate:

$$\tau_w = \frac{f \rho V_\infty^2}{\left(\frac{\rho V_\infty \delta}{\mu} \right)^{1/4}} \quad (2.32)$$

where f is an empirical friction factor taken from Ref. (28) to be 0.021.

Thus, the non-dimensional shears become:

$$\bar{\tau}_{tw} = \frac{C_f \lambda \Gamma V_f}{(1-x) (\bar{V}_f)^{1/4}} \quad (2.33)$$

$$\bar{\tau}_{tw} = \frac{C_f U V_f}{(\bar{\delta} V_f)^{1/4}}$$

where

$$C_f = \frac{f}{\left(\frac{\rho h u_o}{2\mu} \right)^{1/4}}$$

$$V_f = \sqrt{U^2 + \frac{\Gamma^2 \lambda^2}{(1-x)^2}}$$

At the outer periphery, the theoretical values of these non-dimensional variables are:

$$\begin{aligned}\bar{\delta} &= 0.0 \\ U_s &= 0.0 \\ U &= 1.0 \\ \Gamma &= 1.0 \\ P &= \frac{P_o}{\rho U_o^2}\end{aligned}\tag{2.34}$$

However, for a finite difference integration scheme, marching from the outer periphery to the exit, the initial zero value of $\bar{\delta}$ gives infinite shear stresses. Thus, the values used for small x , .001 in the present study, are those given in Reference 21, as follows:

$$\bar{\delta} = \left(18.1 \frac{2r_o}{h} \frac{C_f \sqrt{x}}{\lambda^{1/4}} \right)^{4/5}\tag{2.35}$$

$$U_s = 0.686 \lambda \sqrt{x}\tag{2.36}$$

$$U = \frac{(1.0 + 0.439 \bar{\delta} U_s)}{(1.0 - 0.115 \bar{\delta})}\tag{2.37}$$

With these equations and starting values, the values of the variables as functions of x may be found by numerical integration. The full set of equations are used to the point where $U = 0$, and then the reduced set of equations to $x = x_e$.

The results of Reference 29 show that the solutions of these equations may be obtained when only two parameters, λ and BLC, are specified, where

$$\text{BLC} = \frac{2r_o f}{\left(\frac{\rho u_o h}{2\mu}\right)^{1/4}}$$

Also, the distributions of U and Γ are essentially dependent only on the product of λ and BLC, designated BLC^* , while $\bar{\delta}$ and U_s are functions of both λ and BLC.

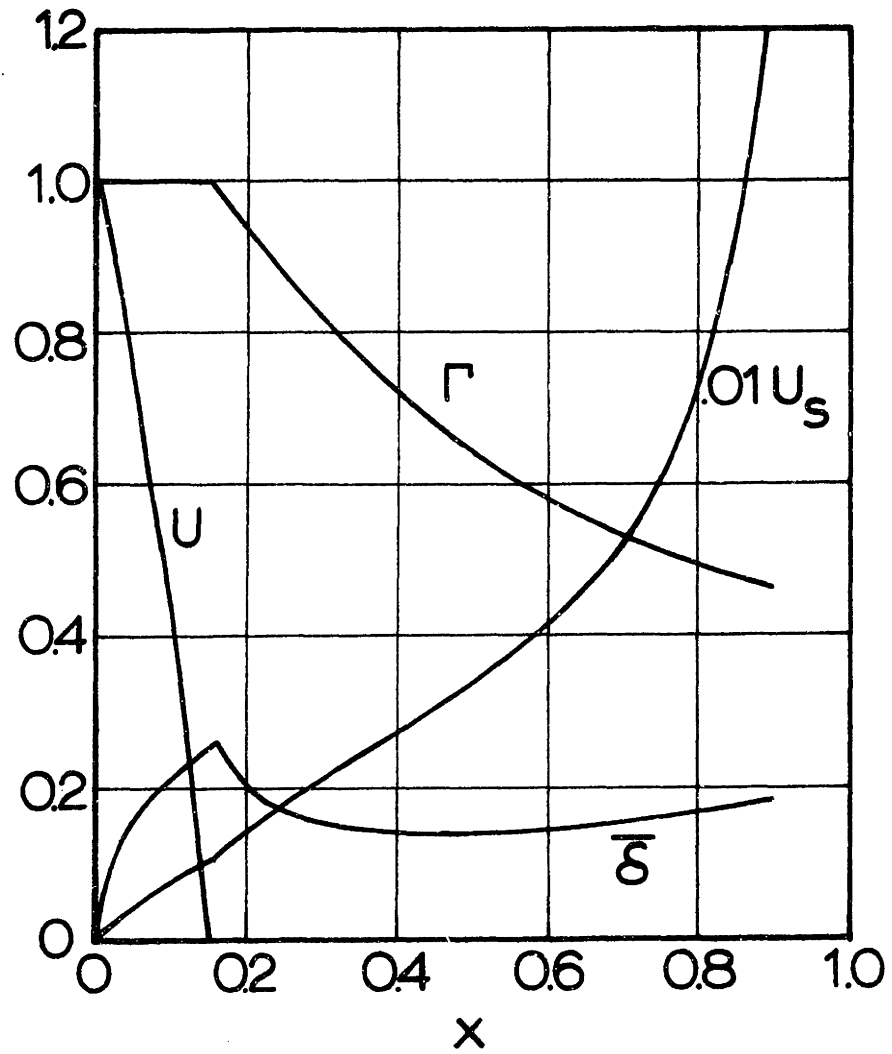
A plot of the distribution of the variables for a typical combination of λ and BLC is shown in Fig. 2.5.

Thus, the steady state flow distribution in a vortex chamber can be determined. It has been shown (28) that the pressure distributions corresponding to the flow agrees closely with experimental data. However, the conceptual model of the dynamic response requires further development.

2.3.2 Dynamic Viscous Model

In order to gain some insight into the dynamic behavior of the viscous vortex region, a dynamic flow visualization study was undertaken. A seven inch diameter chamber with a clear plexiglas cover was run with water as the fluid.

The visualization technique used was the milk injection method, as used in Reference 29. A quantity of reconstituted powdered milk was injected into the vortex valve. After a short period, the milk



$\lambda = 30.9$
BLC = 0.066

Fig. 2.5 Typical Steady State Flow Distribution Variables

had cleared from the areas with radial flow, leaving a spinning donut of milky fluid. The control flow was then changed, and motion pictures of the changes were taken.

During the changes, the spinning donut was observed to speed up or slow down, as expected, and the milkiness remained. This indicated that the region of zero radial flow remained essentially intact during the dynamic changes, with the tangential velocity changes being due to viscous action.

A series of frames from the dynamic visualization motion pictures is shown in Fig. 2.6. As can be seen there is some disruption of the outer boundary of the milky region during the change, but that there is not a marked difference between the initial milkiness and the final condition.

A sketch of the four regions of the valve to be considered in formulating a viscous dynamic model of the vortex chamber is shown in Fig. 2.7. Region I is the portion of the inviscid core where there is radial flow and angular momentum is conserved. In Region III, there is no radial flow and the circulation function, representing the angular momentum, is decreasing. Regions II and IV are the corresponding boundary layers.

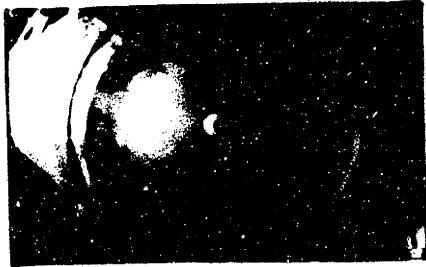
The presence of Region III with no radial flow, resulting from viscous effects, modifies the dynamic response predicted by the inviscid model. Since the major portion of the pressure drop occurs across Region III, the pressure drop cannot change until the momentum of the fluid in this region has changed. The dynamic flow visualization indicates that the radial flow remains essentially zero



a) $t=0$



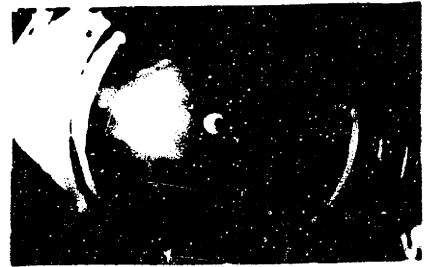
b) $t=1$ sec



c) $t=2$ sec



d) $t=3$ sec



e) $t=4$ sec



f) $t=5$ sec



g) $t=6$ sec



h) $t=7$ sec

Fig. 2.6 Dynamic Flow Visualization

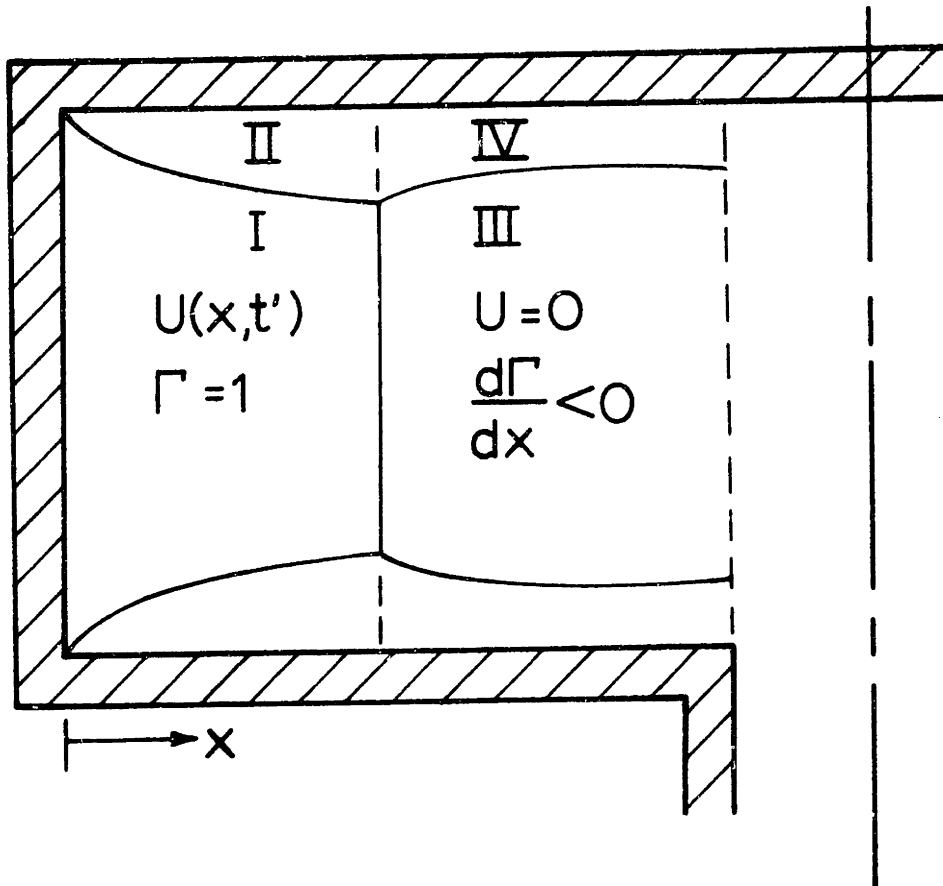


Fig. 2.7 Valve Region Conditions for Steady State Calculations

during the dynamic changes, and the response of this region to a change in outer periphery tangential velocity must occur mainly through viscous action.

Thus the chronological response of the vortex chamber to a step change in v_o , with u_o remaining constant, is illustrated in Fig. 2.8 and is as follows:

1. The new conditions established at the outer periphery are propagated through the boundary layer, Region II, and through the core, Region I, in the developing region. Because the radial flow is slower in the core than in the boundary layers, there are three regions initially.

- a) Near the outer periphery, the flow propagating through both the core and boundary layer regions, I and II, corresponds to the "new" conditions.
- b) Farther in, the boundary layer, Region II, corresponds to the "new" conditions, but the core, Region I does not, so that the flow from the core to the B.L.* will tend to decrease the changes propagating in through the boundary layer.
- c) Even farther in, both the B.L. and the core in all four regions correspond to the "old" conditions, as in the inviscid model.

* B.L. = boundary layer

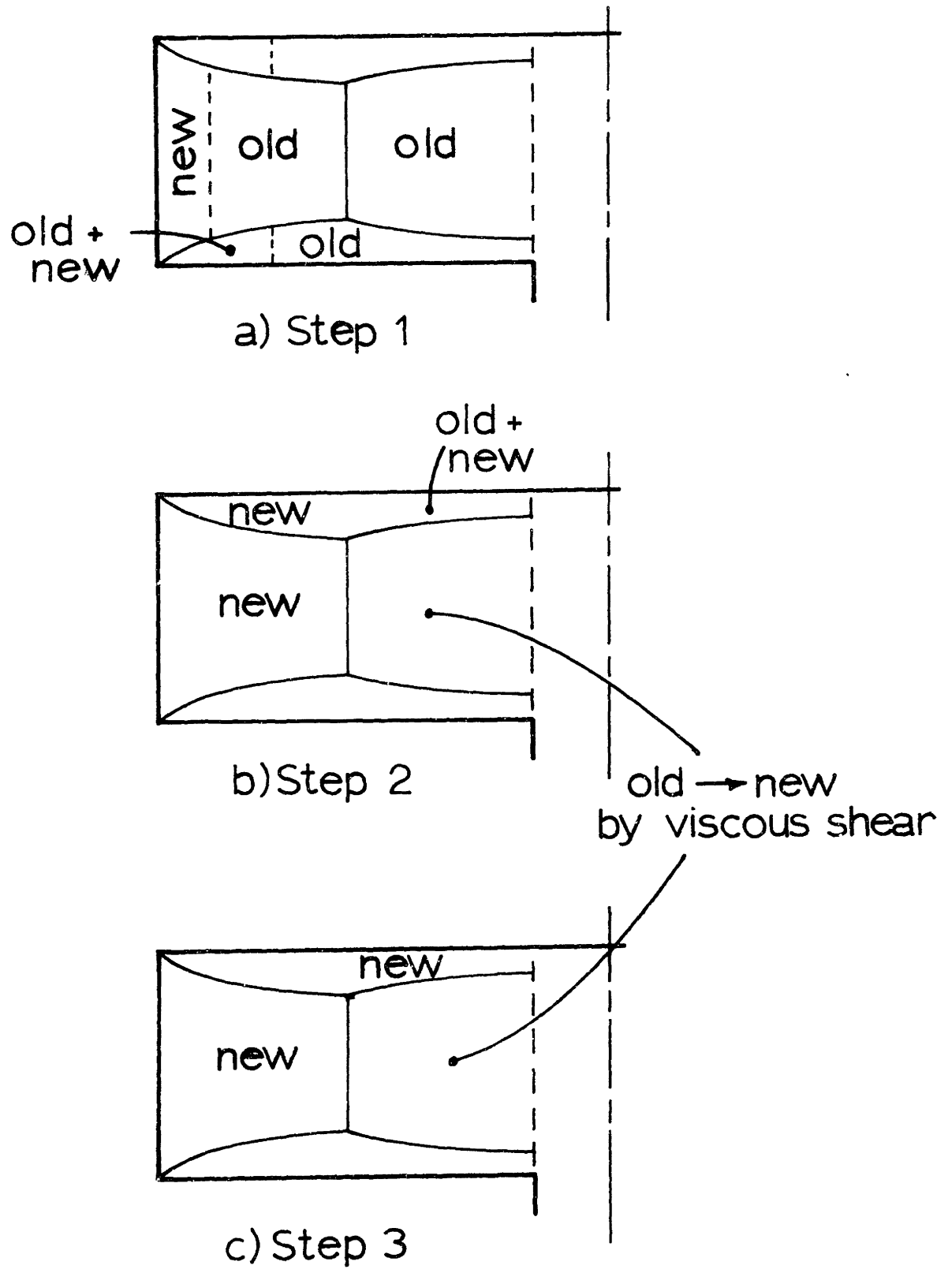


Fig. 2.8 Conceptual Dynamic Response

2. After some time, the conditions propagating into the B.L.'s in Region IV are a mixture of the "new" conditions through the boundary layers and the "old" conditions. Gradually, these conditions will change until the propagating conditions are entirely new, both through the boundary layers, Region II, and the core, Region I.
3. As the "new" conditions propagate through the boundary layers in Region IV, they interact with Region III through turbulent viscous shear at the interface, to drive Region III to its new condition.

For this conceptual model, the shear due to the radial circulation gradient in the core has been assumed negligible. This assumption is verified in the final section of this chapter, after solutions have been found to predict the dynamic response.

In order to calculate a dynamic response based on this conceptual model, the initial and final steady state equations for a step change were solved first to provide a set of velocity distributions and boundary layer dimensions on which to base the dynamic solution. The step change in v_0 is assumed to be small, and u_0 is kept constant. The chamber is divided into a set of eighty finite elements, forty concentric rings in one boundary layer on the matching forty rings extending from the boundary layer to the mid plane, with each element represented by the values of the variables at the mid-point radius. The nondimensional time steps used were $\Delta t u_0 / r_0 = 0.0002$. This was the minimum number of elements required to represent the valve with reasonable accuracy, as judged

by trials with more and less elements. The computer program used is presented in Appendix A.

The regions considered, and the important effects in each region, are shown in Fig. 2.9.

Consider first a finite element of fluid in the outer region, Fig. 2.10, extending from the wall to the mid-plane. The values of U , U_g , and $\bar{\delta}$ at the boundaries $j-1$ and j are calculated from the steady state distributions, as shown below. In the dynamic case, the tangential velocity at the mid-plane of the core does not match the maximum tangential velocity in the boundary layer. Therefore, there are two circulation functions, Γ and Γ_c , associated with these velocities, which are both initially equal to the initial steady state circulation function. This dynamic tangential velocity distribution is shown in Fig. 2.11. The term "boundary layer" in this discussion of the dynamic response will refer to the region up to the maximum velocity, and will be characterized by that velocity. The term "core" will refer to the region between "boundary layers" including the transition region, and will be characterized by the tangential velocity at the mid-plane.

The non-dimensional flows \bar{q}_1 , and \bar{q}_2 may be written as:

$$\bar{q}_1 = U_{j-1}(1 - x_{j-1})(1 - \bar{\delta}_{j-1}) \quad (2.38)$$

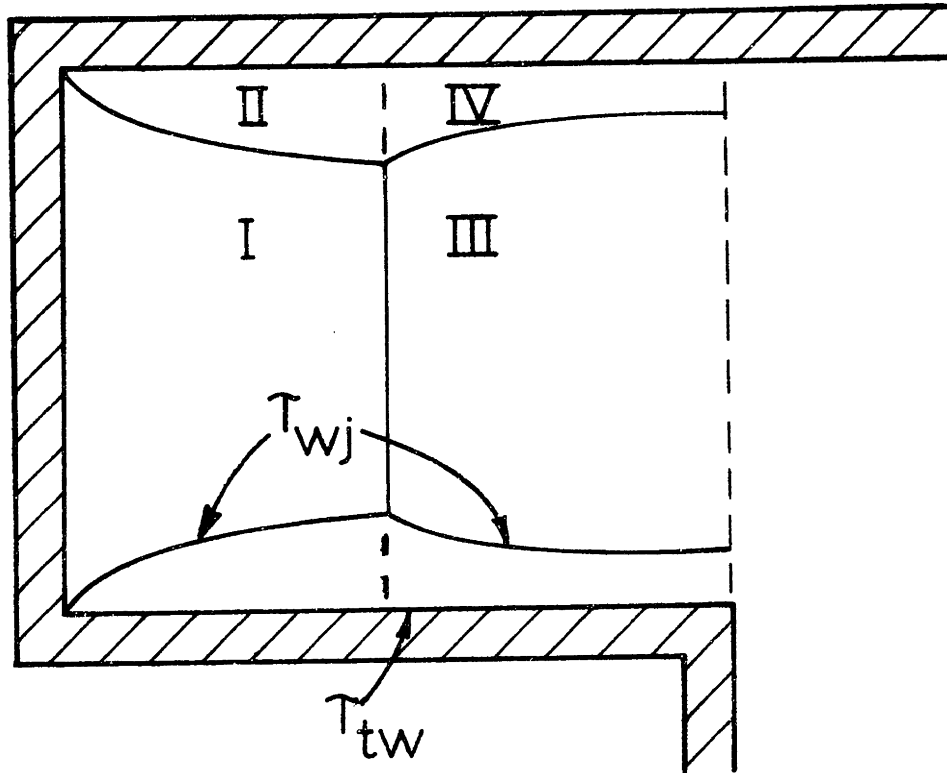
$$\bar{q}_2 = U_j(1 - x_j)(1 - \bar{\delta}_j) \quad (2.39)$$

The axial flow \bar{q}_3 is simply the difference between the two flows:

$$\bar{q}_3 = \bar{q}_1 - \bar{q}_2 \quad (2.40)$$

The non-dimensional volume of the core ring may be written as

$$V_{cj} = (1 - \bar{\delta}_j)(1 - x_j)\Delta x \quad (2.41)$$



| Region | New Conditions by: | Viscous shear |
|--------|--------------------|------------------------|
| I | Flow propagation | τ_{wj} |
| II | Flow propagation | τ_{wj}, τ_{tw} |
| III | Viscous action | τ_{wj} |
| IV | Flow propagation | τ_{wj}, τ_{tw} |

Fig. 2.9 Important Effects for Viscous Dynamic Response, by Regions

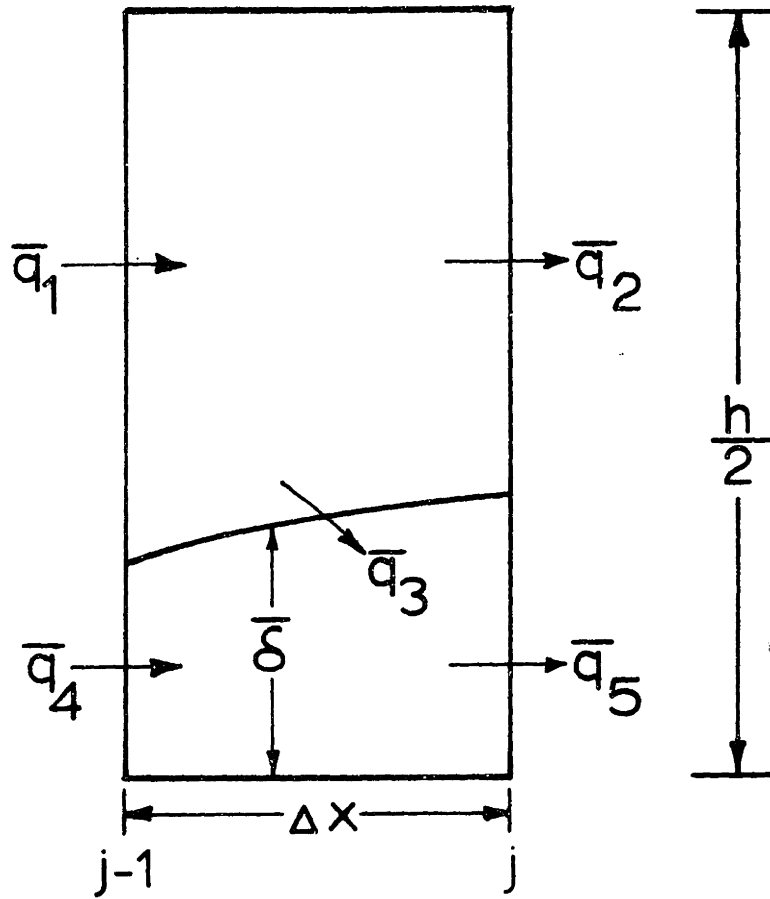
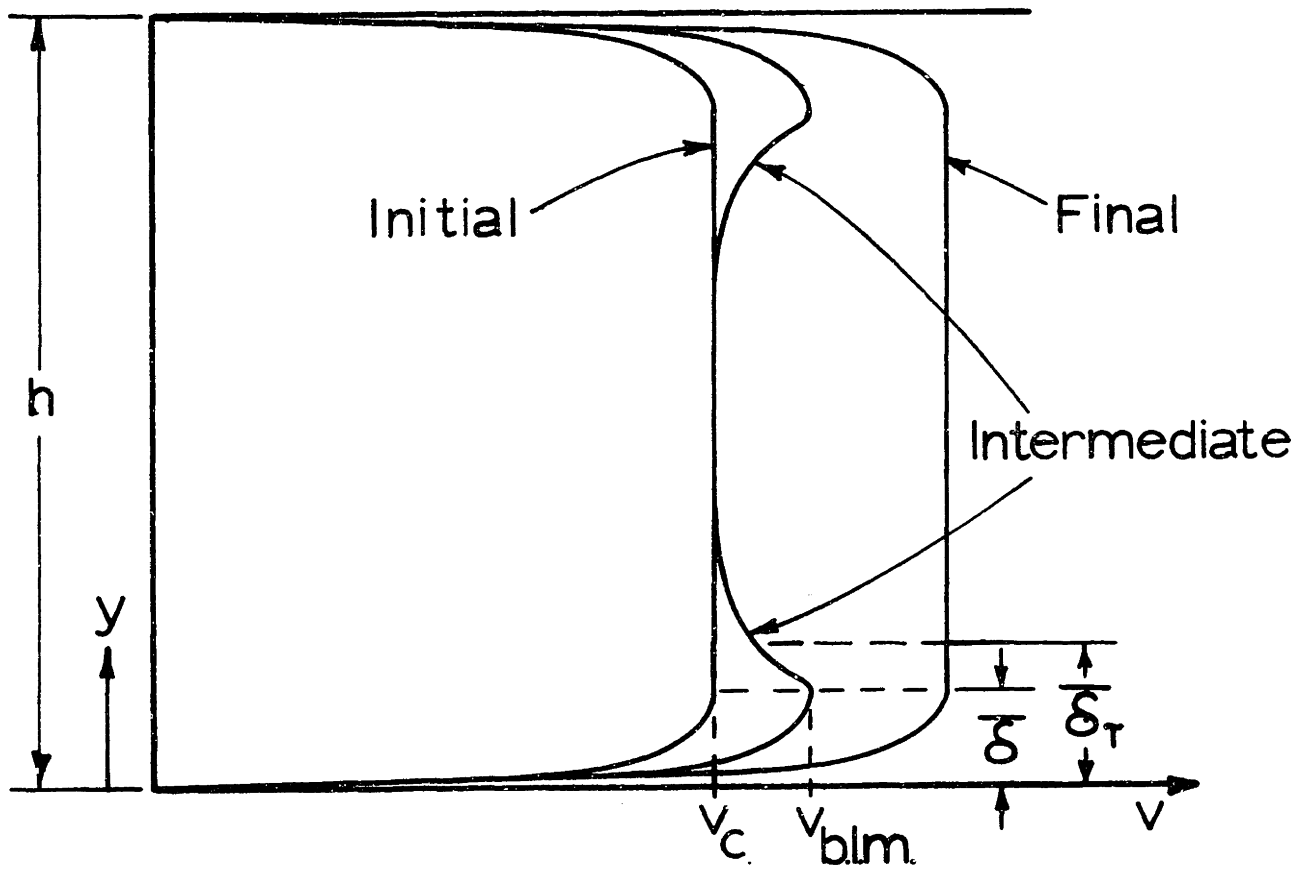


Fig. 2.10 Single Finite Element for Dynamic Response Calculation



$$\Gamma_c = \frac{v_c r}{v_o r_o}$$

$$\Gamma = \frac{v_{blm} r}{v_o r_o}$$

Fig. 2.11 Dynamic Tangential Velocity Axial Distribution

The rate of change of circulation within this volume will be due to two effects, flow propagation, as in the inviscid case, and viscous action. These are designated respectively as

$$\left(\frac{d\Gamma_{c_j}}{dt'} \right)_{\text{prop.}} \quad \text{and} \quad \left(\frac{d\Gamma_{c_j}}{dt'} \right)_{\text{vis.}}$$

Thus, the circulation change equation is:

$$\frac{d\Gamma_{c_j}}{dt'} = \left(\frac{d\Gamma_{c_j}}{dt'} \right)_{\text{prop.}} + \left(\frac{d\Gamma_{c_j}}{dt'} \right)_{\text{vis.}} \quad (2.42)$$

The rate of change of circulation within this volume due to the flow propagation, assuming the fluid in the volume is constantly well mixed, may be written as:

$$\left(\frac{d\Gamma_{c_j}}{dt'} \right)_{\text{prop.}} = \frac{\bar{q}_1 \Gamma_{c,j-1} - (\bar{q}_2 + \bar{q}_3) \Gamma_{c,j}}{V_{c_j}} \quad (2.43)$$

The rate of change of momentum in the boundary layer can be calculated similarly, to give:

$$\left(\frac{d\Gamma_j}{dt'} \right)_{\text{prop.}} = \frac{\bar{q}_3 \Gamma_{c,j} + \bar{q}_4 \Gamma_{j-1} - \bar{q}_5 \Gamma_j}{V_j} \quad (2.44)$$

where $t' = t \frac{u_o}{r_o}$

$$\bar{q}_4 = (\alpha_4 U_{s,j-1} + \alpha_5 U_{j-1})(1 - x_{j-1}) \bar{\delta}_{j-1}$$

$$\bar{q}_5 = (\alpha_4 U_{s,j} + \alpha_5 U_j)(1 - x_j) \bar{\delta}_j$$

The major change of concern is the change in the circulation distribution in Region I and III. However, the distribution of U , U_g , and δ also change slightly between the initial and final conditions. In order to take into account these changes, at each time step and for each element, the U , U_g , and δ values are assumed to have changed by the same proportion of their total change as the circulation changes. Thus, if Γ_{ji} represent the initial value of the circulation for the j^{th} element, and Γ_{jf} is the final value, the proportion of the circulation change may be represented by:

$$\beta = \frac{\Gamma_j - \Gamma_{ji}}{\Gamma_{jf} - \Gamma_{ji}} \quad (2.45)$$

where β will initially be zero and will approach 1.0 for long times. Using the same notation, the value of U_j at any time may also be written as:

$$U_j = U_{ji} + \beta(U_{jf} - U_{ji}) \quad (2.46)$$

and the values of U_g and δ may be calculated similarly.

As the new conditions propagate through the boundary layer ahead of the propagation in the core, the circulation difference causes a turbulent viscous shear which must also be taken into account. It is assumed that the effects of this viscous shear

may be approximated by a shear proportional to the square of the maximum velocity difference;

$$\begin{aligned}\tau_{wj} &= k\rho(\Delta v_m)^2 \\ &= k\rho(v_{B.L.M.} - v_c)^2\end{aligned}\tag{2.47}$$

From the moment of momentum equation, and assuming that the change in velocity is nearly uniform for an element in the core, the non-dimensional change of momentum in the core may be written as:

$$\left(\frac{d\Gamma_c}{dt}\right)_{vis.} = \frac{k\lambda(\Gamma - \Gamma_c)|\Gamma - \Gamma_c|}{H(1-\delta_\tau)(1-x)}\tag{2.48}$$

where $H = \frac{h}{2r_0}$ and δ_τ is the effective shear height. Similarly, the effect of this shear on the boundary layer can be written as:

$$\left(\frac{d\Gamma_j}{dt}\right)_{vis.} = -\frac{k\lambda(\Gamma - \Gamma_c)|\Gamma - \Gamma_c|}{H\delta_\tau(1-x)}\tag{2.49}$$

The form of the turbulent viscous shear equation, with $\tau_{wj} = \rho k(\Delta v_m)^2$, was suggested by wall jet theory, first treated by Glauert (8). While this work is not directly applicable to the vortex chamber flows, it does provide an indication of the form of shear relationship.

Glauert dealt mainly with a jet striking a plane surface and spreading out radially in a still fluid. He separated the flow into two regions, divided at the point of maximum velocity. He postulated that for turbulent flow, the inner flow would be similar

to a plane turbulent boundary layer, and the outer flow would be similar to a plane free jet.

Kruka and Eskinazi (12) reported an extensive experimental work with a plane wall jet issuing from a slot into a parallel free stream. This work found that the shear stresses in the outer flow region were correlated to the square of the velocity difference Δv_m between the maximum jet velocity and the free stream velocity.

Other authors (3,7) have treated wall jets with longitudinal curvature, but none to this author's knowledge have treated transverse curvature. Therefore, the form of the parallel straight flow shear is used in the present work.

In order to calculate the shear, a simple model of the flow was postulated. It was assumed that the maximum velocity occurred at the height of the steady state boundary layer, so that the steady state and dynamic velocity profiles in the boundary layer are similar, as shown in Fig. 2.11. As the core region is spun up, the point of maximum shear will move upward from near the steady state boundary layer height. For simplicity, it was assumed that this point of maximum shear designated $\bar{\delta}_\tau$ be represented by an average value of one and one-half times the boundary layer height, $\bar{\delta}$. The changes due to the shear were assumed to be uniformly distributed within each element, so that the angular momentum change is the same as that of an equivalent solid ring driven by the shear torque. This torque is assumed to be proportional to the square of the maximum velocity difference, as suggested by the wall jet literature.

Thus, the equations for the total changes in circulation in the developing regions are as follows:

$$\begin{aligned} \frac{d\Gamma_{c,j}}{dt'} &= \left(\frac{d\Gamma_{c,j}}{dt'} \right)_{\text{prop.}} + \left(\frac{d\Gamma_{c,j}}{dt'} \right)_{\text{vis.}} \\ &= \frac{\bar{q}_1 \Gamma_{c,j-1} - (\bar{q}_2 + \bar{q}_3) \Gamma_{c,j}}{V_{c,j}} + \frac{k\lambda(\Gamma - \Gamma_c) |\Gamma - \Gamma_c|}{H(1-\bar{\delta}_r)(1-x)} \end{aligned} \quad (2.50)$$

$$\begin{aligned} \frac{d\Gamma_j}{dt'} &= \left(\frac{d\Gamma_j}{dt'} \right)_{\text{prop.}} + \left(\frac{d\Gamma_j}{dt'} \right)_{\text{vis.}} \\ &= \frac{\bar{q}_3 \Gamma_{c,j} + \bar{q}_4 \Gamma_{j-1} - \bar{q}_5 \Gamma_j}{V_j} - \frac{k\lambda(\Gamma - \Gamma_c) |\Gamma - \Gamma_c|}{H\bar{\delta}_r(1-x)} \end{aligned} \quad (2.51)$$

A single value for the constant k in the shear stress equation was selected to correlate the complete set of experimental data discussed in Chapter 4. A different ratio of $\bar{\delta}$ and $\bar{\delta}_r$ would have led to a different value of k , but the responses would have been essentially the same, as can be seen from Eqs. (2.50) and (2.51).

In the developing region, where the steady state Γ is constant with x , the shear at the walls is accounted for implicitly through the radial inward growth of the boundary layer. This effect is represented in the dynamic case only through the change in boundary layer height $\bar{\delta}$ proportional to the change in Γ_j as shown in Eqs. (2.45) and (2.46). In the developed region, where the core radial velocity has gone to zero, the loss of momentum due to the shear at the walls must also be accounted for explicitly, as the value of Γ decreases with x . Thus, in the developed region, the boundary layer circulation change has a third component, $\left(\frac{d\Gamma}{dt'} \right)_{\text{wall}}$,

so that the equation becomes:

$$\frac{d\Gamma_j}{dt'} = \left(\frac{d\Gamma_j}{dt'} \right)_{\text{prop.}} + \left(\frac{d\Gamma_j}{dt'} \right)_{\text{vis.}} + \left(\frac{d\Gamma_j}{dt'} \right)_{\text{wall}} \quad (2.52)$$

In the boundary layer, Region IV, the average radial velocity is $\alpha_4 U_s$. From this, the average amount of non-dimensional time for a particle of fluid to cross an incremental ring may be calculated to be:

$$\Delta t'_j = \frac{\Delta x}{\alpha_4 U_s} \quad (2.53)$$

In crossing this ring, the average rate of loss of momentum of a particle due to the shear at the wall may be calculated as follows:

$$\begin{aligned} \left(\frac{d\Gamma_j}{dt'} \right)_{\text{wall}} &\approx \frac{\Delta\Gamma}{\Delta t'_j} = \frac{\Gamma_j - \Gamma_{j-1}}{\Delta x} \frac{\Delta x}{\Delta t'_j} \\ &= \frac{(\Gamma_j - \Gamma_{j-1})\alpha_4 U_s}{\Delta x} \end{aligned} \quad (2.54)$$

The loss of momentum due to the shear at the core boundary is given by Eq. 2.49, and the gain of momentum of the core is given by Eq. 2.48. Since, in this region \bar{q}_1 , \bar{q}_2 , and \bar{q}_3 go to zero, and \bar{q}_4 and \bar{q}_5 go to 1.0, the circulation change equations become:

$$\frac{d\Gamma_{c_j}}{dt'} = \left(\frac{d\Gamma_{c_j}}{dt'} \right)_{\text{vis}} = \frac{k\lambda(\Gamma_j - \Gamma_{c_j})|\Gamma_j - \Gamma_{c_j}|}{H(1-\bar{\delta}_{\tau_j})(1-x_j)} \quad (2.55)$$

$$\frac{d\Gamma_j}{dt'} = \left(\frac{d\Gamma_j}{dt'} \right)_{\text{prop.}} + \left(\frac{d\Gamma_j}{dt'} \right)_{\text{vis.}} + \left(\frac{d\Gamma_j}{dt'} \right)_{\text{wall}} \quad (2.56)$$

(Cont'd.)

$$= \frac{\Gamma_{j-1} - \Gamma_j}{V_j} - \frac{k\lambda(\Gamma_j - \Gamma_{cj})|\Gamma_j - \Gamma_{cj}|}{H \delta (1-x)} \quad (2.56)$$

$$- \frac{(\Gamma_{j-1} - \Gamma_j)u_{sj}}{\Delta x}$$

The pressure drop across the chamber as a function of time may be found from the static equation:

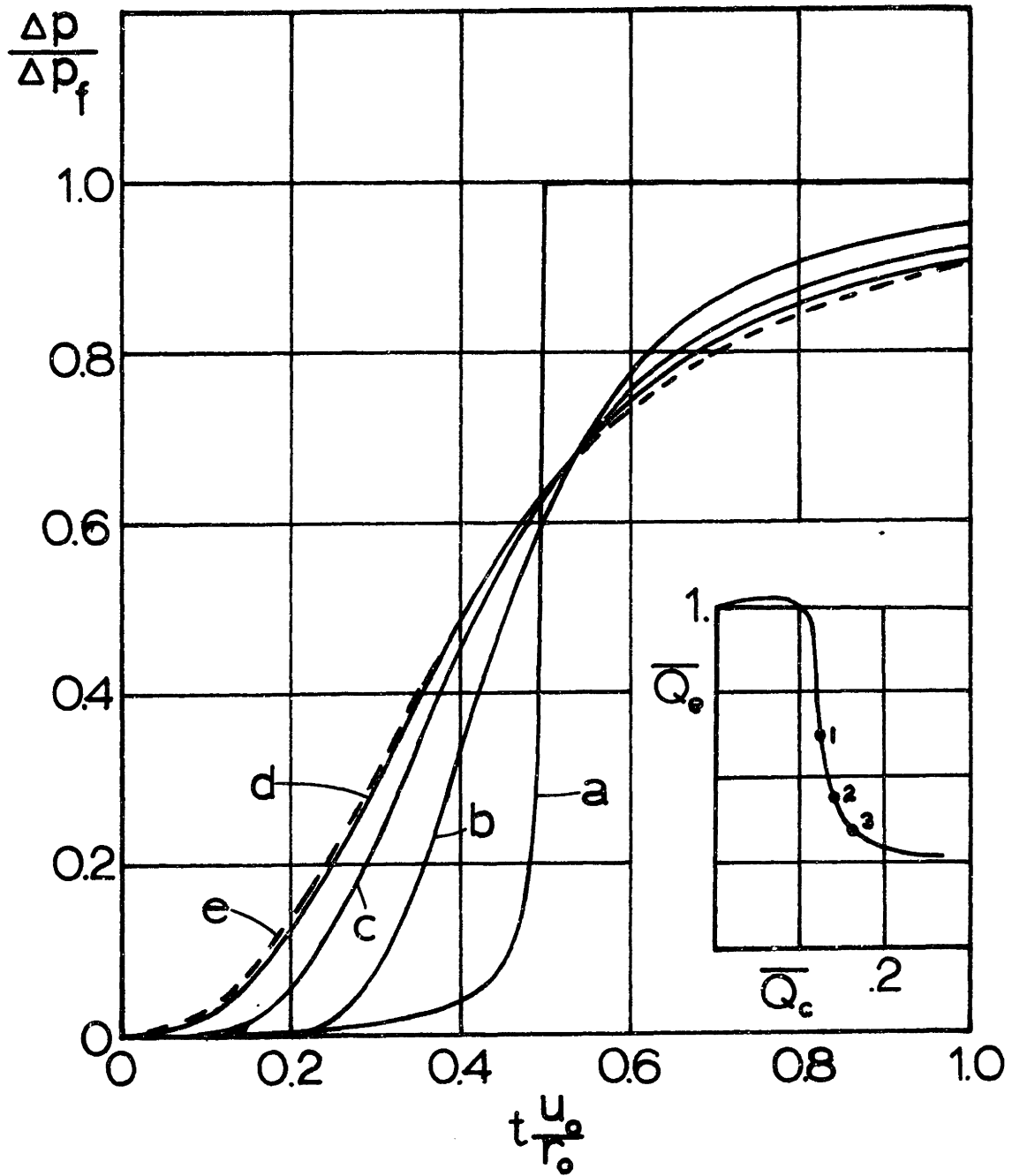
$$\frac{dP}{dx} = - \frac{\lambda^2 - \Gamma^2}{(1-x)^3} \quad (2.57)$$

for the case of $\lambda > 10$ since $\lambda^2 \Gamma^2$ then is of the order of 100 while $U \frac{dU}{dx}$ is of the order of 1 and $\frac{dU}{dt}$ is of the order of 0.1.

These dynamic equations were programmed for solution with a Fortran program, run on an IBM 360/65 computer, and listed in Appendix A. Several typical plots of the change in pressure drop across the chamber versus non-dimensional time are shown in Fig. 2.12. If the fill time, $T_1 = \frac{r_o^2 - r_e^2}{2u_o r_o}$ is approximated by $T_1 = \frac{r_o}{2u_o}$, then $t' = 0.5$ represents the fill time as shown by the equivalent inviscid response. This plot shows that as the viscous effects become more and more important, the response differs more from the inviscid response, as a smaller portion of the fluid momentum is changed by flow transport and more is changed due to viscous action.

The term of the Navier-Stokes equation (24) which gives the radial shear is $(\frac{\partial^2 v}{\partial r^2} + \frac{1}{r} \frac{\partial v}{\partial r} - \frac{v}{r^2})$. It can be shown that this becomes $\frac{v_o r_o}{r} [\frac{\partial^2 \Gamma}{\partial r^2} - \frac{1}{r} \frac{\partial \Gamma}{\partial r}]$. Thus, this term is identically zero for zero radial circulation gradient.

In order to check the assumption that the dynamic radial circulation gradient is similar to the static gradient, a plot of the Γ distribution for a series of values of t' is shown in Fig. 2.13. This plot shows that the dynamic gradient very closely



- a) Inviscid
- b) Point 1, no radial shear
- c) Point 2, no radial shear
- d) Point 3, no radial shear
- e) Point 3, with radial shear

Fig. 2.12 Viscous Vortex Chamber Pressure Step Responses

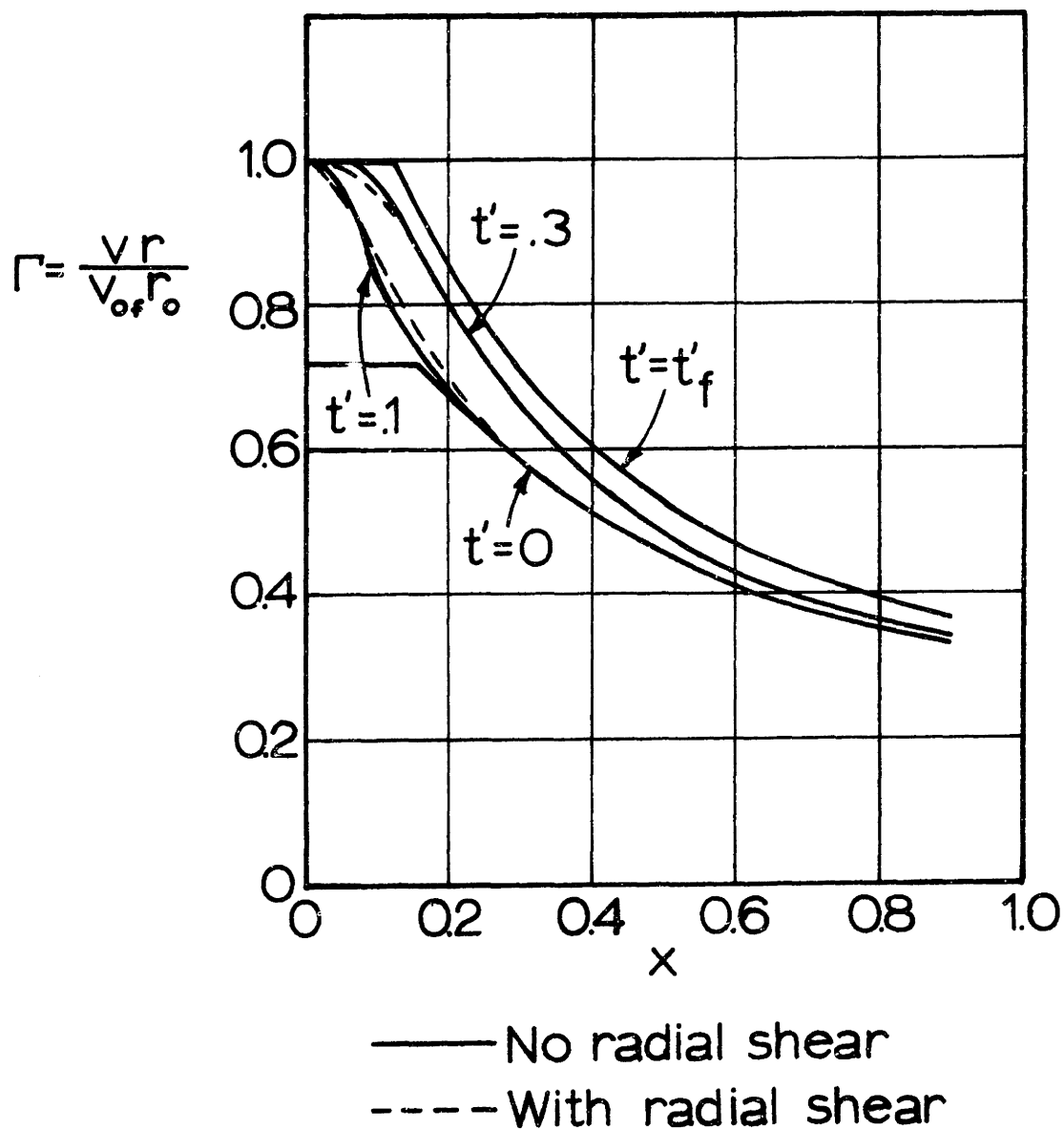


Fig. 2.13 Viscous Circulation Distribution Step Response

parallels the static gradient in the developed region, verifying that the radial shear may be neglected here as it was in the static case. In the developing region, the gradient is quite steep. To verify that the predominant mode of change in this region is due to transport effects rather than viscous action, a step response was run with a shear between concentric elements due to the radial circulation gradient. This shear was of the same form as the shear between the boundary layer and core, proportional to the square of the circulation gradient. The overall step response with this radial shear is also shown in Fig. 2.12, and the Γ distributions are shown in Fig. 2.13. The change in the response is small compared with changes due to the changes in k , as will be shown in Chapter 4, thus in further work the radial shear term is neglected.

Thus, a model of the dynamic viscous response of the vortex flow has been developed. This model forms the basis of the development of a lumped model to represent the entire vortex amplifier dynamic response, presented in the next chapter.

Chapter 3

LUMPED MODEL

3.1 Introduction

In order to complete a dynamic model for the vortex amplifier, the vortex flow field model developed in Chapter 2 must be combined with the appropriate models for the inlet and exit ports of the amplifier and for their interaction with the vortex flow. This chapter presents the development of a dynamic model for the complete vortex amplifier.

In designing a vortex valve, the steady state characteristic may be estimated with reasonable accuracy, using the methods and graphs of Reference 30. Or, if a valve has already been built, it is a relatively simple matter to measure the steady state characteristic. However, as outlined in Chapter 1, there has been no satisfactory method of predicting the dynamic response, and even measuring the dynamic response once a valve is built is a complex and difficult task. Therefore, a method of predicting the dynamic response using either predicted or steady state information is needed.

The design of dynamic fluid power control circuits involves the interconnection of many elements to form the complete circuit. The method used for predicting the response of these total systems during the initial design stages is through the use of linear, lumped transfer function relationships. Thus, in order to be compatible

with other fluid power control component models, the lumped model presented in this chapter will be in terms of a linearized dynamic transfer function.

In general, the linearized dynamic model parameters depend upon the region of operation on the steady state characteristic, as shown in Fig. 3.1. This model, developed using either predicted or measured steady state information, will predict the dynamic parameters for small signal operation about a given operating point. It thus will provide a building block for the design of fluid power control circuits using vortex valves, and basically operating over a small region of the vortex valve steady state characteristic, such as might occur in a servomechanism regulation operation.

The prediction of the dynamic response for full range operation, switching from nearly full flow to nearly cutoff, is beyond the scope of this thesis. This range of operation would be used in circuits where the vortex valve acts essentially as a flow switch, changing between "high" and "low" flow rates.

In the work below, a lumped parameter dynamic model for a control valve is developed for which all dynamic model parameters for a given operating point may be determined directly from the distributed parameter analysis described in Chapter 2. A schematic drawing of a valve including the variables of interest is shown in Fig. 3.2.

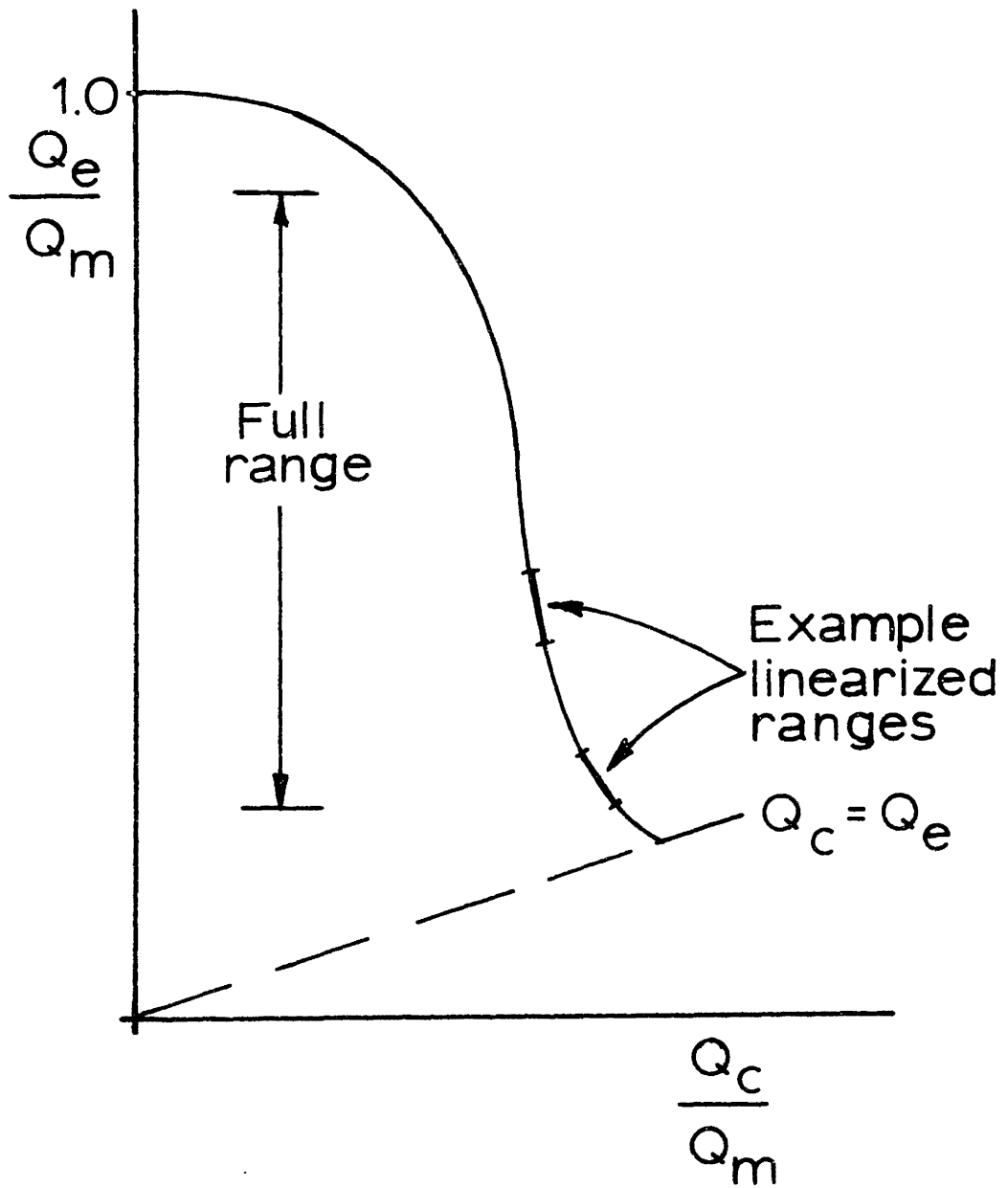


Fig. 3.1 Regions of Dynamic Operation

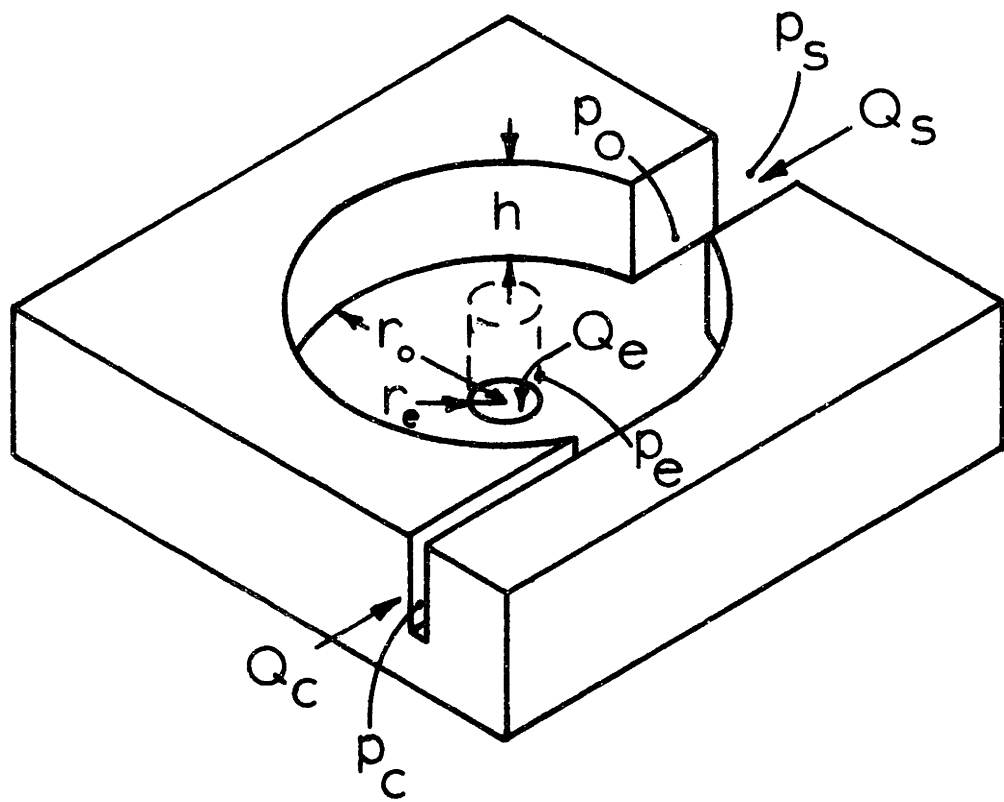


Fig. 3.2 Schematic of Vortex Valve with Definition of Variables

3.2 Inlet Ports

The ideal supply and control ports of a vortex valve are short, straight passages, so that the velocity profiles are nearly uniform. Thus, for incompressible flow, these ports may be represented as quadratic orifices with the following pressure-flow equations:

$$Q_c = c_{dc} A_c \sqrt{\frac{2(p_c - p_o)}{\rho}} \quad (3.1)$$

$$Q_s = c_{ds} A_s \sqrt{\frac{2(p_s - p_o)}{\rho}} \quad (3.2)$$

where Q_c is the control flow and Q_s is the supply flow.

For small signal analysis, these equations may be linearized about an operating point to give incremental linear equations in terms of equivalent resistances:

$$Q_c = \frac{\Delta(p_c - p_o)}{R_c} \quad (3.3)$$

$$Q_s = \frac{\Delta(p_s - p_o)}{R_s} \quad (3.4)$$

where

$$\frac{1}{R_c} = \left. \frac{\partial Q_c}{\partial (p_c - p_o)} \right|_0 = c_{dc} A_c \sqrt{\frac{1}{2\rho(p_c - p_o)}} = \frac{Q_{co}}{2(p_c - p_o)_o}$$

and:

$$\frac{1}{R_s} = \frac{\partial Q_s}{\partial (p_s - p_o)} \Big|_0 = \frac{Q_{so}}{2(p_s - p_o)_o}$$

The second subscript o indicates that the quantities are to be evaluated at the operating point.

Due to the small, short passages, and the assumption of incompressibility, the effects of inertia and capacitance in these inlet chambers are assumed negligible.

3.3 Mixing Region

The supply and control flows are assumed to mix completely at the outer periphery, in a period of time which is short compared to the times associated with the vortex flow field changes. Under these assumptions, the radial and tangential velocities at r_o are uniform. The radial velocity may be expressed as the total flow divided by the outer periphery area:

$$u_o = \frac{Q_c + Q_s}{2\pi r_o h} \quad (3.5)$$

The tangential velocity may be derived from consideration of conservation of momentum. Thus, for lossless mixing, the ideal v_o may be written as:

$$v_o^+ = \frac{Q_c v_c}{Q_c + Q_s} = \frac{Q_c^2}{A_c(Q_c + Q_s)} \quad (3.6)$$

The mixing loss has been studied previously and may be represented by a loss coefficient ϵ , as determined empirically in Reference 28. This coefficient is primarily a function of the swirl, represented by the ideal ratio v_o^+/u_o , and is shown in Fig. 3.3.

Thus, the tangential velocity expression becomes:

$$v_o = \frac{\epsilon Q_c^2}{A_c (Q_c + Q_s)} \quad (3.7)$$

and the swirl parameter λ may be written as:

$$\lambda = \frac{v_o}{u_o} = \frac{\epsilon A_o Q_c^2}{A_c (Q_c + Q_s)^2} \quad (3.8)$$

For incompressible flow, the sum of the control and supply flows is equal to the exit flow Q_e . Thus, the linearized equations for the incremental changes in velocity due to changes in flow may be written as:

$$\Delta u_o = \frac{1}{2\pi r_o h} \Delta Q_e = k_u \Delta Q_e \quad (3.9)$$

$$\Delta v_o = \frac{\epsilon_o 2Q_{co}}{A_c Q_{eo}} \Delta Q_c - \frac{\epsilon_o Q_{co}^2}{A_c Q_{eo}^2} \Delta Q_e \quad (3.10)$$

$$= k_c \Delta Q_c - k_e \Delta Q_e$$

where

$$k_u = \frac{1}{2\pi r_o h} \quad k_c = \frac{2\epsilon_o Q_{co}}{A_c Q_{eo}} \quad k_e = \frac{\epsilon_o Q_{co}^2}{A_c Q_{eo}^2}$$

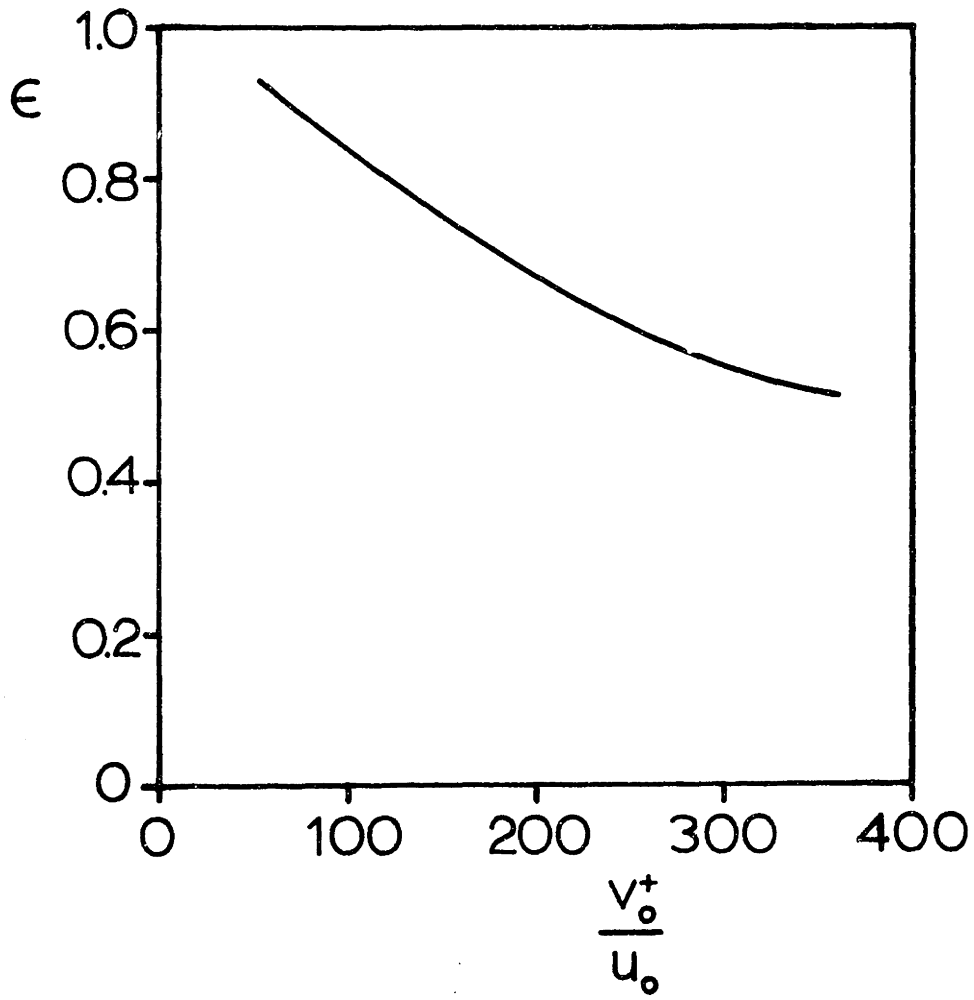


Fig. 3.3 Jet Recovery Factor ϵ

3.4 Main Vortex Region

Chapter 2 presented a distributed system analysis for the dynamic response of the main vortex region. This section presents a lumped system model, in which the values of the dynamic lumped parameters are determined from the distributed system analysis.

A typical distributed dynamic response from the analysis of Chapt. 2 is shown in Fig. 3.4. There are two important aspects of this response which must be represented for any realistic lumped model. They are:

- 1) The time delay associated with the fluid transport of the new conditions, and
- 2) the response as the viscous action between the boundary layer and the core drives the spinning donut to its new state.

These two physical phenomena may be represented in terms of lumped parameters as a pure transportation delay and as a first order lag, as shown also in Fig. 3.4. Specifically, in Laplace transform notation, the response in pressure drop from r_o to r_e due to a change in v_o , with u_o held constant, may be expressed as:

$$\Delta(p_o - p_e) \Big|_{\substack{\Delta v_o \\ \Delta u_o = 0}} = \frac{k_1 e^{-T_1 s}}{1 + T_2 s} \Delta v_o \quad (3.11)$$

where the total pressure drop response consists of two parts:

$$\Delta(p_o - p_e) = \Delta(p_o - p_e) \Big|_{\substack{\Delta v_o \\ \Delta u_o = 0}} + \Delta(p_o - p_e) \Big|_{\substack{\Delta u_o \\ \Delta v_o = 0}} \quad (3.12)$$

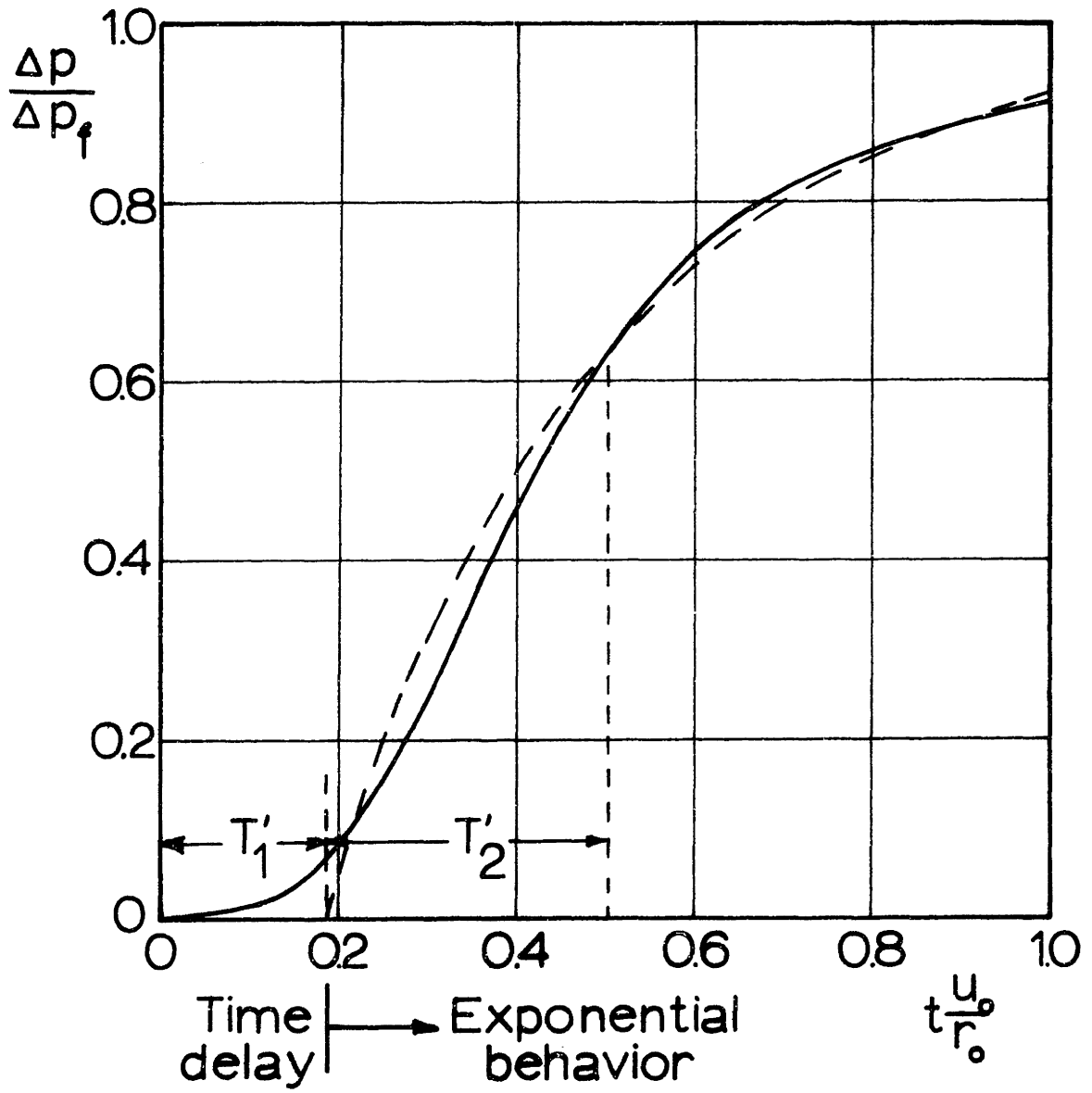


Fig. 3.4 Distributed Response with Lumped Model Response Approximation

and where k_1 represents the steady-state gain $\left. \frac{\partial(p_o - p_e)}{\partial v_o} \right|_0$.

In the non-dimensional time domain, this response is:

$$\left. \Delta(p_o - p_e) \right|_{\substack{\Delta v_o \\ \Delta u_o = 0}} = k_1 \left(1 - e^{-\frac{t' - T'_1}{T'_2}} \right) \delta'(t' - T'_1) \Delta v_o \quad (3.13)$$

where $\delta'(t' - T'_1)$ is the unit step function delayed by a time constant T'_1 and T'_1 and T'_2 are the non-dimensional times $\frac{T'_1 r_o}{u_o}$ and $\frac{T'_2 r_o}{u_o}$.

The lumped approximation to the distributed response is shown in Fig. 3.4, where the values of T'_1 and T'_2 are determined to match the distributed responses in the following manner:

- 1) A tangent is drawn through the point of inflection of the distributed system response, and T'_1 is determined as the zero intercept of the tangent line.
- 2) The value of T'_2 is chosen so that the lumped and distributed responses coincide at $t' = T'_1 + T'_2$, which is the point where the response value is 0.632, which is $1 - e^{-1}$.

As can be seen from Fig. 3.4, this lumped model is a reasonable approximation to the distributed response and as will be shown in Chapter 4 provides reasonable agreement with the experimental data. Thus, it was not felt that a more sophisticated approximation was justified or necessary within the scope of this thesis.

In the main vortex region for operation with high swirl there is also a change in pressure drop due to a change in u_0 . For incompressible flow, a change in radial flow must occur instantaneously throughout the chamber. The change in pressure drop due directly to the changes in radial velocity are negligible. However, changing u_0 changes the circulation distribution due to the different radial momentum at the outer periphery. For instance, a decrease in u_0 decreases the region of potential vortex flow, where the circulation is constant, as shown in Fig. 3.5. The radial flow is forced into the boundary layers at a larger radius due to the decreased radial momentum of the fluid introduced at the outer periphery.

The experimental results discussed in Chap. 4 have shown that the time required to establish the effects due to this change is small compared with T_2 in all of the cases considered, and therefore this time is neglected in this study. Thus, the full dynamic lumped expression for the main vortex chamber may be written as:

$$\Delta(p_o - p_e) = \frac{k_1 e^{-T_1 s}}{1 + T_2 s} \Delta v_o + k_2 \Delta u_o \quad (3.14)$$

The method of calculating k_1 and k_2 will be demonstrated below.

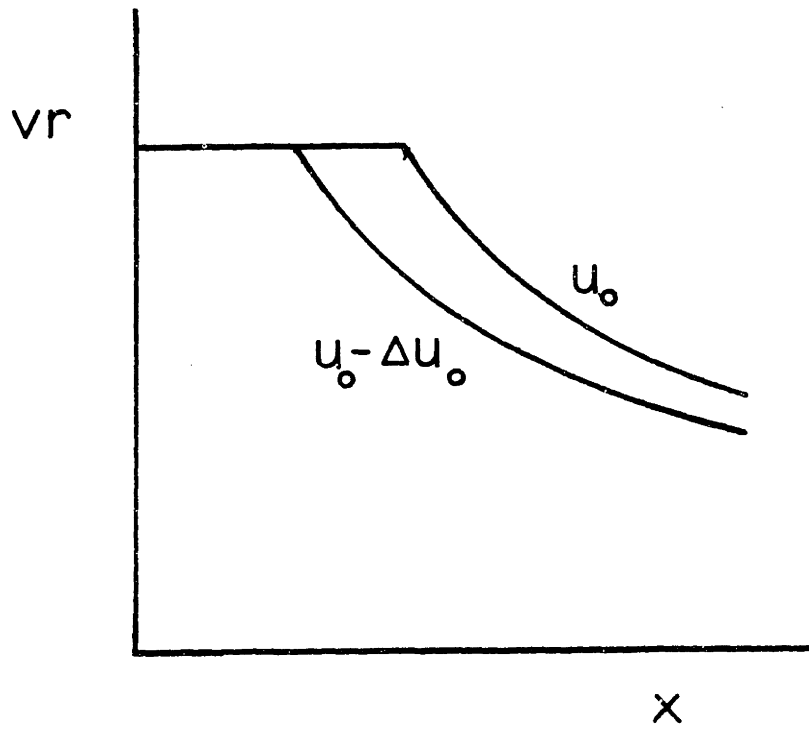


Fig. 3.5 Change in Circulation Distribution for Change in u_0

3.5 Exit Port

Since the exit port is small compared with the main chamber, just as for the supply and control ports, and the fluid velocities are higher than the vortex chamber velocities, this port is also treated as a static resistance. Thus, the exit port equation is:

$$\Delta Q_e = \frac{\Delta p_e - \Delta p_c}{R_e} \quad (3.15)$$

3.6 Total Lumped Model

For the maximum efficiency in a vortex valve, as shown in Reference 30, the supply port resistance should be small, so that its pressure drop is small compared to the pressure drop across the valve chamber and exit port. If this resistance is small, as it should be, then a simplification of the port equations is obtained, i.e. p_o may be assumed constant and equal to p_s . Thus, for the case of constant supply and ambient pressures, p_s and p_a , the flow equations reduce to:

$$\begin{aligned} \Delta Q_c &= \frac{\Delta p_c}{R_c} \\ \Delta Q_e &= \frac{\Delta p_e}{R_e} \end{aligned} \quad (3.16)$$

$$\Delta Q_s = \Delta Q_e - \Delta Q_c$$

assuming incompressible flow.

The change in pressure drop across the valve is a function of the outer periphery velocities as follows:

$$-\Delta p_e = \frac{k_1 e^{-T_1 s}}{1 + T_2 s} \Delta v_o + k_2 \Delta u_o \quad (3.17)$$

The velocity flow relations are given by Eqs. (3.9) and (3.10), so that the change in chamber pressure drop may be written in terms of flows as follows:

$$\begin{aligned} -\Delta p_e &= \frac{k_1 e^{-T_1 s}}{1 + T_2 s} (k_c \Delta Q_c - k_e \Delta Q_e) + k_2 k_u \Delta Q_e \\ &= G_1(s) \Delta Q_c + G_2(s) \Delta Q_e = -R_e \Delta Q_e \end{aligned} \quad (3.18)$$

Thus, the transfer functions for changes in flows at each valve port due to changes in the control port pressure with the supply and exit pressures held constant are given in Table 3.1.

The block diagram, which explicitly indicates the relationship between the input control pressure and the output system flows is shown in Fig. 3.6.

These equations may be solved to obtain the valve supply and exit flow responses to a sinusoidal input by letting $s \rightarrow j\omega$ in the equations, as also shown in Table 3.1. A typical frequency response plot is shown in Fig. 3.7, with the dynamic gains normalized with respect to the static gains. This analytical model is compared with the experimental frequency and step response data in Chap. 4.

Table 3.1

| <u>Output</u> | <u>Laplace Notation</u> | <u>Frequency Notation</u> |
|---------------------------------|--|----------------------------------|
| $\frac{\Delta Q_c}{\Delta p_c}$ | $\frac{1}{R_c}$ | $\frac{1}{R_c}$ |
| $\frac{\Delta Q_s}{\Delta p_c}$ | $-\frac{G_1(s) + G_2(s) + R_e}{R_c(R_e + G_2(s))}$ | $-\frac{(A-C) + j(B-D)}{C + jD}$ |
| $\frac{\Delta Q_e}{\Delta p_e}$ | $-\frac{G_1(s)}{R_c(R_e + G_2(s))}$ | $-\frac{A + jB}{C + jD}$ |

where

$$A = \frac{k_1 k_c}{R_c} \cos \omega T_1$$

$$B = -\frac{k_1 k_c}{R_c} \sin \omega T_1$$

$$C = -k_1 k_e \cos \omega T_1 + (R_e + k_2 k_u)$$

$$D = k_1 k_e \sin \omega T_1 + T_2 \omega (R_e + k_2 k_u)$$

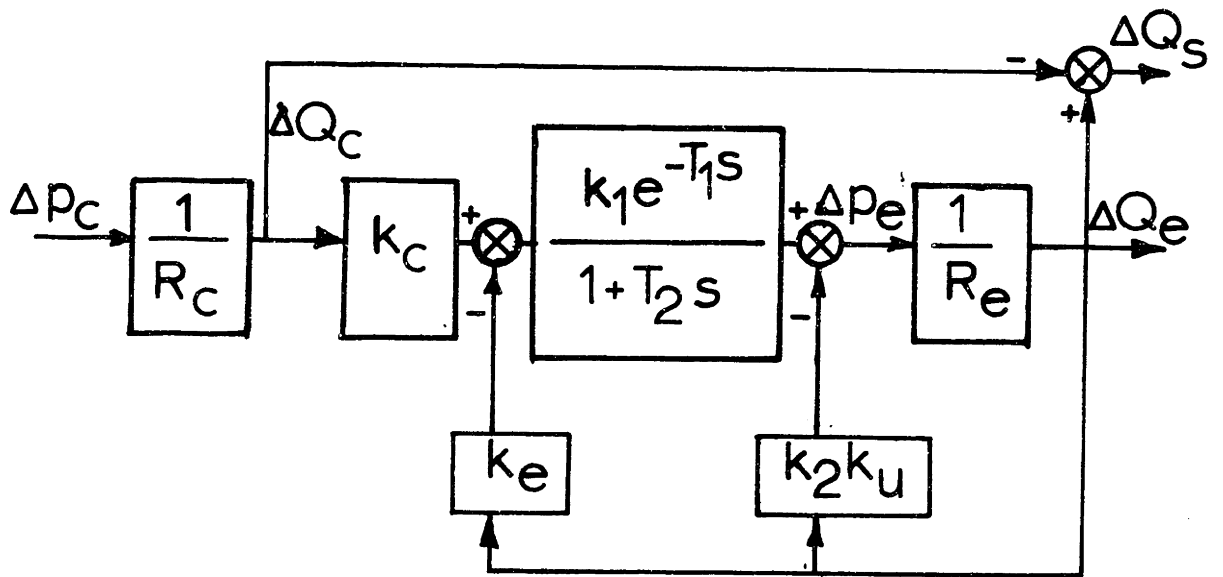


Fig. 3.6 Lumped Model Block Diagram

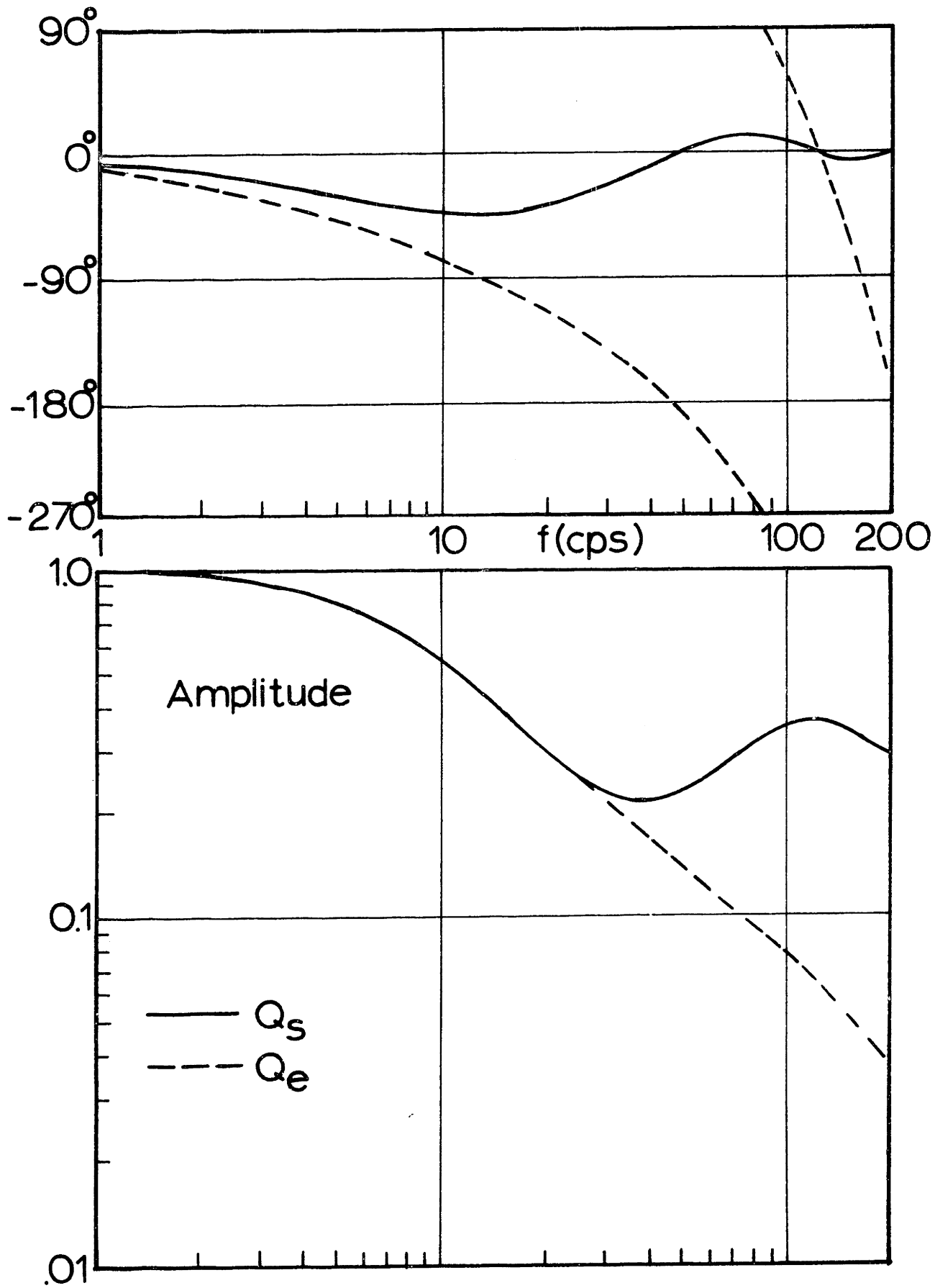


Fig. 3.7 Typical Lumped Model Frequency Response

Thus, a lumped linearized model has been developed which may be used by a fluid control circuit designer to predict the dynamic response of a vortex valve in a circuit. This model has been based on the two fundamental physical phenomena of the vortex chamber, the time delay due to the transport effects and the time lag due to the viscous effects.

3.7 Calculation of k_1 , k_2 and R_e

The gains k_1 , k_2 , and R_e may be calculated by considering the pressure gradient described by Eq. 2.57 for $\lambda > 10$, which may be written as:

$$\frac{1}{\lambda^2} \frac{dP}{dx} = - \frac{\Gamma^2}{(1-x)^3} \quad (3.19)$$

In Reference 29, it has been shown that the Γ distribution is essentially a function only of the parameter BLC^* , so that P/λ^2 is a function only of BLC^* at any value of x , where:

$$BLC^* = \frac{2r_o}{h} \frac{v_o}{u_o} \frac{f}{\left(\frac{\rho u_o h}{2\mu} \right)^{1/4}} \quad (3.20)$$

The relationship of P/λ^2 and BLC^* is shown in Fig. 3.8. Thus, the pressure distribution and specifically the pressure at the exit radius may be found from this graph, once BLC^* has been calculated, since

$$P_o - P_e = \frac{P}{\lambda^2} \Big|_{x_e} (\rho v_o^2) \quad (3.21)$$

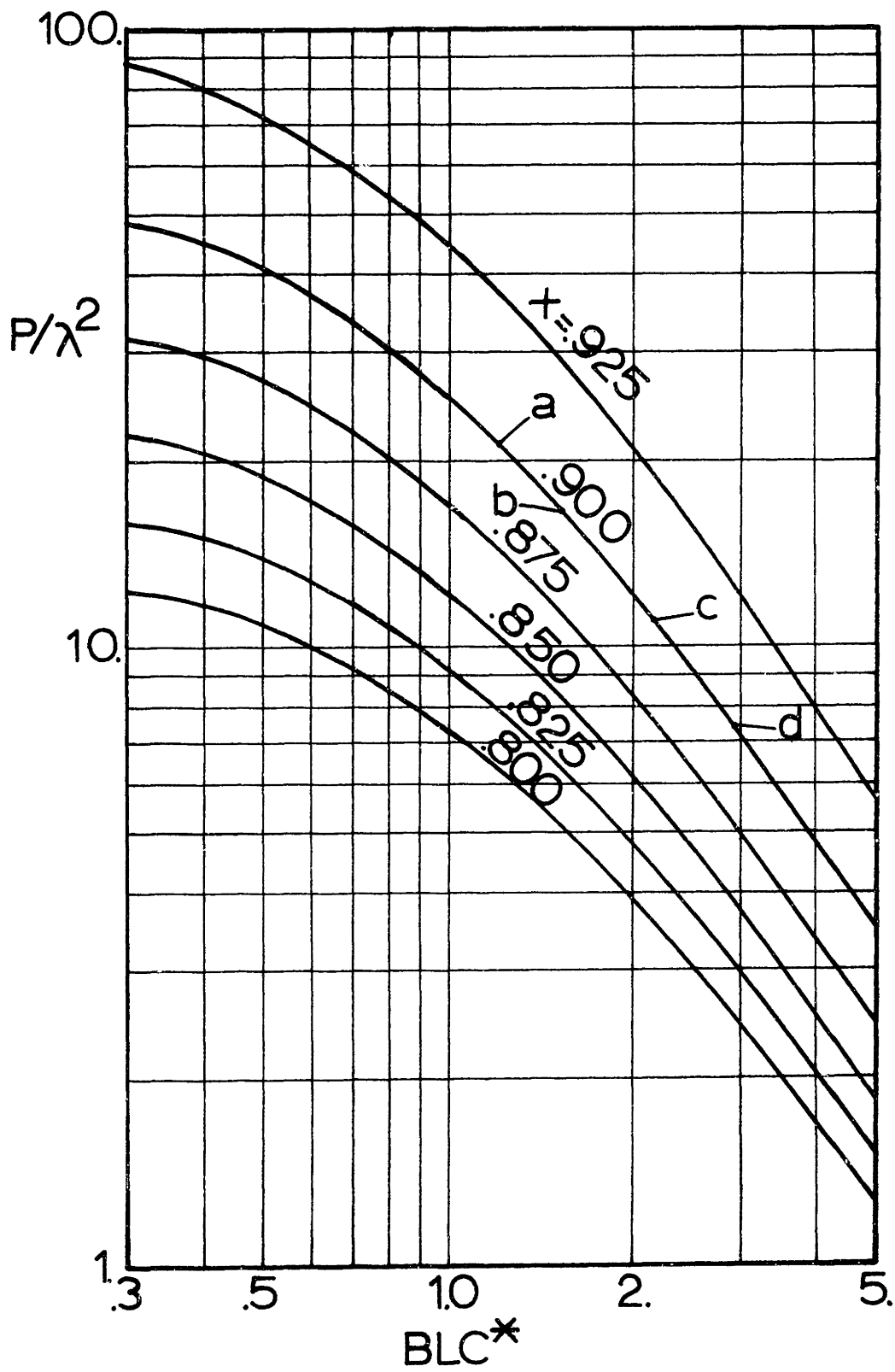


Fig. 3.8 Plot of P/λ^2 vs. BLC^*

Thus, by calculating changes in BLC^* for changes in the appropriate flows and velocities, the changes in pressures and thus the gains may be calculated.

For the calculation of the gains, it is useful to break the response up into three parts:

- 1) The control flow changes, changing the outer periphery tangential velocity. The change in pressure drop due to this change, maintaining a constant u_o , may be calculated.
- 2) The supply flow changes due to the change in control flow. The amount of this change is determined by the steady state characteristic, and its effects on the pressure drop across the valve may also be calculated.
- 3) The tangential velocity, v_o , changes due to the change in supply flow, which cause another change in the pressure drop across the vortex chamber.

The gain k_1 is associated with steps 1 and 3, while the gain k_2 is associated with step 2. Thus, consider the points in Table 3.2, which are the end points of these three processes for case D of Chap. 4.

Table 3.2

| Point | a → 1 → | b → 2 → | c → 3 → | d |
|---------------|---------------------------------------|---------------------------------------|-------------------------------------|---------------------------------------|
| Q_c | 17.9 $\frac{\text{in}^3}{\text{sec}}$ | 20.5 $\frac{\text{in}^3}{\text{sec}}$ | | 20.5 $\frac{\text{in}^3}{\text{sec}}$ |
| Q_e | 57.4 $\frac{\text{in}^3}{\text{sec}}$ | 57.4 $\frac{\text{in}^3}{\text{sec}}$ | | 43.6 $\frac{\text{in}^3}{\text{sec}}$ |
| u_o | 29.2 $\frac{\text{in}}{\text{sec}}$ | 29.2 $\frac{\text{in}}{\text{sec}}$ | 22.2 $\frac{\text{in}}{\text{sec}}$ | 22.2 $\frac{\text{in}}{\text{sec}}$ |
| v_o | 592 $\frac{\text{in}}{\text{sec}}$ | 756 $\frac{\text{in}}{\text{sec}}$ | 756 $\frac{\text{in}}{\text{sec}}$ | 1022 $\frac{\text{in}}{\text{sec}}$ |
| BLC* | 1.208 | 1.539 | 2.175 | 2.935 |
| P/λ^2 | 21.3 | 16.7 | 11.1 | 7.5 |
| $(p_o - p_e)$ | .836 psi | 1.070 psi | 0.711 psi | 0.879 psi |

Thus, k_1 can be calculated as:

$$\begin{aligned}
 k_1 &= \frac{\Delta(p_o - p_e)}{\Delta v_o} = \frac{(1.070 - 0.836) + (.879 - .711)}{(756 - 592) + (1022 - 756)} \\
 &= \frac{.234 + .168}{430} = \frac{.402}{430} = 9.34(10)^{-4} \frac{\text{lb}_f \text{sec}}{\text{in}^3}
 \end{aligned}$$

and

$$k_2 = \frac{\Delta(p_o - p_e)}{\Delta u_o} = \frac{0.711 - 1.070}{22.2 - 29.2} = \frac{-.359}{-7.0} = 5.13(10)^{-2} \frac{\text{lb}_f \text{sec}}{\text{in}^3}$$

and

$$R_e = \frac{\Delta p_e}{\Delta Q_e} = \frac{0.043}{13.9} = 3.09(10)^{-3} \frac{\text{lb}_f \text{sec}}{\text{in}^5}$$

Chapter 4

EXPERIMENTAL RESULTS

4.1 Objectives of the Experiments

The objectives of the experimental work were to provide guidance in formulating a dynamic model for the vortex valve and to provide verification of that model once it had been formulated. To accomplish these objectives, both step response and small signal sinusoidal frequency tests were made using low pressure air, along with the dynamic flow visualization already discussed in Chapter 2.

4.2 Apparatus

The basic experimental vortex amplifier used in this study is shown disassembled in Fig. 4.1. It consists of five circular plates bolted together to form the chamber and its ports. The top plate contains the ducts to distribute the control ports. The second plate separates the control flow passages from the valve chamber. The third and fourth plates form the vortex chamber itself as well as containing the supply and control ports. The fifth plate contains the exit port. There is also a sixth plate which fits between the third and fourth plates to double the height of the chamber.

The diameter of the vortex chamber is 2.5 inches. The supply ports consist of four slots, each 0.10 inch high by 0.75 inches wide. The four control ports are each 0.031 inches by 0.079 inches. Two bottom plates may be used, one with a 0.25 inch diameter exit and the

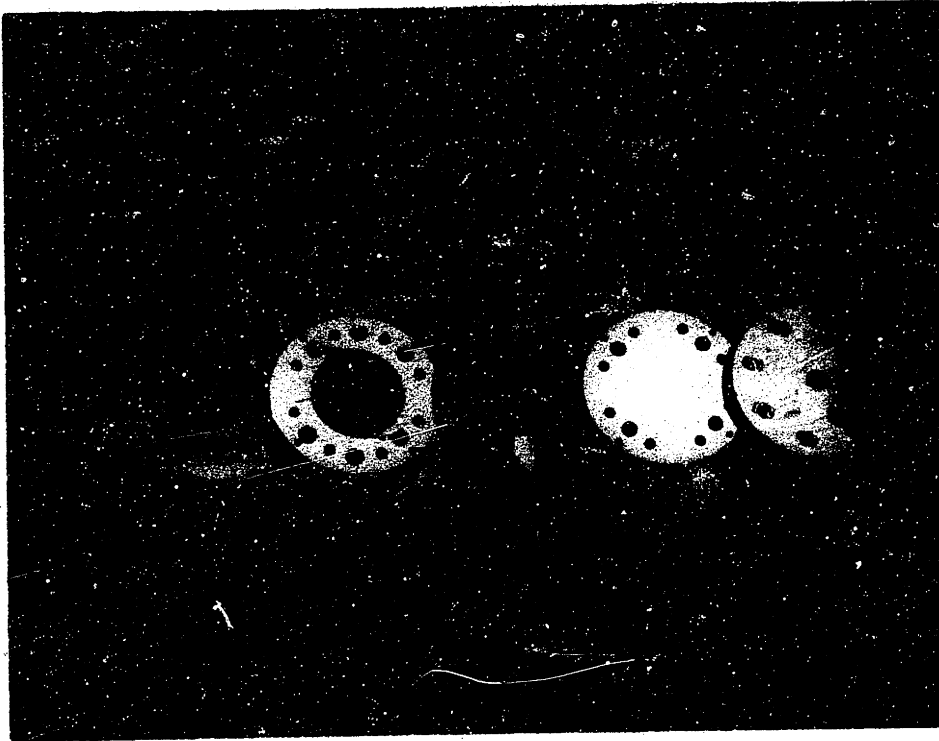


Fig. 4.1 Disassembled Vortex Valve

other with a 0.188 inch diameter exit. The height of the chamber may be adjusted to either 0.25 inches or 0.50 inches with the spacer. The outer diameter of the plates is 5 inches.

The two end plates are grooved for O-rings to seal the valve in a 5 inch clear acrylic tube such that the supply ports mate with holes in the tube which passes to the supply chamber. The supply chamber is kept at constant pressure by a pressure regulator. This arrangement is shown in the schematic drawing, Fig. 4.2.

For the experiments, the control pressure signal was monitored by a Kistler piezoelectric pressure transducer. The control, supply, and exit flows were inferred from velocity measurements using Disa hot-wire probes with a constant temperature anemometer servo. The flow measurements were obtained by calibrating the output of the constant temperature anemometer for static flow conditions of the valve, and assuming that the dynamic and static velocity profiles were similar, since the dynamic changes in the flow were small compared with the quiescent flow, and there was no reverse flow. This method provides about the only reasonable method for measuring dynamic flows in the frequency range of interest for this study.

The dynamic input signal to the valve was provided by a flapper nozzle valve arrangement, shown schematically in Fig. 4.3. The flapper was a rotating disc, driven by a variable speed D.C. motor. This apparatus is shown in Fig. 4.4.

By using radial slots on the rotating disc which were slightly narrower than the nozzle, so that the effective area of the nozzle was constantly changing, a reasonable sinusoidal pressure wave was

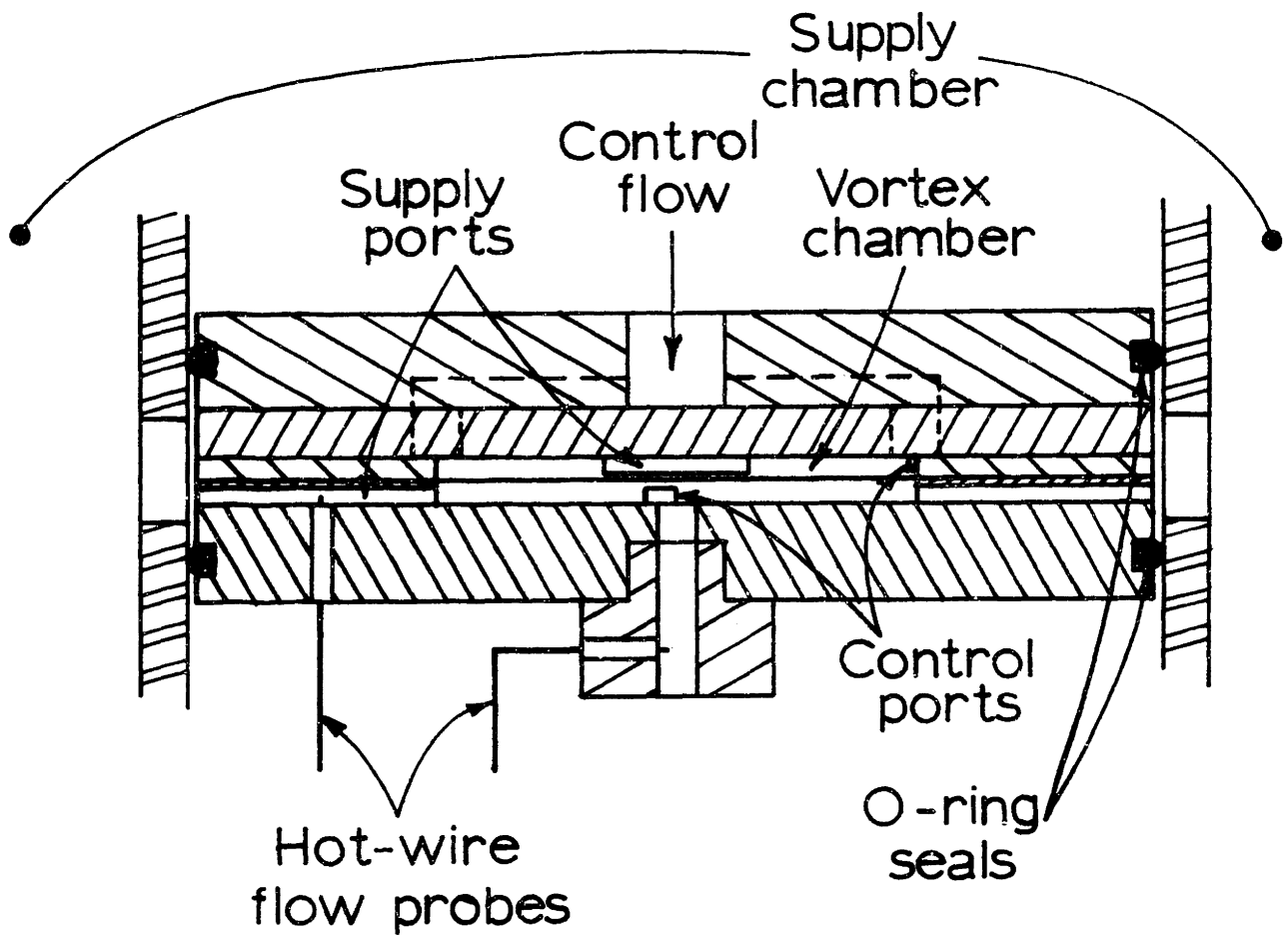


Fig. 4.2 Schematic of Experimental Apparatus

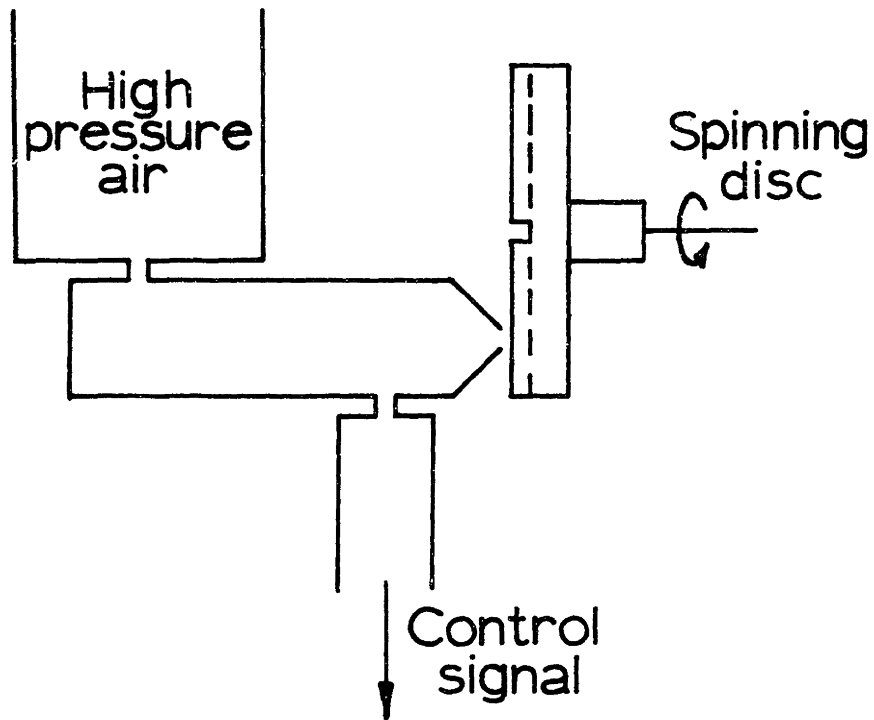


Fig. 4.3 Schematic of Signal Generator



Fig. 4.4 Signal Generating Apparatus

generated. Using another disc with the nozzle open for half a revolution and then closed for the other half of the disc revolution, the opening and closing times are negligible compared with the open and closed times, providing a reasonable square wave for step response tests.

The variable speed D.C. motor had an attached 24:1 gear reduction unit, so that the changing from the low to high speed shaft and using the speed controller, the sinusoidal signal could be varied over a range of frequencies from 1 cps to over 500 cps.

4.3 Experimental Valve Configurations

As discussed in Chapter 5, the analytical model predicts that the two major parameters affecting the dynamic time constants are the internal flow field, as characterized by the parameters λ and BLC, and the ratio of the height to the outer periphery radius. Thus, several different tests were run to confirm the predicted effects of these changes.

For the comparison of experimental and theoretical responses, four specific different configurations of the experimental vortex valve are considered.

The first configuration, designated A, is considered the basic configuration. The significant dimensions and ratios are as follows:

$$\begin{array}{ll} r_o = 1.25 \text{ in.} & A_c/A_c = .356 \\ r_e = .094 \text{ in.} & p_s = 30 \text{ in. H}_2\text{O} \\ h = 0.25 \text{ in.} & A_s/A_e = 10.9 \end{array}$$

Configuration B has the same physical dimensions as configuration A, but the supply pressure used was 80 inches of water, so that the basic flow rate through the valve is higher and the transport dynamics are faster.

Configuration C has a supply pressure of 30 inches of water, as the basic valve does, but the height is 0.50 inches, to verify the effect of height on the dynamic response.

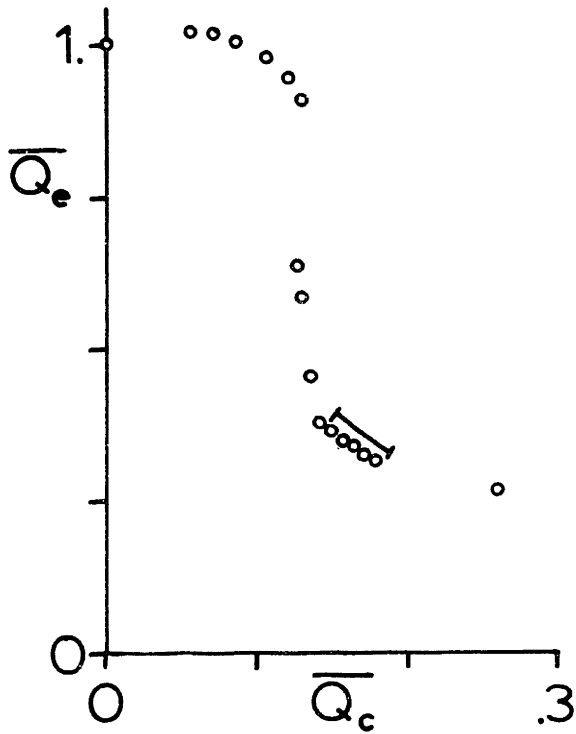
Configuration D is identical with the basic configuration with the exception of the exit radius, which is 0.25 inches. This also decreases the A_c/A_e ratio to .20.

The non-dimensional, steady state valve characteristics of these four configurations are shown in Fig. 4.5. The dynamic data for one representative operating point will be presented, and these operating points are also indicated in the figure.

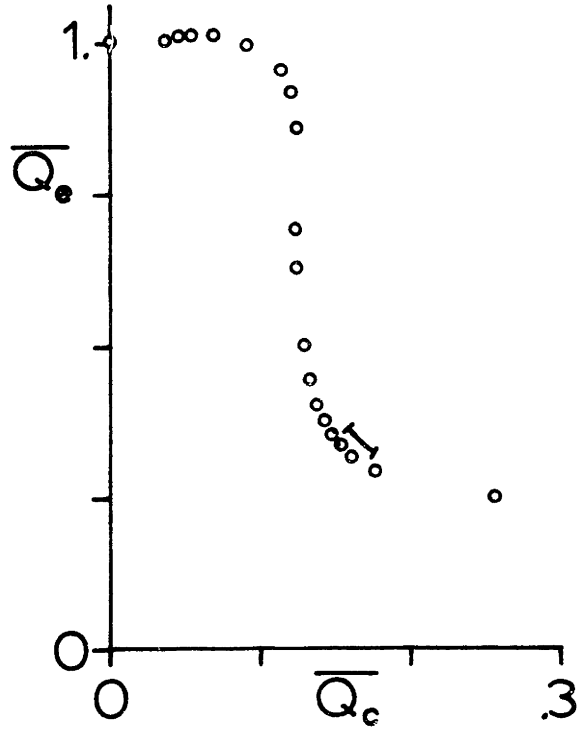
4.4 Calculation of Theoretical Responses

In order to calculate analytical step and frequency responses, it is necessary to find the dynamic time parameters and the gains of the valve at the operating point. This section will give a fuller explanation of the calculation of the gains for case D discussed briefly in Chapter 3, and will list these parameters for the other cases.

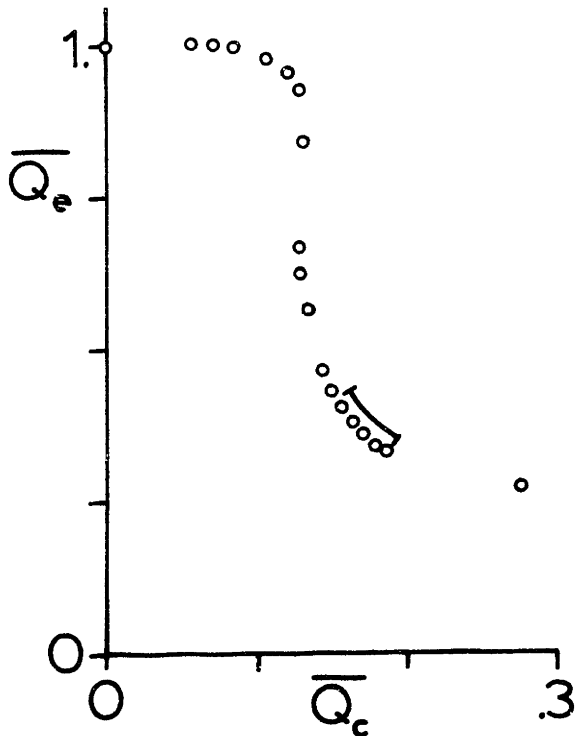
Consider the two end points of the range of operation indicated for case D in Fig. 4.5. These are the two end points, a and d, of Fig. 3.8 and Table 3.2. The two intermediate points, b and c, are calculated from these points. Point b is the point which



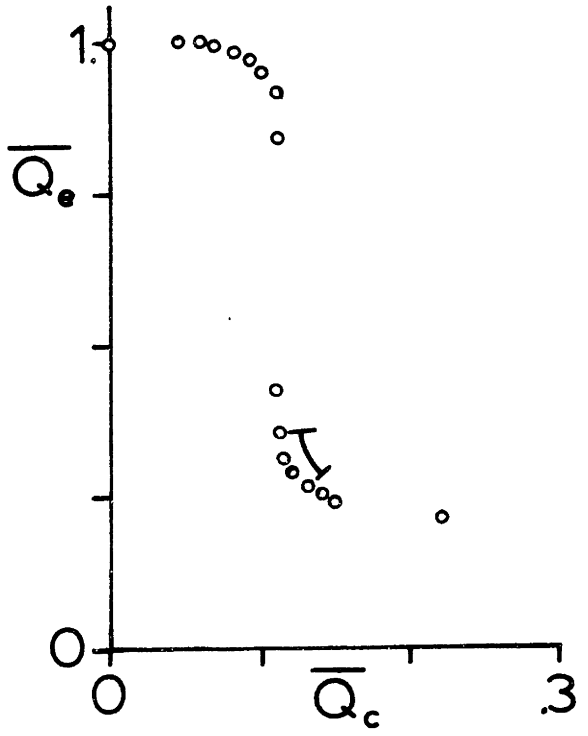
a) Case A



b) Case B



c) Case C



d) Case D

Fig. 4.5 Experimental Steady State Characteristics

corresponds to changing the control flow Q_c and the tangential velocity v_o without changing u_o and Q_e . Point c is the point which corresponds to changing Q_e and u_o without considering the effect of Q_e in changing v_o . It should be noted that these intermediate conditions do not occur in the actual valve, since all three changes are taking place simultaneously. However, they are useful conceptual points for the calculation of the gains, as discussed in Chapter 3.

The gain k_1 is calculated from the changes from a to b and from c to d, while the gain k_2 is calculated from the change from b to c. The exit resistance R_e is calculated from the entire change, a to d. The other three gains, k_c , k_e , and k_u may be calculated directly from the difference relationships:

$$k_c = \frac{\Delta v_o}{\Delta Q_c} = \frac{756 - 592}{20.5 - 17.9} = \frac{164}{2.6} = 63.1/\text{in}^2 \quad (4.1)$$

$$k_e = -\frac{\Delta v_o}{\Delta Q_e} = \frac{1022 - 756}{57.4 - 43.6} = \frac{266}{13.8} = 19.3/\text{in}^2 \quad (4.2)$$

$$k_u = \frac{\Delta u_o}{\Delta Q_e} = \frac{7.0}{13.8} = .507/\text{in}^2 \quad (4.3)$$

The dynamic time constants T_1 and T_2 are solved by the computer program of Chapter 3 by considering the change from a to b. These two non-dimensional times are .181 and .321, which when dimensionalized by the time factor $\frac{r_o}{u_o} = \frac{1.25}{29.2} \text{ sec.} = .0428 \text{ sec.}$ become $T_1 = .0078 \text{ sec.}$ and $T_2 = .0138 \text{ sec.}$

The gains and time constants for the four cases are shown in Table 4.1. The gains G_{os} and G_{oe} are the steady state flow gains $\frac{\Delta Q_s}{\Delta Q_c}$ and $\frac{\Delta Q_e}{\Delta Q_c}$, respectively.

4.5 Step Responses

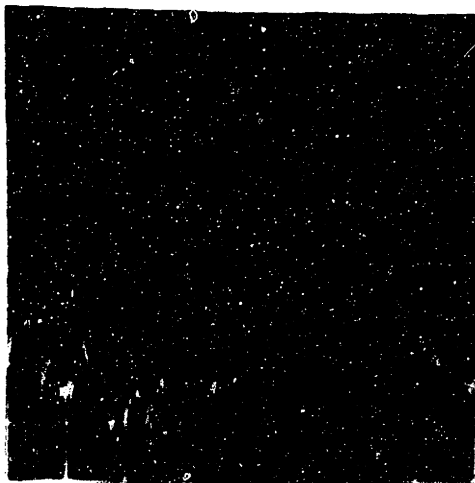
Once the lumped system parameters had been found, the analytical step and frequency responses were calculated. The experimental step responses of the change in exit flow to a step change in input control pressure are shown in Fig. 4.6, and the analytical and experimental step responses are compared in Fig. 4.7.

As can be seen, the analytical and experimental results agree reasonably well, to the extent possible considering the noisy experimental response. This noise, which was also observed in steady state operation, was due to local turbulence in the vicinity of the hot wire, rather than to overall flow changes. In order to get a better comparison between analysis and experiment, frequency responses were taken.

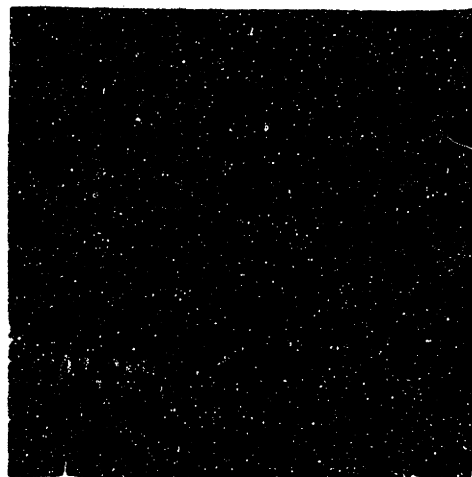
The step response of the entire valve depends upon the two time constants, T_1 and T_2 , and upon the steady state gain at the operating point. The time delay T_1 of the vortex flow remains a time delay in the total vortex valve. The rise time of the vortex valve response is proportional to T_2 , for a given value of gain. The steady state gain is a measure of the extent to which supply flow changes are due to the positive feedback effects of the supply flow on itself compared with the changes due directly to the control flow

Table 4.1

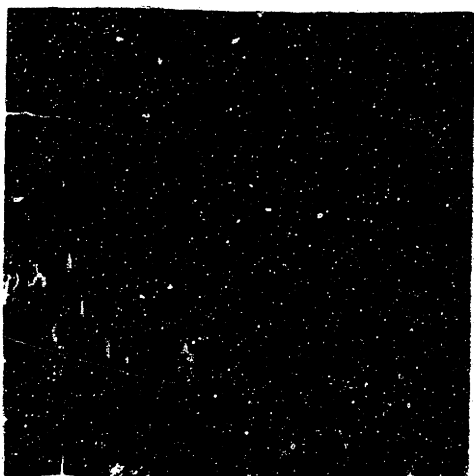
| <u>Case</u> | A | B | C | D |
|---|-----------------|------------------|------------------|-----------------|
| $k_1 \left(\frac{\text{lb}_f \text{sec}}{\text{in}^3} \right)$ | $8.25(10)^{-4}$ | $13.17(10)^{-4}$ | $9.67(10)^{-4}$ | $9.34(10)^{-4}$ |
| $k_2 \left(\frac{\text{lb}_f \text{sec}}{\text{in}^3} \right)$ | $9.54(10)^{-2}$ | $1.68(10)^{-1}$ | $1.74(10)^{-1}$ | $5.13(10)^{-2}$ |
| $k_c (\text{in}^{-2})$ | 78.6 | 78.8 | 64.6 | 63.1 |
| $k_e (\text{in}^{-2})$ | 2.45 | 20.2 | 10.94 | 19.3 |
| $k_u (\text{in}^{-2})$ | .507 | .507 | .254 | .507 |
| $R_e \left(\frac{\text{lb}_f \text{sec}}{\text{in}^5} \right)$ | $1.74(10)^{-3}$ | $-9.47(10)^{-3}$ | $-6.79(10)^{-3}$ | $3.09(10)^{-3}$ |
| $T_1 (\text{sec})$ | .0094 | .0061 | .0162 | .0078 |
| $T_2 (\text{sec})$ | .0232 | .0135 | .0446 | .0138 |
| $\frac{T_1 u_o}{r_o}$ | .147 | .153 | .139 | .181 |
| $\frac{T_2 u_o}{r_o}$ | .349 | .336 | .381 | .321 |
| G_{os} | -2.35 | -3.12 | -3.33 | -6.30 |
| G_{oe} | -1.35 | -2.12 | -2.33 | -5.30 |



a) Case A



b) Case B



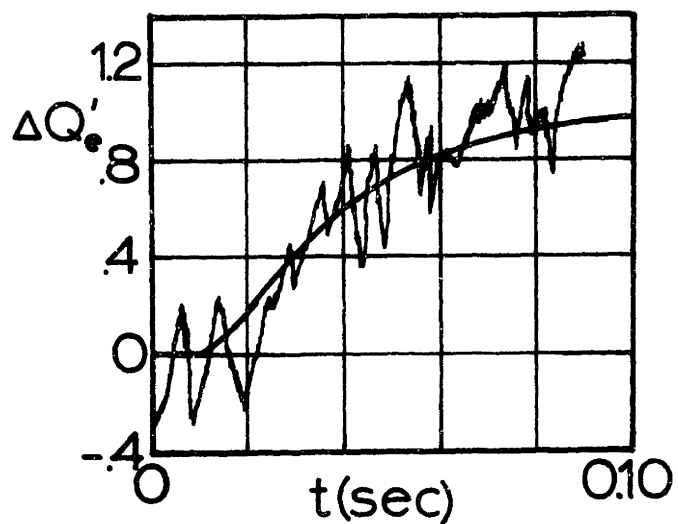
c) Case C



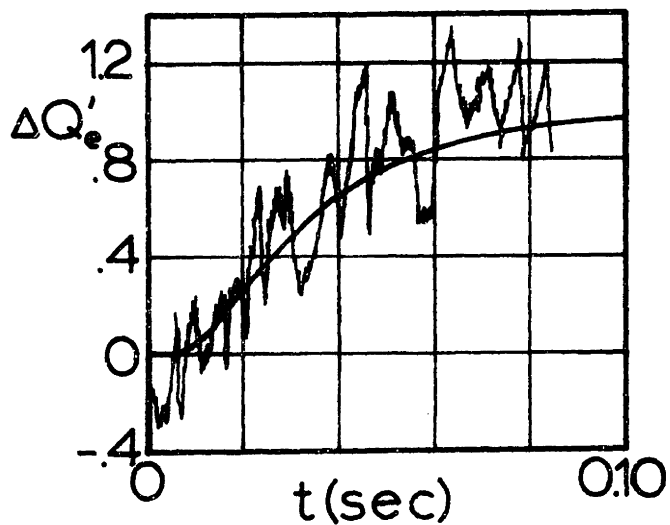
d) Case D

20 msec/cm. for all responses

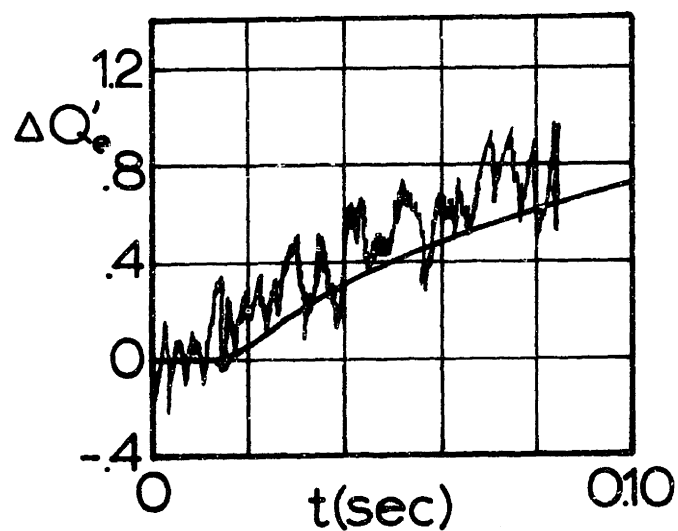
Fig. 4.6 Small Signal Step Responses



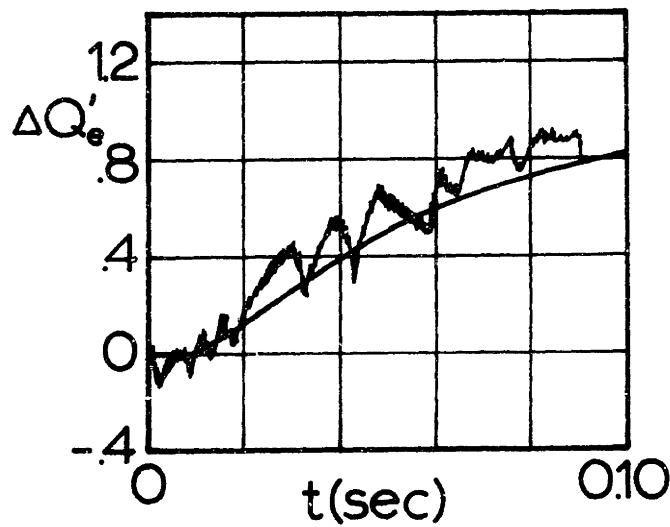
a) Case A



b) Case B



c) Case C



d) Case D

Fig. 4.7 Comparison of Theoretical and Experimental Step Responses

changes. Thus, a valve with a higher gain will be slower, since more of the response will be due to the positive feedback effect. This can be thought of conceptually by considering increments of change in flow, each taking about the same time to occur. Thus, if the initial increment due to the control flow change is a large portion of the total change, fewer increments due to the supply flow feedback will be needed, and the response will be faster.

These effects are illustrated in Fig. 4.7. Thus, the responses of A and B are similar, since the shorter T_2 of case B is compensated by the increase in gain. Case C is much slower because of its much larger T_2 , while D is slower because of its higher gain.

4.6 Frequency Response

In order to eliminate the turbulent noise from the flow measurement of the sinusoidal frequency response, a Fourier decomposition technique was used.

The basic concept of the Fourier decomposition is shown in Fig. 4.8. The input signal is $\sin \omega t$, and $\cos \omega t$ is also available. The output of the system is represented by $\alpha \sin (\omega t + \phi) + w(t)$, where $w(t)$ represents the random noise and harmonic frequency output component. Using geometric identities, the output may be written as

$$A \sin \omega t + B \cos \omega t + w(t) \quad (4.4)$$

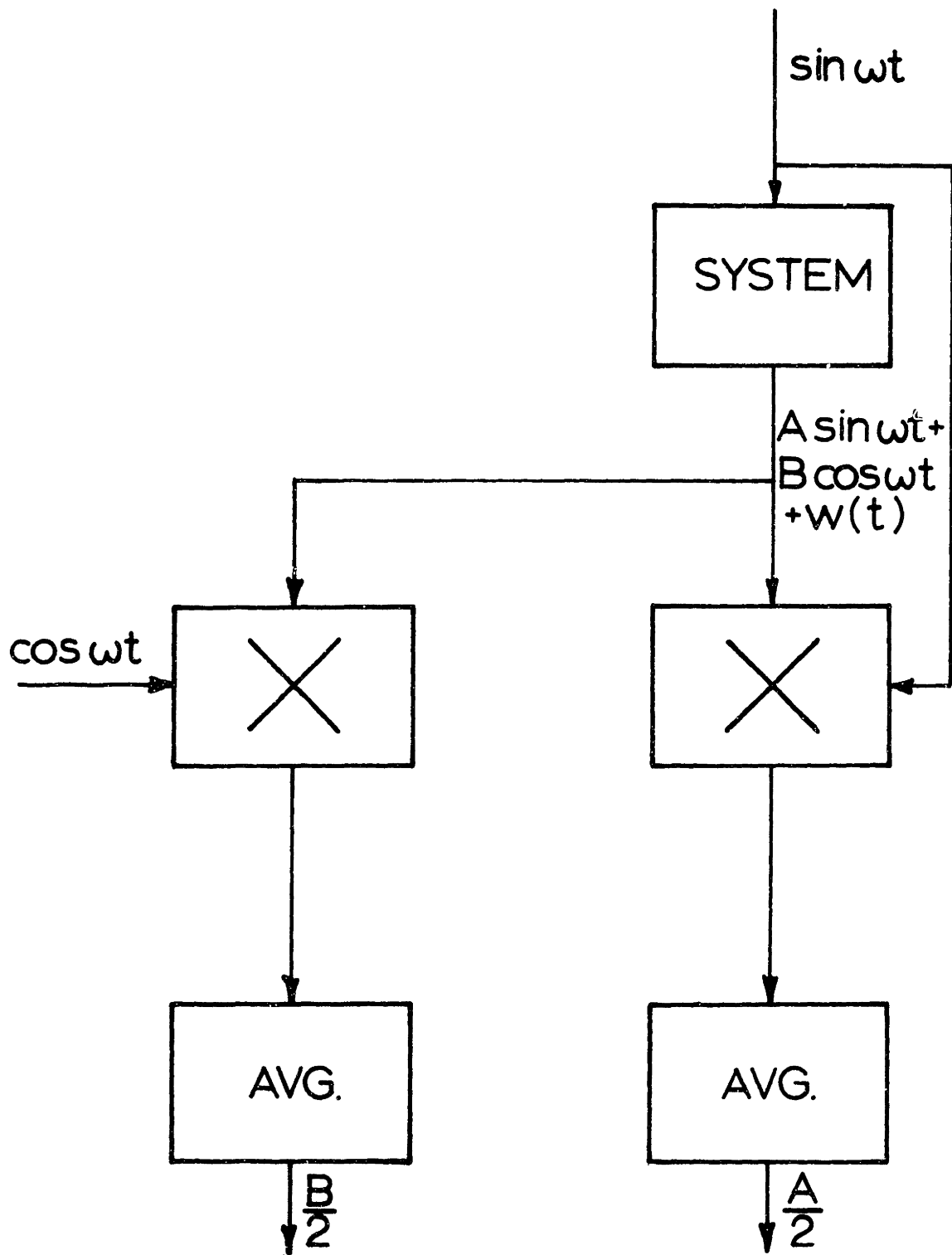


Fig. 4.8 Block Diagram of Frequency Response Fourier Decomposition

where

$$A = \alpha \cos \phi$$

$$B = \alpha \sin \phi$$

The output is multiplied by the original sine and cosine signals, then integrated and averaged over an integral number of cycles of the sinusoid, as follows:

$$\frac{1}{2N\pi} \int_0^{2N\pi} \sin \omega t (A \sin \omega t + B \cos \omega t + w(t)) dt = \frac{A}{2} \quad (4.5)$$

$$\frac{1}{2N\pi} \int_0^{2N\pi} \cos \omega t (A \sin \omega t + B \cos \omega t + w(t)) dt = \frac{B}{2} \quad (4.6)$$

From these averages, the amplitude ratio α may be found as:

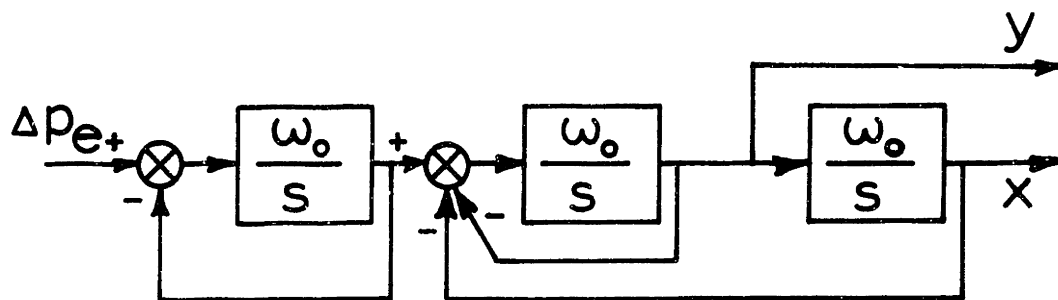
$$\alpha = \sqrt{A^2 + B^2} \quad (4.7)$$

and the phase shift ϕ is simply:

$$\phi = \tan^{-1} \frac{B}{A} \quad (4.8)$$

In practice, the averaging is performed by first order lag networks with time constants much greater than the period of the sinusoid.

In the experimental system a third order Butterworth filter operating at its break frequency, as shown in Fig. 4.9, was used to provide a sine and cosine which were out of phase with the input pressure by a constant angle, and which could be used for the Fourier decomposition.



Note: For ω_0 equal to the fundamental frequency of Δp_{e+} , x and y are equal amplitude sine and cosine.

Fig. 4.9 Butterworth Filter for Pressure Signal

The four analytical and experimental frequency responses are shown in Figs. 4.10 - 4.13. The responses for the supply and exit flows are shown, each normalized with respect to its steady state gain. The control flow response is not shown, since for the frequency range of interest, it essentially followed the control pressure, as predicted by the analysis. The phase angles are plotted as zero in the steady state, although since the gain of the valve is negative, the supply and exit flow changes are opposite in sign to the control pressure signal.

Consider first the characteristics which are common to all four of the responses. The exit flow response shows a steadily decreasing amplitude response, accompanied by a steadily increasing phase lag. The decreasing amplitude response is due to the constantly decreasing time available for the spinning donut to change conditions during each cycle. The increasing phase lag is due to the transportation delay, which has a phase lag of $T_1\omega$.

The supply flow response is completely different. Since the supply resistance is negligible, the supply flow is essentially just the difference between the exit and control flows. Thus, as the exit flow changes become small, the supply flow amplitude becomes equal to the control flow, and opposite in sign. These conditions are represented by an amplitude asymptote equal to the inverse of the steady state gain, and a phase asymptote of zero degrees. The peaks and valleys in the supply amplitude response occur as the exit response is in phase or out of phase with the control flow.

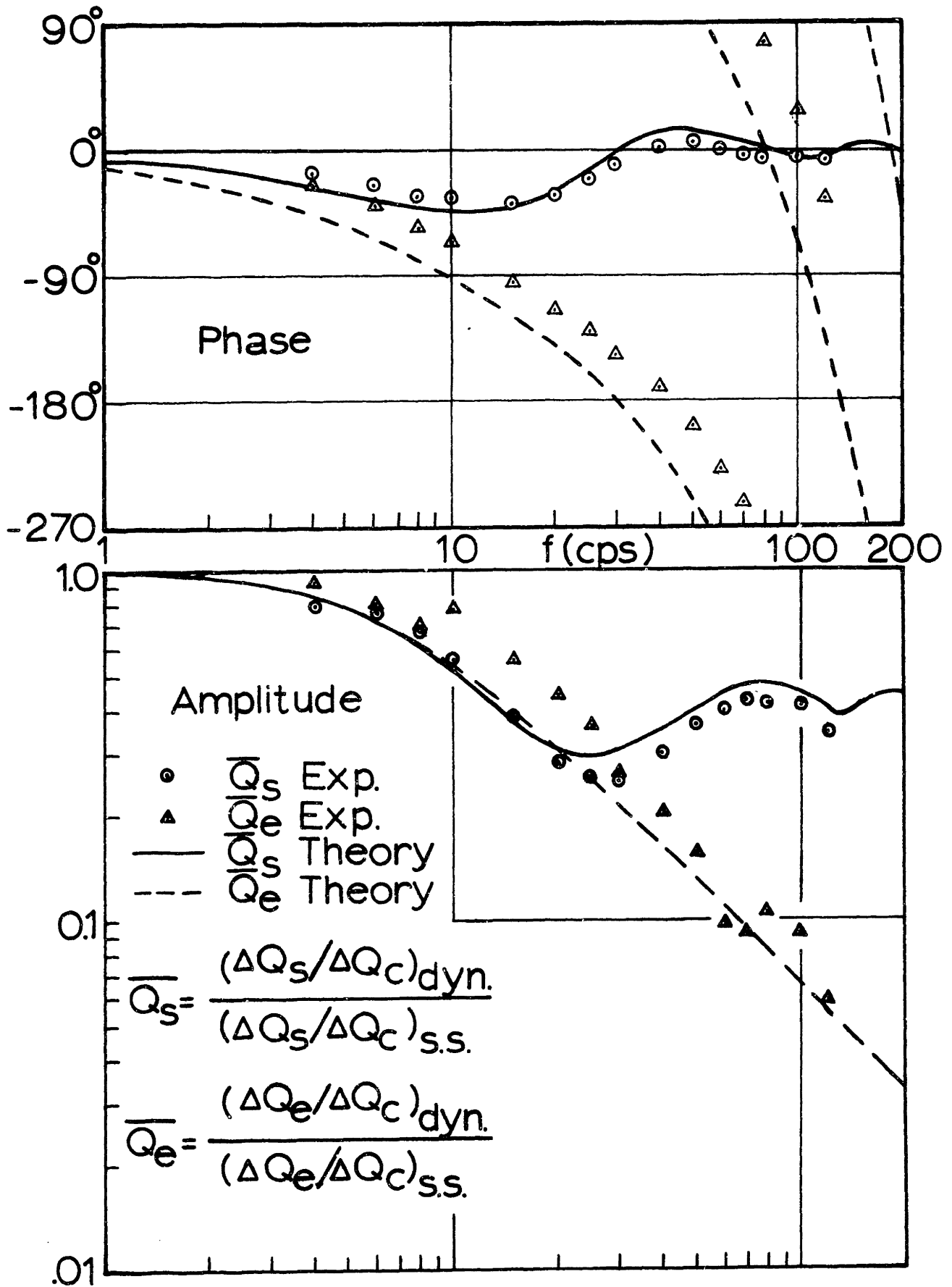


Fig. 4.10 Theoretical and Experimental Frequency Responses - Case A

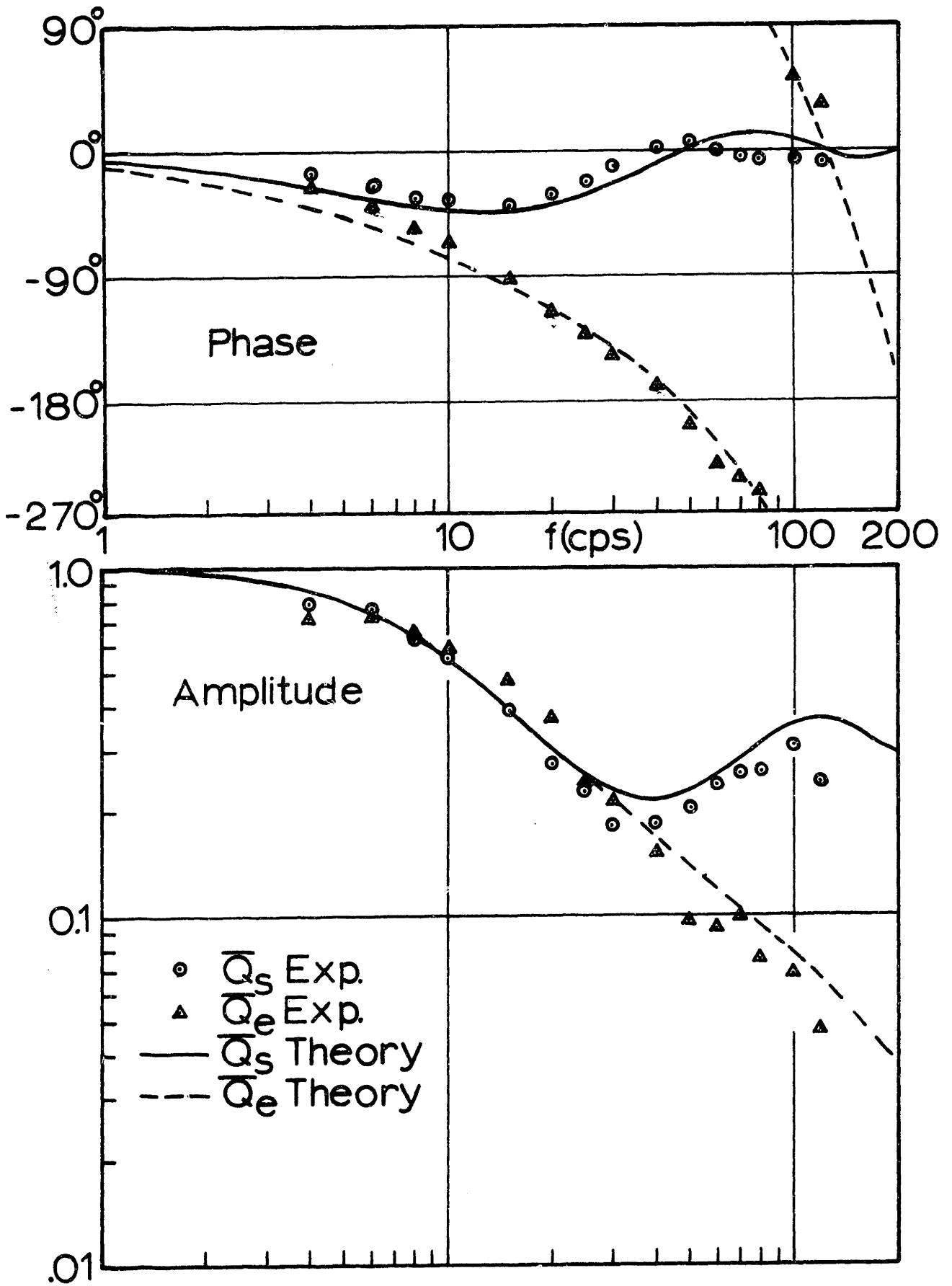


Fig. 4.11 Theoretical and Experimental Frequency Responses - Case B

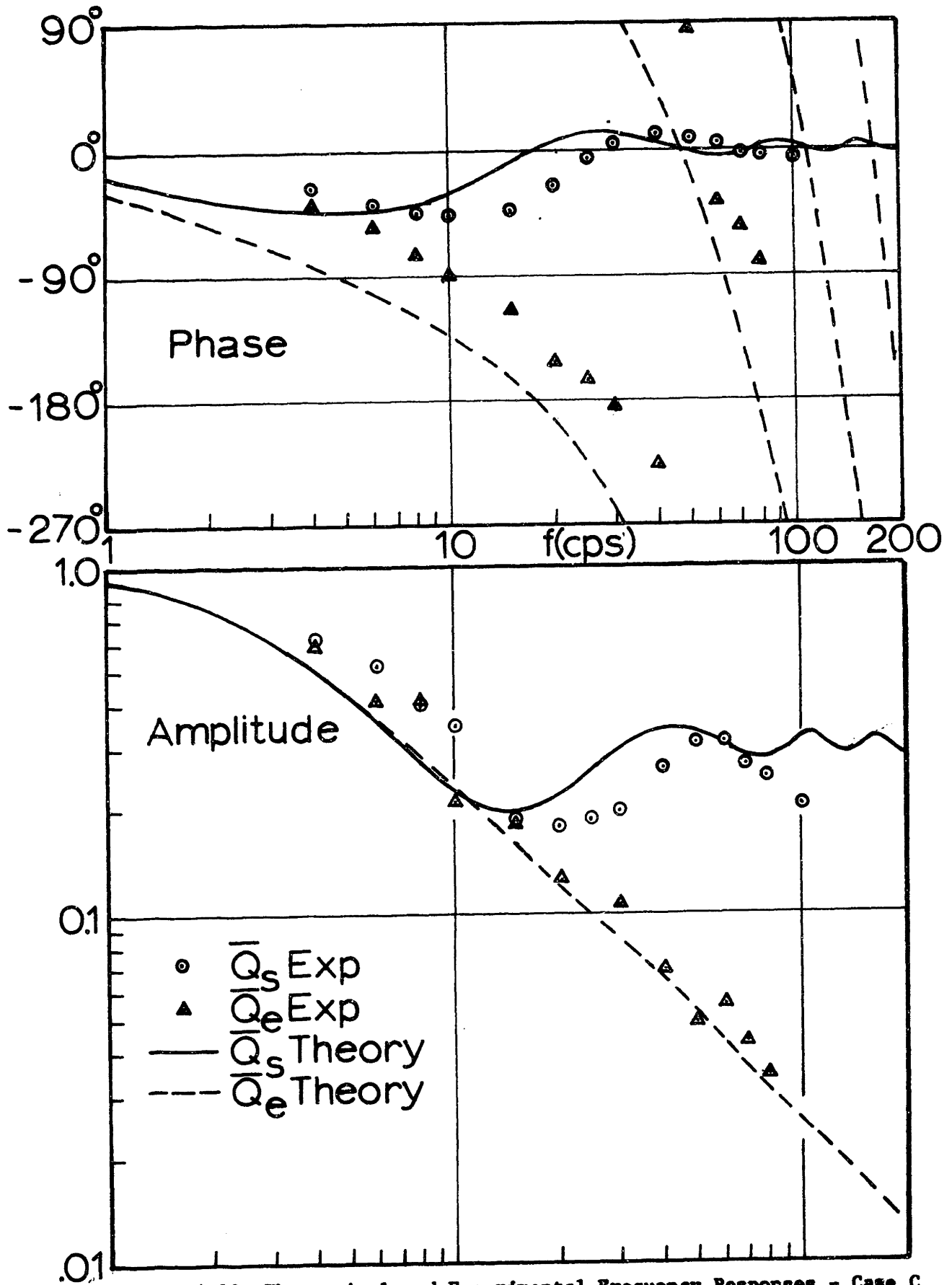


Fig. 4.12 Theoretical and Experimental Frequency Responses - Case C

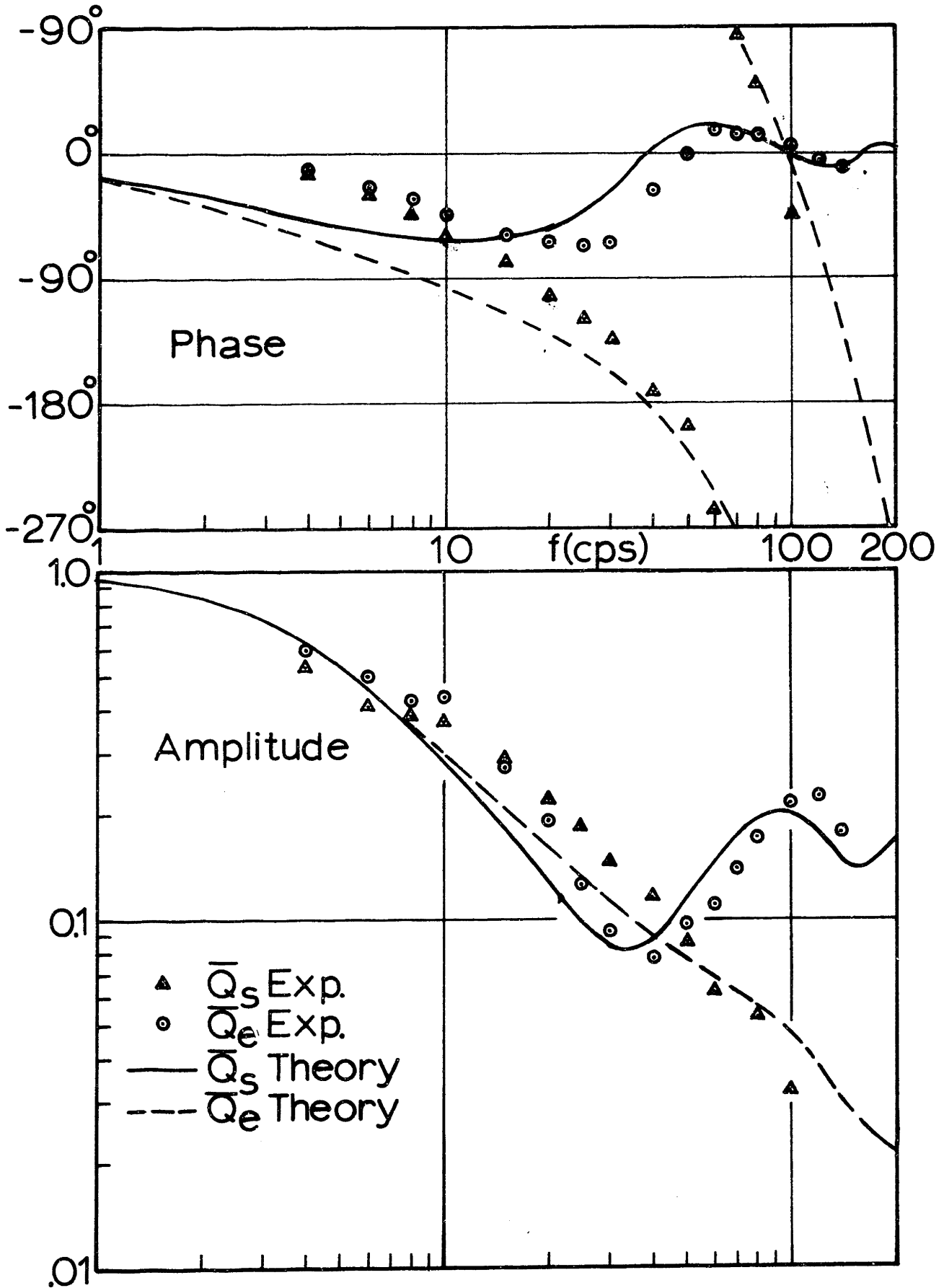


Fig. 4.13 Theoretical and Experimental Frequency Responses - Case D

These characteristics are well illustrated by the frequency response of case A. The major difference between the different cases, in terms of this study, is the speed of response. This difference is represented effectively by consideration of the frequency at which the peak in supply flow response occurs, which corresponds to a phase shift of 360° for the exit flow, and a zero phase shift of the supply flow. For case A, this point falls at a frequency of about 82 cps. The time constants associated with this case are T_1 equal to just over 9 milliseconds and T_2 equal to just over 23 msec.

For case B, the frequency of the supply flow peak occurs at about 120 cps, while the time constants are $T_1 \approx 6$ msec and $T_2 \approx 14$ msec. This faster response is associated with the fact that the radial flow rate through the valve is 1.6 times faster, while the operating point on the steady state characteristic and the internal flow fields are similar to case A. Thus, as would be expected, for similar operating conditions, the speed of response is essentially proportional to the flow rate through the valve.

For case C, the height of the valve was doubled, with the flow rates approximately the same as for case A, so that the outer periphery radial velocity was one-half that of case A. The steady state theory predicts that the boundary layers should be about the same height as for case A, so that the core region is over twice the height of case A. Thus, T_2 would be expected to be longer because of the increased inertia of the spinning donut, and T_1 would also be expected to be longer due to the increased effect of the

core region on the boundary layers. The distributed system response gives $T_1 \approx 16$ msec and $T_2 \approx 45$ msec, while the lumped model gives the supply response peak at about 45 cps. Note that T_1 for case C is less than twice the T_1 for case A, which means it is a smaller fraction of the fill time. The experimental response indicates that the T_1 for case C should be even less than predicted. This example illustrates one disadvantage of using a fixed fraction of the fill time to represent the time constants, since changing the height for the same flows changes the fill time proportionately, but T_1 is changed less. The exact changes in T_1 and T_2 cannot be predicted by any simple relationship, but may be estimated with the use of the distributed model and computer program.

For case D, the exit hole of the vortex valve is larger, so that the basic flow rate is larger, tending to decrease T_1 . However, the spinning donut is smaller, decreasing the effect of the concentration of the flow in the boundary layers, and tending to increase T_1 . Compared with case A, T_1 is smaller with a value of just under 8 milliseconds, but is larger compared with its fill time. This again illustrates the inadequacy of using a fixed fraction of the fill time as the time constant T_1 . In this case, the time lag T_2 is smaller compared with T_1 than in the other cases, also because of the decreased size and momentum of the spinning donut.

Thus, the effects of changes in operating point and height of the valve on the lumped model response have been demonstrated qualitatively, and have been confirmed by experimental results. These effects are discussed further in Chap. 5, and some quantitative indications of the effects are given.

4.7 Choice of Friction Constant k

The numerical value of the friction constant k of Eq. 2.48 used in the distributed system program of Appendix A was chosen as 0.50 to provide a reasonable match with all of the experimental data. The effect on T_1 due to changing this constant is small, since the major factor in determining T_1 is the transport time. As expected, T_2 is changed substantially by changes in k , since this time constant is associated with the viscous effects. As an example, the effects of changing k between 0.40 and 0.60 for case A are listed in Table 4.2. For the range of experimental data considered, the values of T_1 and T_2 for $k = 0.50$ provided the most reasonable fit.

The tangential Reynolds number $\frac{\rho v_o r_o}{\mu}$ for all the experimental operating points was greater than 10^4 , justifying the use of turbulent shear expressions in the calculation of the friction effects.

4.8 Large Signal Step Response

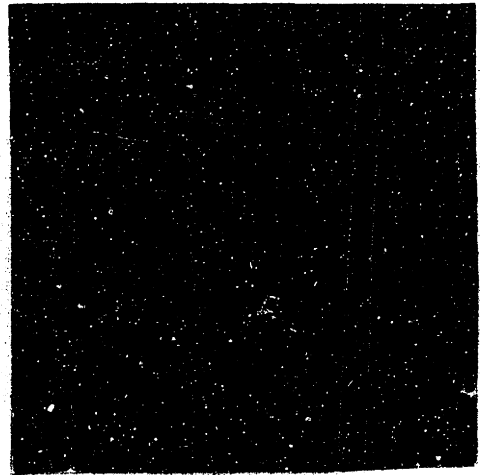
Although the prediction of large signal dynamic responses, involving flow changes from nearly maximum to nearly minimum conditions, is beyond the scope of this thesis, step response experiments were run for these conditions to gain some insight into the approximate range of dynamics involved. These step responses of exit flow changes due to step changes in control pressure are shown in Fig. 4.14 for the four configurations tested. The flow changes are on the order of ten times the small signal flow changes, but the time delays and rise times are only on the order of twice the small signal times. This indicates that the large signal response could also be modelled by a pure delay and a first order lag, although the linearized analysis of

Table 4.2

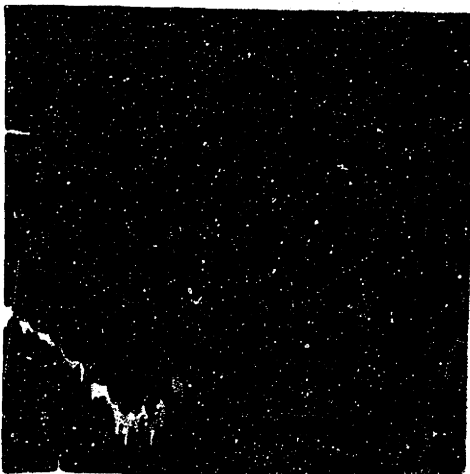
| | | | |
|-----------------------|-------|-------|-------|
| k | 0.40 | 0.50 | 0.60 |
| $T_1 \frac{r_o}{u_o}$ | 0.143 | 0.147 | 0.151 |
| $T_2 \frac{r_o}{u_o}$ | 0.375 | 0.349 | 0.329 |



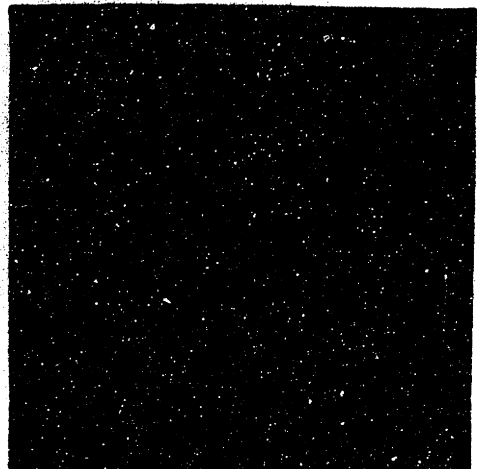
a) Case A



b) Case B



c) Case C



d) Case D

50 msec/cm for all responses

Fig. 4.14 Large Signal Step Responses

Chapters 2 and 3 would not be valid for response prediction. The large signal dynamic behavior of vortex valves would provide a possible area of further investigation.

4.9 Frequency Response Sensitivity to Gain and Time Constant Changes

The effects of parameter changes on system response may be investigated through the use of the techniques of the next chapter and through use of a computer program to give the frequency response from the equations of Table 3.1. In order to show the sensitivity of the response to these changes, several responses have been calculated for modifications to case A. Case A_1 is the original case with $T_1 = 0.0094$, $T_2 = 0.0232$, and $G_{oe} = -1.35$. For Case A_2 , T_1 is decreased by 20% to 0.0075, and for case A_3 , T_2 is also decreased by 20% to 0.0186. Finally, for case A_4 , the amplitude of the gain is increased by 25% to give $G_{oe} = -1.69$. These responses are shown in Fig. 4.15, where the cumulative effects of these changes can be seen.

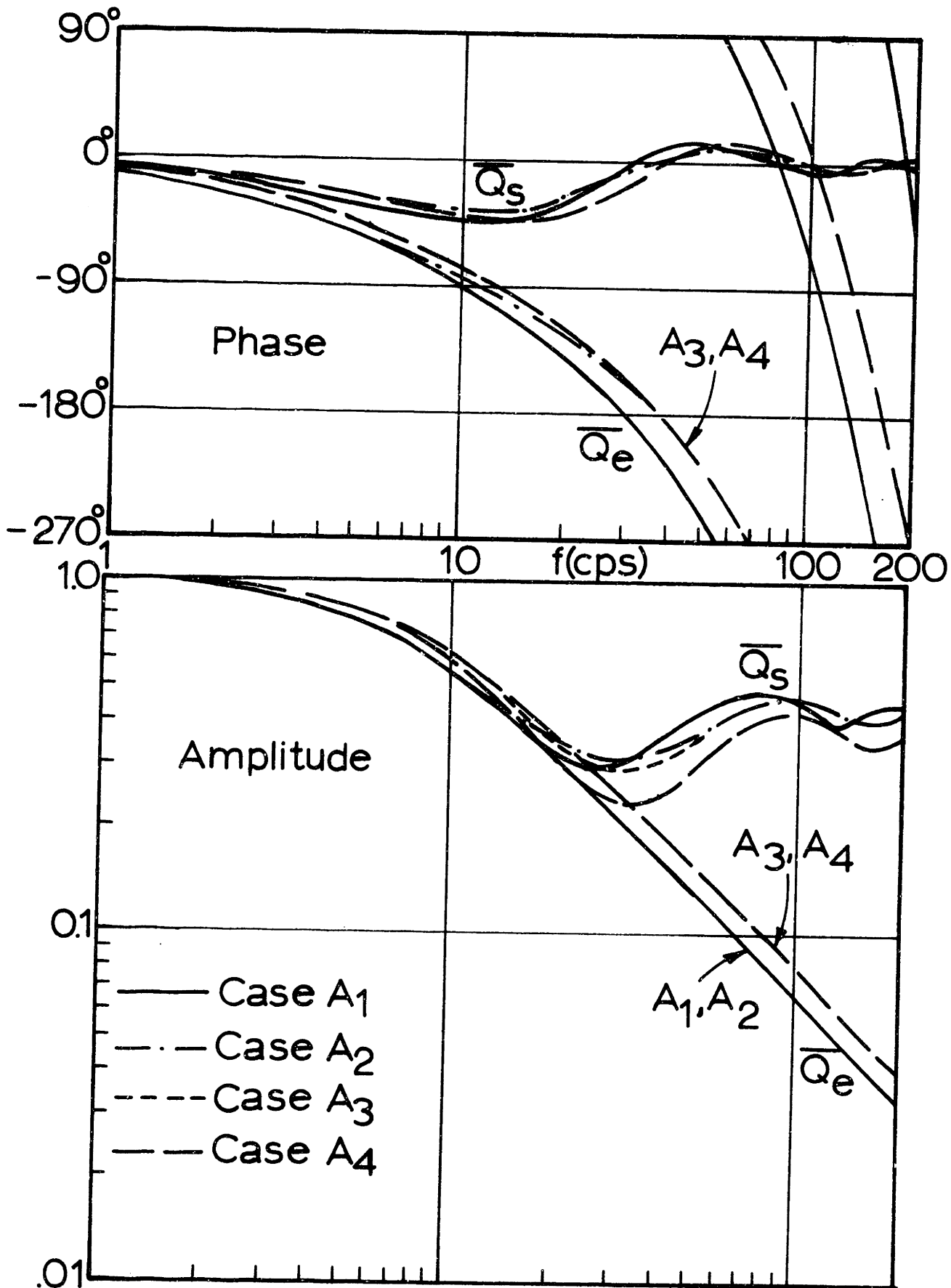


Fig. 4.15 Frequency Responses with Gain and Time Constant Changes

Chapter 5

DYNAMIC VORTEX VALVE DESIGN

5.1 General Dynamic Design

In the design of a vortex valve for a specific application, there are many criteria by which the valve must be judged, and many parameters which determine to what extent these criteria will be met. Some of the criteria for judging the valve may include the steady state flow requirements, the gain of the valve in a proportional region, the minimum quiescent flow, the ratio of control and supply flow at an operating point, and the speed of the dynamic response.

The parameters which affect the steady state performance include the size of the valve, the control port area to exit port area ratio, the fluid density and viscosity, and the ratio of the outer periphery radius to the exit radius. In the vortex flow itself, the velocity

distributions are determined by the two factors, λ and BLC, discussed in Chap. 3, where $\lambda = \frac{v_o}{u_o}$ and $BLC = \frac{2r_o}{h} \frac{f}{\left(\frac{\rho u_o h}{2\mu} \right)^{1/4}}$.

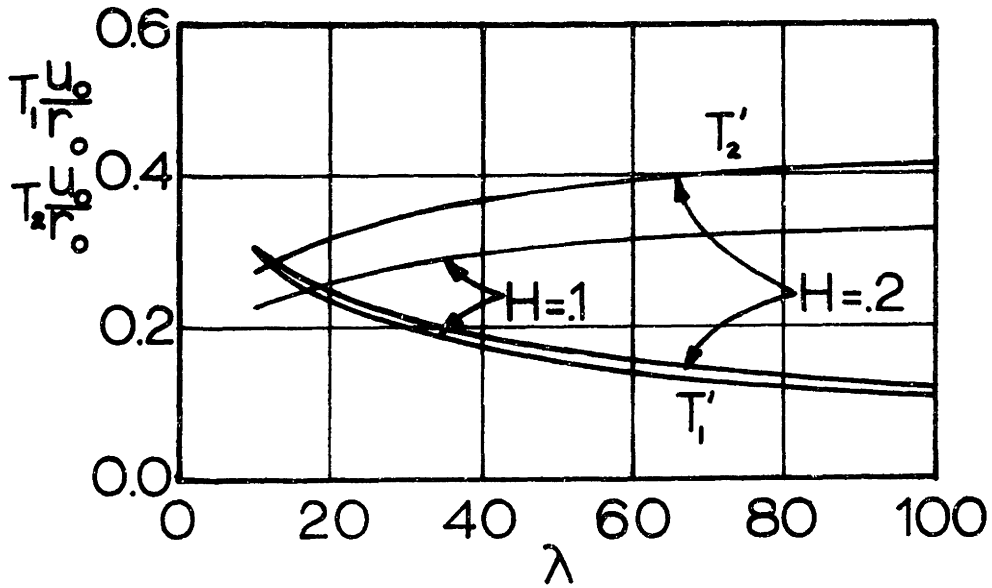
The dynamic time constants, T_1 and T_2 , depend upon the velocity distributions, and thus are functions of BLC and λ . In addition, since it influences the relationship between the boundary layer and the spinning core, the parameter $H = h/2r_o$ also affects the time constants. Since the entire spinning core responds essentially as a unit, as discussed in Chap. 2, the radius ratio does not have a strong influence on the time constants, as has been verified by results of the computer program of Appendix A.

The gains, k_1 , k_2 , k_c , k_e , k_u and R_e are functions of the steady state characteristic, and must be calculated for any particular case individually, as discussed in Chapters 3 and 4.

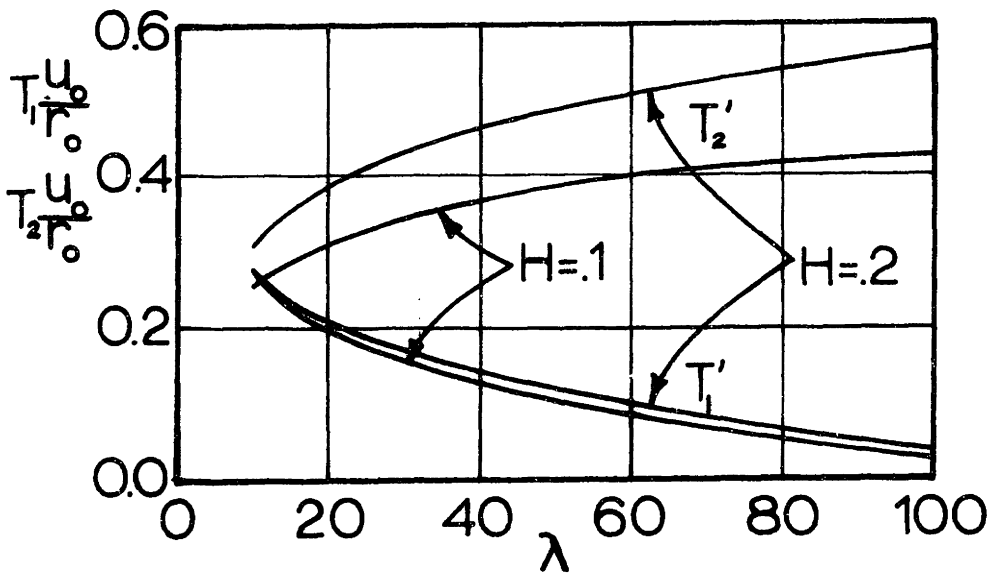
Because of the wide range over which the parameters BLC, λ , and H may differ, it is not practicable to present here a complete set of time constants for all possible conditions. Therefore, for specific applications, a designer is urged to use the computer program of Appendix A. However, some insight into the magnitude of these effects may be gained from the data summarized in Fig. 5.1. As can be seen, increasing λ , which corresponds to operating further down the steady state characteristic, with less exit flow, decreases T_1 and increases T_2 with respect to the fill time, due to the increased region of zero radial flow. An increase in BLC has the same tendency to decrease T_1 and increase T_2 with respect to the fill time. Doubling the height of a valve and maintaining the corresponding flow rates, doubles H, doubles λ , and halves BLC. An example of the effect of doubling the height is going from $\lambda = 20$, BLC = 0.050, H = 0.1 to $\lambda = 40$, BLC = 0.025, H = 0.2, which shows a decrease in T_1 and an increase in T_2 as the increased height increases the effect of the core compared with the boundary layer.

5.2 Example Design

As an example of dynamic considerations in the design of a vortex valve, consider a valve with $A_c/A_e = 0.1$ and $r_e/r_o = 0.15$. From Ref. (19), the three x'ed points of Fig. 5.2 may be determined analytically and an estimate of the characteristic sketched where in the present case three approximations are sketched to illustrate the possible variations in the approximation. For a valve with



a) BLC = 0.025



b) BLC = 0.050

Fig. 5.1 Changes in T_1 and T_2 Due to Swirl and Height Changes

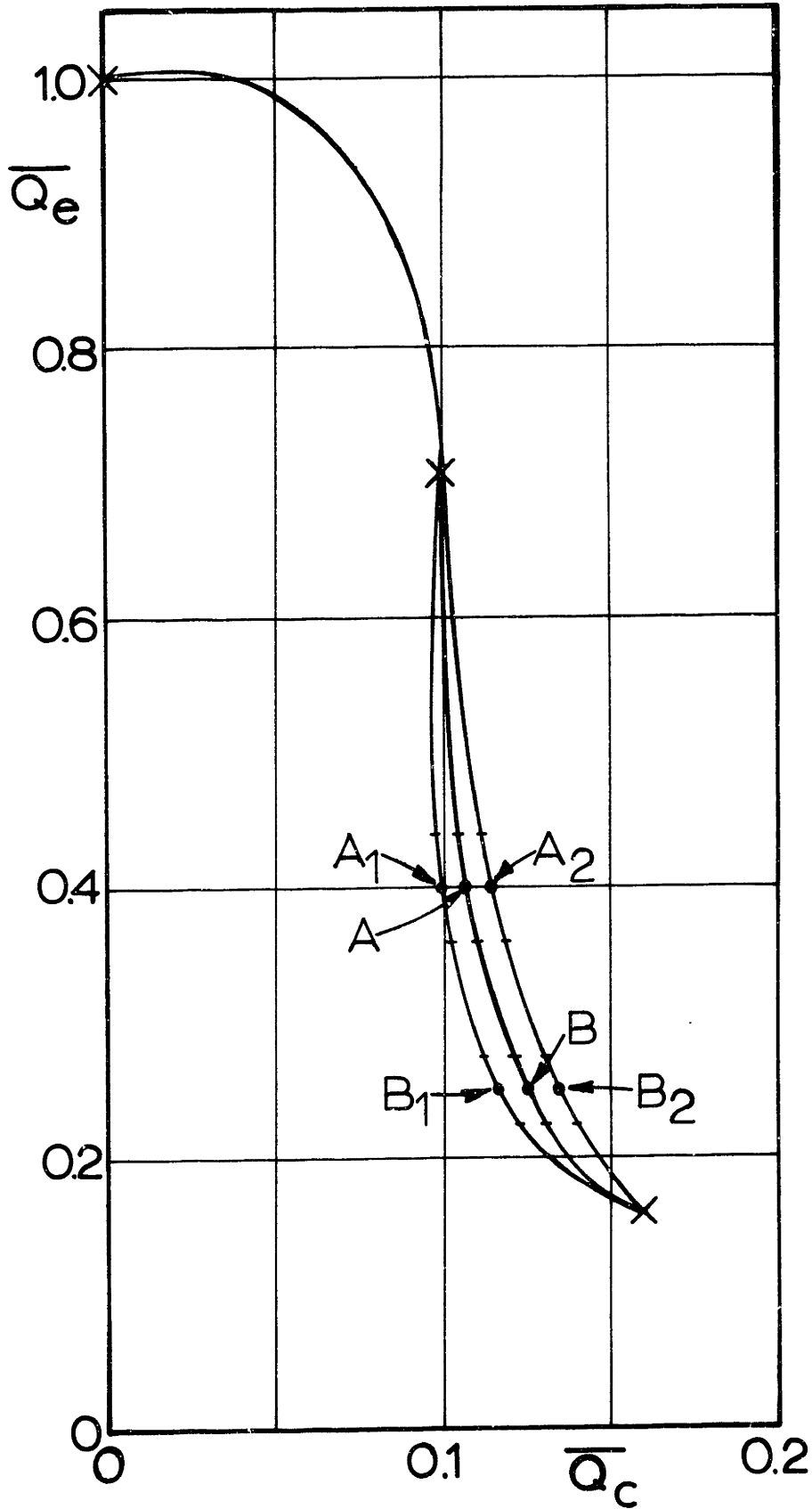


Fig. 5.2 Estimated Steady State Characteristic for Example Design

an outer radius of 1.0 in. and a height of 0.3 in, the flow at point A is 84 in³/sec of air at 1.0 psig supply pressure. This same flow would occur at point B for a valve of 1.26 in. outer radius and 0.38 in height with the same supply pressure. However, the dynamic response would be different for the two valves.

The fill time for case A would be 20.5 msec while for case B it would be 41.3 msec. The full comparisons of the operating conditions for cases A and B and the alternative points are shown in Table 5.1. The step responses of the two operating conditions are shown in Fig. 5.3. This figure illustrates two relationships, the changes from the A to B points on each characteristic and the changes from one possible characteristic to the others. The changes for each particular comparison depend upon the interaction of the changes due to different T_1 , T_2 , and gains. Increases in each of these tend to slow down the step responses. Thus, as can be seen, the responses at the A points tend to be faster than the B points, although the quickest B response is close to the slowest A response. The changes in the T's and the gains make the alternate characteristics slower at both points.

The estimated steady state response gives a good approximation to the dynamic characteristics, within the limitations of the steady state theory. For the best estimate of the dynamic characteristics, an experimental steady state response is probably desirable.

Table 5.1

| | A | A ₁ | A ₂ | B | B ₁ | B ₂ |
|---|-------|----------------|----------------|-------|----------------|----------------|
| $Q_m \left(\frac{\text{in}^3}{\text{sec}} \right)$ | 209 | 209 | 209 | 335 | 335 | 335 |
| \bar{Q}_{eo} | .40 | .40 | .40 | .25 | .25 | .25 |
| \bar{Q}_{co} | .107 | .100 | .115 | .125 | .116 | .134 |
| $\frac{\Delta Q_e}{\Delta Q_c}$ | -13.5 | -19.1 | -12.1 | -5.05 | -4.90 | -5.21 |
| $\frac{T_1 u_o}{r_o}$ | .236 | .251 | .220 | .115 | .128 | .102 |
| $\frac{T_2 u_o}{r_o}$ | .375 | .388 | .390 | .414 | .390 | .436 |
| T_1 (msec) | 4.8 | 5.1 | 4.5 | 4.7 | 5.3 | 4.2 |
| T_2 (msec) | 7.7 | 7.9 | 8.0 | 17.1 | 16.1 | 18.0 |

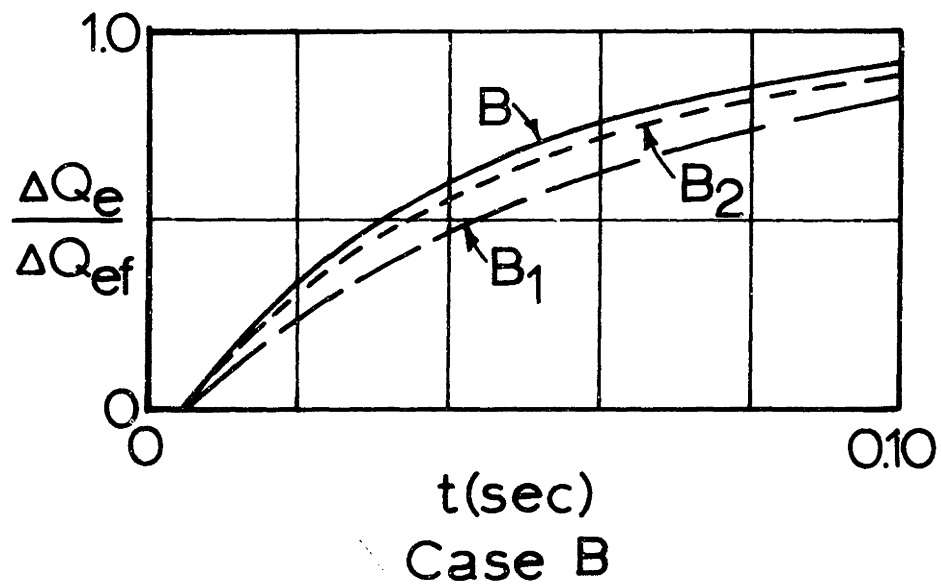
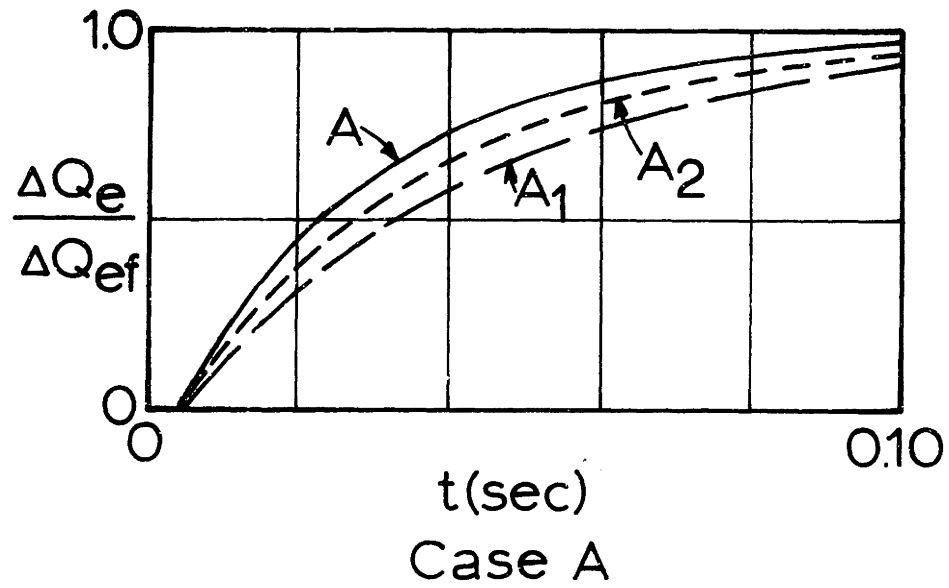


Fig. 5.3 Comparison of Step Responses for Example Design

Chapter 6

CONCLUSIONS AND RECOMMENDATIONS

6.1 Conclusions

This study has considered the small signal dynamic response of a vortex valve to changes in control pressure, with the supply and exit pressure held constant. The analysis is valid for incompressible flows in a valve operating with high swirl conditions, such that there is a significant pressure drop across the vortex chamber due to the centrifugal flow field. A method has been presented for the prediction of the gains and time constants of the dynamic model from a predicted or measured steady state characteristic. Experimental step responses and sinusoidal frequency responses have been presented to verify the analytical model. Thus, this study has presented an initial building block in the design of fluid power control circuits containing vortex valves as dynamic system components.

The main contribution of this thesis, compared with past work (1,5,11,25,26), is the prediction of dynamic model parameters based on the fluid and geometric characteristics of the valve and the experimental verification of those parameters.

6.2 Recommendations

Although this study represents a significant step in the understanding and prediction of the dynamic response of vortex valves, there are several areas of study which would be useful to refine and extend the findings of this study.

The first area of proposed further study is working for a better understanding of the phenomena associated with the exit region

For this study, this region was represented as a linearized resistance relating the exit flow and pressure drop. A more complete representation would probably include separate consideration of the effects of swirl and axial flow on the exit pressure drop. The simpler representation used for this study was sufficient since the changes in exit flow were always associated with changes in the swirl conditions in the chamber and exit, and because the linearized resistance effects enter the lumped model transfer function in the same form as the larger effect of changes in the radial flow on the chamber pressure drop. However, for cases with non-constant supply and exit pressures, these effects are not so closely related and it is felt that a more complete model of the exit flows would be necessary for reasonable representation of the dynamic behavior.

Another area of further study, mentioned in Chapter 4, is work on the modelling of the large signal dynamic switching behavior of the valve. This involves a more complete understanding of the phenomena involved in the development and elimination of the spinning donut region, since it changes drastically in this type of operation.

The third possible area of study is further work on the prediction of the high gain region of the static characteristic. In this region, the predominant resistance of the valve is changing from the exit port resistance to the centrifugal flow field resistance, and this change tends to be unstable for valves with flows approaching the axisymmetric assumption of the static analysis. Thus a fuller understanding of the phenomena associated with this change, which would also relate to the other two areas of study indicated above, would be desirable.

These three areas of further study give only an indication of the rich possibilities for continuing research in the vast and complex area of vortex flows in general and vortex amplifiers in particular.

Appendix A - Distributed Dynamic Response Computer Program

The computer program listed on the following pages consists of a main program and six subroutines which calculate the distributed dynamic response of a vortex chamber to a step in the outer periphery tangential velocity v_o . The equations used are those developed in Chapt. 2.

The first subroutine, DHPCG, is a predictor-corrector subroutine, only slightly modified from the IBM 360 Scientific Subroutine package (31) to guarantee that all of the desired outputs are computed. This program automatically adjusts the integration step size to limit the maximum error, and is used to determine the steady state operating conditions.

The other five subroutines are called by DHPCG to calculate the derivatives and output results. DERIV 1 calculates the derivatives in the outer region, for U greater than zero, and DERIV 2 calculates the derivatives in the central region where there is no radial flow. OUTPT1 prints out the values of the variables at the initial segment, OUTPT2 prints out the values for U greater than zero and signals when U goes to zero, and OUTPT3 prints the values for the zero radial flow region.

The main program reads one data card for each step response to be calculated, with the five inputs being the initial and final values of λ , the value of BLC, the height parameter H , and XMAX equal to the non-dimensional value of $1 - \frac{r_e}{r_o}$. These parameters are used to calculate the initial and final steady states, using the equations of Sect. 2.3.1. The initial conditions are then

re-normalized with respect to the final v_0 , which changes the Γ values, and then the dynamic equations of Sect. 2.3.2 are solved for non-dimensional time steps of 0.0002. The fraction of the exit pressure change, PE , is printed at regular intervals, along with the distributions of Γ and Γ_c . When the non-dimensional time reaches 1, which equals two fill times, the program stops and prints out the values of $TAU1 = T_1 \frac{r_0}{u_0}$ and $TAU2 = T_2 \frac{r_0}{u_0}$. From these values, the dimensional time constants may be calculated.

```

SUBROUTINE DHPCG(PRMT, Y, DERY, NDIM, IHLF, FCT, DJT P, AUX)
DIMENSION PRMT(1), Y(1), DERY(1), AUX(16,1)
DOUBLE PRECISION Y, DERY, AUX, PRMT, X, H, Z, DELT
N=1
IHLF=0
X=PRMT(1)
H=PRMT(3)
PRMT(5)=0.00
DO 1 I=1,NDIM
AUX(16,I)=0.00
AUX(15,I)=DERY(I)
1 AUX(1,I)=Y(I)
IF(H*(PRMT(2)-X))3,2,4
2 IHLF=12
GOTO 4
3 IHLF=13
4 CALL FCT(X, Y, DERY)
CALL OUTP(X, Y, DERY, IHLF, NDIM, PRMT)
IF(PRMT(5))6,5,6
5 IF(IHLF)7,7,6
6 RETURN
7 DO 8 I=1,NDIM
8 AUX(8,I)=DERY(I)
ISW=1
GOTO 100
9 X=X+H
DO 10 I=1,NDIM
10 AUX(2,I)=Y(I)
11 IHLF=IHLF+1
X=X-H
DO 12 I=1,NDIM
12 AUX(4,I)=AUX(2,I)
H=.5D0*H
N=1
ISW=2
GOTO 100
DHC11120
DHC11130
DHC11140
DHC11150
DHC11160
DHC11170
DHC11180
DHC11190
DHC11200
DHC11210
DHC11220
DHC11230
DHC11260
DHC11270
DHC11280
DHC11310
DHC11340
DHC11350
DHC11360
DHC11370
DHC11380
DHC11390
DHC11420
DHC11430
DHC11450
DHC11460
DHC11470
DHC11500
DHC11510
DHC11520
DHC11530
DHC11540
DHC11550
DHC11560
DHC11570

```

```
13 X=X+H
   CALL FCT(X,Y,DERY)
   N=2
   DO 14 I=1,NDIM
     AUX(2,I)=Y(I)
14  AUX(9,I)=DERY(I)
   ISW=3
   GOTO 100
15 DELT=0.00
   DO 16 I=1,NDIM
     DELT=DELT+AUX(15,I)*DABS(Y(I)-AUX(4,I))
     DELT=.06666666666666667D0*DELT
16  IF(DELT-PRMT(4))19,19,17
17  IF(IHLF-10)11,18,18
18  IHLF=11
   X=X+H
   GOTO 4
19 X=X+H
   CALL FCT(X,Y,DERY)
   DO 20 I=1,NDIM
     AUX(3,I)=Y(I)
20  AUX(10,I)=DERY(I)
   N=3
   ISW=4
   GOTO 100
21 N=1
   X=X+H
   CALL FCT(X,Y,DERY)
   X=PRMT(1)
   DO 22 I=1,NDIM
     AUX(11,I)=DERY(I)
22  Y(I)=AUX(1,I)+H*(.375D0*AUX(8,I)+.7916666666666667D0*AUX(9,I)
     1-.2083333333333333D0*AUX(10,I)+.04166666666666667D0*DERY(I))
23  X=X+H
   N=N+1
   CALL FCT(X,Y,DERY)
```

DHCG1590
DHCG1600
DHCG1610
DHCG1620
DHCG1630
DHCG1640
DHCG1650
DHCG1660
DHCG1690
DHCG1700
DHCG1710
DHCG1720
DHCG1730
DHCG1740
DHCG1770
DHCG1780
DHCG1790
DHCG1820
DHCG1830
DHCG1840
DHCG1850
DHCG1860
DHCG1870
DHCG1880
DHCG1890
DHCG1910
DHCG1920
DHCG1930
DHCG1940
DHCG1950
DHCG1960
DHCG1970
DHCG1980
DHCG1990
DHCG2000
DHCG2010


```
DHCG2480
DHCG2490
DHCG2500
DHCG2510
DHCG2520
DHCG2580
DHCG2590
DHCG2620
DHCG2630
DHCG2640
DHCG2650
DHCG2660
DHCG2690
DHCG2720
DHCG2730
DHCG2740
DHCG2750
DHCG2760
DHCG2770
DHCG2780
DHCG2790
DHCG2800
DHCG2810
DHCG2850
DHCG2880
DHCG2890
DHCG2900
DHCG2910
DHCG2920
DHCG2950
DHCG2960
DHCG2970
DHCG2980
DHCG3010
DHCG3020
DHCG3030

DO 104 I=1,NDIM
1040 Y(I)=AUX(N,I)+.1747602822626903700*AUX(5,I)-.5514806628787329400*
1AUX(6,I)+1.205535599396523500*AUX(7,I)+.1711847812195190300*
2H*DERY(I)
GOTO(9,13,15,21),ISW
200 ISTEP=3
201 IF(N-8)204,202,204
202 DO 203 N=2,7
DO 203 I=1,NDIM
AUX(N-1,I)=AUX(N,I)
203 AUX(N+6,I)=AUX(N+7,I)
N=7
204 N=N+1
DO 205 I=1,NDIM
AUX(N-1,I)=Y(I)
205 AUX(N+6,I)=DERY(I)
X=X+H
206 ISTEP=ISTEP+1
DO 207 I=1,NDIM
0DELTA=AUX(N-4,I)+1.333333333333333300*H*(AUX(N+6,I)+AUX(N+6,I))-
1AUX(N+5,I)+AUX(N+4,I)+AUX(N+4,I))
Y(I)=DELTA-.925619834710743800*AUX(16,I)
207 AUX(16,I)=DELTA
CALL FCT(X,Y,DERY)
DO 208 I=1,NDIM
0DELTA=.12500*(9.00*AUX(N-1,I)-AUX(N-3,I)+3.00*H*(DERY(I)+AUX(N+6,I)
1+AUX(N+6,I)-AUX(N+5,I)))
AUX(16,I)=AUX(16,I)-DELTA
208 Y(I)=DELTA+.0743801652892562000*AUX(16,I)
DELTA=0.00
DO 209 I=1,NDIM
DELTA=DELTA+AUX(15,I)*DABS(AUX(16,I))
IF(DELTA-PRMT(4))210,222,222
210 CALL FCT(X,Y,DERY)
CALL OUTP(X,Y,DERY,IHLF,NDIM,PRMT)
IF(PRMT(5))212,211,212
```


DHCG3040
DHCG3050
DHCG3060
DHCG3070
DHCG3080
DHCG3130
DHCG3140

DHCG3180
DHCG3190
DHCG3200
DHCG3210
DHCG3220
DHCG3230
DHCG3240
DHCG3250
DHCG3260
DHCG3270
DHCG3280
DHCG3290
DHCG3300
DHCG3310
DHCG3320
DHCG3360
DHCG3370
DHCG3380
DHCG3390
DHCG3400
DHCG3410
DHCG3420
DHCG3430
DHCG3440
DHCG3450

```

211 IF(IHLF-11)213,212,212
212 RETURN
213 IF(H*(X-PRMT(2))214,212,212
214 IF(DABS(X-PRMT(2))-1D)*DABS(H)212,215,215
215 IF(DEL T-.02D0*PRMT(4))216,216,201
216 IF(IHLF)201,201,217
217 IF(N-7)201,218,218
218 IF(ISTEP-4)201,421,421
421 IJH = (X+0.10D0*H-PRMT(1))/H
IKH = IJH/2
IF (IJH-IKH-IKH) 201,220,201

```

```

220 H=H+H
IHLF=IHLF-1
ISTEP=0
DO 221 I=1,NDIM
AUX(N-1,I)=AUX(N-2,I)
AUX(N-2,I)=AUX(N-4,I)
AUX(N-3,I)=AUX(N-6,I)
AUX(N+6,I)=AUX(N+5,I)
AUX(N+5,I)=AUX(N+3,I)
AUX(N+4,I)=AUX(N+1,I)
DELT=AUX(N+6,I)+AUX(N+5,I)
DELT=DELT+DELT+DELT
2210AUX(16,I)=8.962962962963D0*(Y(I)-AUX(N-3,I))
1-3.3611111111111111D0*H*(DERY(I)+DELT+AUX(N+4,I))
GOTO 201

```

```

222 IHLF=IHLF+1
IF(IHLF-10)223,223,210
223 H=.5D0*H
ISTEP=0
DO 224 I=1,NDIM
OY(I)=.390625D-2*(8.D1*AUX(N-1,I)+135.D0*AUX(N-2,I)+4.D1*AUX(N-3,I)
1+AUX(N-4,I))-1171875D0*(AUX(N+6,I)-6.D0*AUX(N+5,I)-AUX(N+4,I))*H
O AUX(N-4,I)=-.390625D-2*(12.D0*AUX(N-1,I)+135.D0*AUX(N-2,I)+
1108.D0*AUX(N-3,I)+AUX(N-4,I))-C234375D0*(AUX(N+6,I)+
218.D0*AUX(N+5,I)-9.D0*AUX(N+4,I))*H

```

DHCG3460
 DHCG3470
 DHCG3480
 DHCG3490
 DHCG3500
 DHCG3510
 DHCG3520
 DHCG3530
 DHCG3540
 DHCG3550
 DHCG3560
 DHCG3570
 DHCG3580
 DHCG3590
 DHCG3600
 DHCG3610
 DHCG3620
 DHCG3630
 DHCG3640

```

AUX(N-3,I)=AUX(N-2,I)
224 AUX(N+4,I)=AUX(N+5,I)
X=X-H
DELT=X-(H+H)
CALL FCT(DELT,Y,DERY)
DO 225 I=1,NDIM
AUX(N-2,I)=Y(I)
AUX(N+5,I)=DERY(I)
225 Y(I)=AUX(N-4,I)
DELT=DELT-(H+H)
CALL FCT(DELT,Y,DERY)
DO 226 I=1,NDIM
DELT=AUX(N+5,I)+AUX(N+4,I)
DELT=DELT+DELT+DELT
0AUX(16,I)=8.962962962962963D0*(AUX(N-1,I)-Y(I))
1-3.361111111111111D0*H*(AUX(N+6,I)+DELT+DERY(I))
226 AUX(N+3,I)=DERY(I)
GOTO 206
END

```

```

SUBROUTINE DERIV1(Z,Y,DERY)
DIMENSION Y(3),DERY(3),A(3,3),B(3),C(3),ALPH(5)
DOUBLE PRECISION Y,DERY,A,B,C,D,Z,R,U,US,DEL,VF,RLAM,BLC,ALPH
COMMON /DERIV/RLAM,BLC/ALL/ALPH
R = 1.-Z
U = Y(1)
US = Y(2)
DEL = Y(3)
VF = DSQRT(U**2+(RLAM/R)**2)
A(1,1) = ALPH(4)*US-(1.-ALPH(5))*U
A(1,2) = 1.-(1.-ALPH(5))*DEL
A(1,3) = ALPH(4)*DEL
A(2,1) = (ALPH(5)-ALPH(1))*U**2+(ALPH(4)-2.*ALPH(2))*U*US-
1 ALPH(3)*US**2
A(2,2) = DEL*((1.+ALPH(5)-2.*ALPH(1))*U-2.*ALPH(2))*US)
A(2,3) = DEL*((ALPH(4)-2.*ALPH(2))*U-2.*ALPH(3))*US)
A(3,1) = (ALPH(1)-ALPH(5))*U+(ALPH(2)-ALPH(4))*US
A(3,2) = DEL*(ALPH(1)-ALPH(5))
A(3,3) = DEL*(ALPH(2)-ALPH(4))
B(1) = ((1.-DEL*(1.-ALPH(5)))*U+DEL*ALPH(4)*US)/R
B(2) = (DEL/R)*((ALPH(1)-1.)*RLAM**2/R**2+(ALPH(5)-ALPH(1))*U**2+
1 (ALPH(4)-2.*ALPH(2))*U*US-ALPH(3)*US**2)+BLC*VF*U/
2 (DEL*VF)**0.25
B(3) = -(DEL/R)*((ALPH(5)-ALPH(1))*U+(ALPH(4)-ALPH(2))*US)-
1 BLC*VF/(DEL*VF)**0.25
C(1) = B(1)*(A(2,2)*A(3,3)-A(2,3)*A(3,2))+A(1,2)*(A(2,3)*B(3)-
1 B(2)*A(3,3))+A(1,3)*(B(2)*A(3,2)-A(2,2)*B(3))
C(2) = A(1,1)*(B(2)*A(3,3)-A(2,3)*B(3))+B(1)*(A(2,3)*A(3,1)-
1 A(2,1)*A(3,3))+A(1,3)*A(2,1)*B(3)-B(2)*A(3,2))+A(1,2)*(B(2)*A(3,1)-
1 C(3) = A(1,1)*A(2,2)*B(3)-B(2)*A(3,2)-A(2,2)*A(3,1))
1 A(2,1)*B(3))+B(1)*(A(2,1)*A(3,2)-A(2,2)*A(3,1))
D = A(1,1)*A(2,2)*A(3,3)-A(2,3)*A(3,2))+A(1,2)*A(3,1)-
1 A(2,1)*A(3,3))+A(1,3)*A(2,1)*A(3,2)-A(2,2)*A(3,1))
DERY(1) = C(2)/D
DERY(2) = C(3)/D
DERY(3) = C(1)/D

```

RETURN
END

9

```
SUBROUTINE DERIV2(Z,Y,DERY)
DIMENSION Y(3),DERY(3),A(2,2),B(2),C(2),ALPH(5)
DOUBLE PRECISION Y,DERY,A,B,C,D,Z,R,US,DEL,VF,RLAM,BLC,ALPH,GAM
COMMON /DERIV/RLAM,BLC/ALL/ALPH
R = 1.-Z
GAM = Y(1)
US = Y(2)
DEL = Y(3)
VF = GAM*RLAM/R
A(1,1) = US
A(1,2) = DEL
A(2,1) = -ALPH(3)*US**2
A(2,2) = -2.*ALPH(3)*DEL*US
B(1) = DEL*US/R
B(2) = (ALPH(1)-1.)*DEL*RLAM**2 *GAM**2/R**3-ALPH(3)*DEL*US**2/R
C(1) = B(1) *A(2,2)- B(2) *A(1,2)
C(2) = A(1,1)* B(2) -A(2,1)* B(1)
D = A(1,1)*A(2,2)-A(2,1)*A(1,2)
DERY(3) = C(1)/D
DERY(2) = C(2)/D
DERY(1) = -BLC*ALPH(4)*R *GAM*VF/(ALPH(2))*((DEL*VF)**C.25)
RETURN
END
```

```
SUBROUTINE OUTPT1(Z,Y,DERY,IHLF,NDIM,PRMT)
DIMENSION Y(3),DERY(3),PRMT(5),X(40),U(40,2),US(40,2),DEL(40,2),
1 GAM(40,2),Q1(40,2),Q2(40,2),Q3(40,2),ALPH(5),R(40)
DOUBLE PRECISION X,Y,DERY,PRMT,Z,U,US,DEL,GAM,Q1,Q2,Q3,R,ALPH
COMMON /OUTPT/X,U,US,DEL,GAM,J,K,R,G1,Q2,Q3/ALL/ALPH
IF ((Z+0.1D0*PRMT(3)*0.5*IHLF-PRMT(2)) .LT. 0.0) GO TO 40
X(J) = Z
R(J) = 1.-X(J)
GAM(J,K) = 1.00
U(J,K) = Y(1)
US(J,K) = Y(2)
DEL(J,K) = Y(3)
Q1(J,K) = U(J,K)*R(J)*(1.-DEL(J,K))
Q2(J,K) = (ALPH(4)*US(J,K)+ALPH(5)*U(J,K))*R(J)*DEL(J,K)
Q3(J,K) = 1.0-Q1(J,K)
WRITE (6,10) X(J),DEL(J,K),U(J,K),US(J,K),GAM(J,K),J
10 FORMAT (I10,F10.4,4D16.6,I6)
40 RETURN
END
```

```
SUBROUTINE OUTPT2(Z,Y,DERY,IHLF,NDIM,PRMT)
DIMENSION Y(3),DERY(3),PRMT(5),X(40),U(40,2),US(40,2),DEL(40,2),
1 GAM(40,2),Q1(40,2),Q2(40,2),Q3(40,2),ALPH(5),R(40),DGAMT(40,2),
2 DT1INV(40,2),DT2INV(40,2)
DOUBLE PRECISION X,Y,DERY,PRMT,Z,U,US,DEL,GAM,Q1,Q2,Q3,ALPH,R,
1 DT1INV,DT2INV,DGAMT
COMMON /OUTPT/X,U,US,DEL,GAM,J,K,R,Q1,Q2,Q3,DT1INV,DT2INV,DGAMT
1 /ALL/ALPH
ICHEK = (Z+0.1D0*PRMT(3)*0.5**IHLF+X(1))/(5*PRMT(3))
IF (ICHEK .NE. J) GO TO 40
X(J) = Z
R(J) = 1.-X(J)
GAM(J,K) = 1.00
U(J,K) = Y(1)
US(J,K) = Y(2)
DEL(J,K) = Y(3)
DGAMT(J,K) = 0.0
Q1(J,K) = U(J,K)*R(J)*(1.-DEL(J,K))
Q2(J,K) = (ALPH(4)*US(J,K)+ALPH(5)*U(J,K))*R(J)*DEL(J,K)
Q3(J,K) = Q1(J-1,K)-Q1(J,K)
DT1INV(J,K) = ((U(J,K)*ALPH(5)+US(J,K)*ALPH(4))/(5*PRMT(3)))
DT2INV(J,K) = U(J,K)/(5*PRMT(3))
WRITE (6,10) X(J),DEL(J,K),U(J,K),US(J,K),GAM(J,K),J
10 FORMAT (1H ,F10.4,4D16.6,I6)
J = J+1
40 IF (Y(1) .GE. 0.0) GO TO 50
KCK1 = (Z+0.1D0*PRMT(3)*0.5**IHLF-X(J-1))/PRMT(3)
KCK2 = (Z-0.1D0*PRMT(3)*0.5**IHLF-X(J-1))/PRMT(3)
IF (KCK1 .EQ. KCK2) GO TO 50
IF (ICHEK .NE. J) J = J+1
X(J-1) = Z
PRMT(5) = 1.0
WRITE (6,45) X(J-1),Y(3),Y(1),Y(2)
45 FORMAT (1H ,F10.4,3D16.6,6X,14HLIMIT OF DONUT)
50 RETURN
END
```

```
SUBROUTINE OUTPT3(Z, Y, DERY, IHLF, NDIM, PRMT)
DIMENSION Y(3), DERY(3), PRMT(5), X(40), U(40,2), US(40,2), DEL(40,2),
1 GAM(40,2), Q1(40,2), Q2(40,2), Q3(40,2), ALPH(5), R(40), DGAMT(40,2),
2 DT1INV(40,2), DT2INV(40,2)
DOUBLE PRECISION X, Y, DERY, PRMT, Z, U, US, DEL, GAM, Q1, Q2, Q3, ALPH, R,
1 DT1INV, DT2INV, DGAMT
COMMON /OUTPT/X, U, US, DEL, GAM, J, K, R, Q1, Q2, Q3, DT1INV, DT2INV, DGAMT
1 /ALL/ALPH
ICHEK = (Z+0.1D0*PRMT(3)*0.5*IHLF+X(1))/(5*PRMT(3))
IF (ICHEK .NE. J) GO TO 40
X(J) = Z
R(J) = 1.-X(J)
U(J,K) = 0.0
GAM(J,K) = Y(1)
US(J,K) = Y(2)
DEL(J,K) = Y(3)
DGAMT(J,K) = (GAM(J,K)-GAM(J-1,K))*ALPH(4)*US(J,K)/(5*PRMT(3))
Q1(J,K) = U(J,K)*R(J)*(1.-DEL(J,K))
Q2(J,K) = (ALPH(4)*US(J,K)+ALPH(5)*U(J,K))*R(J)*DEL(J,K)
Q3(J,K) = Q1(J-1,K)-Q1(J,K)
DT1INV(J,K) = ((U(J,K)*ALPH(5)+US(J,K))*ALPH(4))/(5*PRMT(3))
DT2INV(J,K) = U(J,K)/(5*PRMT(3))
WRITE (6,10) X(J), DEL(J,K), U(J,K), US(J,K), GAM(J,K), J
10 FORMAT (1H, F10.4, 4D16.6, I6)
J = J+1
40 RETURN
END
```



```
DIMENSION PRMT(5), DERY(3), X(40), US(40,2), DEL(40,2), U(40,2),
1 Y(3), ALPH(5), AUX(16,3), GAM(40,2), R(40), Q1(40,2), Q2(40,2),
2 Q3(40,2), DT1INV(40,2), DT2INV(40,2), GAMC(40,2), GAMDF(40),
3 QJ1(40), QJ2(40), DT1(40), DT2(40), DTM1(40), DTM2(40), P(2),
4 TRQ1(40), TRQ2(40), PMLT(40), GAM1(40), DGAMT(40,2), FRGAM(40),
5 FRMGAM(40)
DOUBLE PRECISION RLAM, BLC, ALPH, X, U, LS, DEL, GAM, R, DT1INV, DT2INV,
1 Q1, Q2, Q3, H, PDF, PE, RLMSQ, TRQ, DELT, GAMSQ, RLAM1, RLAM2, GAMAX,
2 GAMAX2, TIME, PRMT, DERY, Y, AUX, GAMC, GAMDF, GAM1, QJ1, QJ2,
3 DT1, DT2, DTM1, DTM2, GAMCG, T, TRG1, TRG2, P, PMLT, XMAX, DGAMT, FRGAM,
4 FRMGAM
COMMON /DERIV/RLAM, BLC/ALL/ALPH/OUTPT/X, U, US, DEL, GAM, J, K, R, Q1, Q2,
1 Q3, DT1INV, DT2INV, DGAMT
EXTERNAL DERIV1, DERIV2, OUTPT1, OUTPT2, OUTPT3
ALPH(1) = 0.778
ALPH(2) = 0.350
ALPH(3) = 0.313
ALPH(4) = 0.439
ALPH(5) = 0.875
10 READ (5,20) RLAM1, RLAM2, BLC, H, XMAX
20 FORMAT (5F10.0)
IF (RLAM1 .LE. 0.0) GO TO 200
J = 1
K = 2
RLAM = RLAM2
25 PRMT(1) = 0.0010
PRMT(2) = 0.01250
PRMT(3) = 0.00050
PRMT(4) = 0.00001
NDIM = 3
DERY(1) = 0.4
DERY(2) = 0.4
DERY(3) = 0.2
X(1) = PRMT(1)
US(1,1) = 0.686*RLAM*DSQRT(X(1))
DEL(1,1) = (18.1*BLC*DSQRT(X(1)))/(RLAM**0.25)**0.8
```

```
U(1,1) = (1.+0.439*DEL(1,1)*US(1,1))/(1.-0.115*DEL(1,1))
Y(1) = U(1,1)
Y(2) = US(1,1)
Y(3) = DEL(1,1)
WRITE (6,30) RLAM,BLC
30 FORMAT (1H1,5HLAM =,F6.2,5X,5HBLC = ,F3.4/1H0,6X,1HX,10X,3HDEL ,
1 14X,1HU,15X,2HUS,14X,3HGAM,10X,1HJ/1H )
CALL DHPGCG(PRMT,Y,DERY,NDIM,IHLF,DERIV1,OUTPT1,AUX)
J = 2
PRMT(1) = 0.01250
PRMT(2) = XMAX
PRMT(3) = 0.00500
DERY(1) = 0.4
DERY(2) = 0.4
DERY(3) = 0.2
CALL DHPGCG(PRMT,Y,DERY,NDIM,IHLF,DERIV1,OUTPT2,AUX)
J = J-1
IF (K .EQ. 2) JM = J
JM1 = JM+1
PRMT(1) = X(J)
DERY(1) = 0.4
DERY(2) = 0.4
DERY(3) = 0.2
Y(1) = 1.00
CALL DHPGCG(PRMT,Y,DERY,NDIM,IHLF,DERIV2,OUTPT3,AUX)
JMAX = J-1
P(K) = 0.0
DO 35 J = 2,JMAX
35 P(K) = P(K)-RLAM**2*GAM(J,K)**2*5.*PRMT(3)/R(J)**3
IF (K .EQ. 1) GO TO 40
J = 1
K = 1
RLAM = RLAM1
GO TO 25
40 CONTINUE
GAMC(1,1) = 1.00
```

```
GAMAX = 0.0
GAMAX2 = 0.0
PDF = P(2)-P(1)
PE = 0.0
PE1 = 0.0
DPE1 = 0.0
DPE2 = 0.0
RLMSQ = RLAM2**2
PMLT(1) = RLMSQ*5.*PRMT(3)/R(1)**3
TRQ = 0.50*RLAM/H
DELT = 0.0002
DO 50 J = 2,JMAX
PMLT(J) = RLMSQ*5.*PRMT(3)/R(J)**3
GAM(J,1) = RLAM1*GAM(J,1)/RLAM2
DGAMT(J,1) = RLAM1*DGAMT(J,1)/RLAM2
GAMC(J,1) = GAM(J,1)
GAMC(J,2) = GAMC(J,1)
GAMDF(J) = GAM(J,2)-GAM(J,1)
50 GAM1(J) = GAM(J,1)
ITIME = 0
70 ITIME = ITIME+1
TIME = ITIME*DELT
DO 80 J = 2,JMAX
FRGAM(J) = (GAM(J,1)-GAM1(J))/GAMDF(J)
FRMGAM(J) = 1.0-FRGAM(J)
TRQ1(J) = TRQ/((1.-1.5*(DELT(J,1)*FRMGAM(J)+DELT(J,2)*FRGAM(J)))*
1 R(J))
TRQ2(J) = TRQ/(1.5*R(J)*(DELT(J,1)*FRMGAM(J)+DELT(J,2)*FRGAM(J)))
QJ1(J) = (FRMGAM(J)*Q3(J,1)/Q2(J,1))+(FRGAM(J)*Q3(J,2)/Q2(J,2))
QJ2(J) = 1.0-QJ1(J)
DT1(J) = DELT*(FRMGAM(J)*DT1INV(J,1)+FRGAM(J)*DT1INV(J,2))
DT2(J) = DELT*(FRMGAM(J)*DT2INV(J,1)+FRGAM(J)*DT2INV(J,2))
DTM1(J) = 1.-DT1(J)
DTM2(J) = 1.-DT2(J)
GAM(J,2) = (QJ1(J)*GAMC(J,1)+QJ2(J)*GAMC(J-1,1))*DT1(J)+GAM(J,1)*
1 DTM1(J)
```

```
80 GAMC(J,2) = GAMC(J-1,1)*DT2(J)+GAMC(J,1)*DTM2(J)
DO 90 J = 2, JMAX
GAMSQ = DABS(GAM(J,1)-GAMC(J,1))*(GAM(J,1)-GAMC(J,1))
GAM(J,1) = GAM(J,2)+(FRGAM(J)*DGAMT(J,2)+FRMGAM(J)*DGAMT(J,1))-
1 TRQ2(J)*GAMSQ)*DELT
90 GAMC(J,1) = GAMC(J,2)+TRQ1(J)*GAMSQ*DELT
110 GAMCG = (GAM(JM,1)-GAMI(JM))/GAMDF(JM)
GAMAX = (GAM(JMAX,1)-GAMI(JMAX))/GAMDF(JMAX)
GAMAX2 = (GAMC(JMAX,1)-GAMI(JMAX))/GAMDF(JMAX)
150 ICHK = ITIME/125
IF (ITIME-125*ICHK) 70,155,70
155 P(2) = 0.0
DO 160 J = 2, JMAX
160 P(2) = P(2)-PMLT(J)*GAMC(J,1)**2
PE = (P(2)-P(1))/PDF
WRITE (6,165) TIME, GAMCG, GAMAX, GAMAX2, PE
165 FORMAT (1H4,4HT = ,F7.4,6X,8HGAMCG = ,F9.6,6X,8HGAMAX = ,F9.6,
1 6X,9HGAMAX2 = ,F9.6,6X,5HPE = ,F5.6)
WRITE (6,170) (X(J),GAM(J,1),GAMC(J,1)),J = 1,JMAX)
170 FORMAT (1H ,F10.4,2F10.6,F10.4,2F10.6,F10.4,2F10.6,F10.4,2F10.6)
DPE1 = PE-PE1
IF (DPE1 .LT. DPE2) GO TO 180
DPE2 = DPE1
TMAX = TIME
PEMAX = PE
180 IF (PE1 .LT. 0.632 .AND. PE .GT. 0.632) TAU2 = TIME-((PE-0.632)*
1 125*DELT/(PE-PE1))
PE1 = PE
IF (PE .LE. 0.95 .AND. TIME .LT. 1.00) GO TO 70
190 TAU1 = TMAX-PEMAX*125*DELT/DPE2
TAU2 = TAU2-TAU1
WRITE (6,260) TAU1,TAU2
260 FORMAT (1H0, 7HTAU1 = ,F8.4,5X, 7HTAU2 = ,F8.4)
GO TO 10
200 CONTINUE
END
```

REFERENCES

1. Bell, A.C., "Optimization of a Vortex Valve", S.M. Thesis, Dept. of Mech. Eng., Massachusetts Institute of Technology, December, 1965.
2. Bichara, R.T. and Orner, P.O., "Analysis and Modeling of the Vortex Amplifier", Journal of Basic Engineering, Trans. ASME, Series D, Vol. 91, December, 1969.
3. Bradshaw, P., "The Analogy Between Streamline Curvature and Buoyancy in Turbulent Shear Flow", Journal of Fluid Mechanics, Vol. 36, 1969.
4. Deissler, R.G., "Unsteady Viscous Vortex with Flow Toward the Center", NASA TN D-3026.
5. Duff, J., K. Foster and D.G. Mitchell, "Some Experiments on the Vortex Valve", First Cranfield Fluidics Conference, British Hydromechanics Research Association, Cranfield, England, 1965.
6. Foster, K. and G.A. Parker, Fluidics: Components and Circuits, Wiley-Interscience, London, 1970.
7. Giles, J.A., A.P. Hays, and R.I. Sawyer, "Turbulent Wall Jets on Logarithmic Spiral Surfaces", Aeronautical Quarterly, Vol. XVII, August, 1966.
8. Glauert, M.B., "The Wall Jet", Journal of Fluid Mechanics, Vol. 1, 1956.

9. Hilsch, R., "The Use of the Expansion of Gases in a Centrifugal Field as a Cooling Process", Review of Scientific Instruments, Vol. 18, 1947.
10. Kirshner, J.M., ed., Fluid Amplifiers, McGraw-Hill Book Company, New York, 1966.
11. Knapp, A.B., "The Development and Control of a Vented Vortex Amplifier", Third Cranfield Fluidics Conference, British Hydromechanics Research Association, Cranfield, England, 1968.
12. Kruka, V. and S. Eskinazi, "The Wall-Jet in a Moving Stream", Journal of Fluid Mechanics, Vol. 20, 1964.
13. Larson, R.H., "The Vortex Amplifier; Its Performance and Application", Third Cranfield Fluidics Conference, 1968, British Hydromechanics Research Association, Cranfield, England, 1968.
14. Mayer, E.A., "Large-Signal Vortex Valve Analysis", Advances in Fluidics, ASME, 1967.
15. Ostrach, S. and D.E. Loper, "An Analysis of Confined Vortex Flows", AIAA Paper No. 66-88, 1966.
16. Otsap, B.A., "Experimental Study of a Proportional Vortex Fluid Amplifier", Proceedings of the Fluid Amplification Symposium, Vol. II, Harry Diamond Laboratories, Washington, D.C., 1964.
17. Phillips, T.A. and A. Blatter, "Hydraulic Fluid Interaction Servo valve", Report for NASA Contract NAS8-11928, Government Clearinghouse number N69-16736.

18. Rakowsky, E.L., L.S. Galowin, and M.J. DeSantis, "Vortex Phenomena Study Continuation Program", Final Report GPSI 1590-6707, Government Clearinghouse No. AD 664, 198.
19. Rivard, J.G., "Secondary-Injection Thrust Vector Control Systems", Bendix Technical Journal, Vol. 1, No. 4, Winter 1969.
20. Rosenzweig, M.L., W.S. Lewellan and D.H. Ross, "Confined Vortex Flows with Boundary-Layer Interaction", AIAA Journal, Vol. 2, No. 12, December 1964.
21. Rott, N., "Turbulent Boundary Layer Development on the End Walls of a Vortex Chamber", Aerospace Corp. Report, ATN-62(9202)-1, 1962.
22. Sarpkaya, T., J.M. Goto and J.M. Kirshner, "A Theoretical and Experimental Study of Vortex Rate Gyro", Advances in Fluidics, ASME, New York, 1967.
23. Savino, J.M. and E.G. Keshock, "Experimental Profiles of Velocity and Radial Pressure Distributions in a Vortex Contained in a Short Cylindrical Chamber", NASA TN D-3072, 1965.
24. Schlichting, H., Boundary-Layer Theory, Sixth Edition, McGraw-Hill, New York, 1968.
25. Taplin, L.B., "Phenomenology of Vortex Flow and its Application to Signal Amplification", Paper at Engineering Seminar on Fluid Control Systems, July, 1965. Pennsylvania State University Engineering Proceedings, P-45, 1967.
26. Taplin, L.B., "Small Signal Analysis of Vortex Amplifiers", Notes, M.I.T. Summer Session on Fluid Power Control, 1966.

27. Vonnegut, B., "A Vortex Whistle", Journal of the Acoustical Society of America, Vol. 26, 1954.
28. Wormley, D.N., "An Analytical and Experimental Investigation of Vortex-Type Fluid Modulators", Ph.D. Thesis, Dept. of Mech. Eng., Massachusetts Institute of Technology, October, 1967.
29. Wormley, D.N., "An Analytical Model for the Incompressible Flow in Short Vortex Chambers", Journal of Basic Engineering, Trans. ASME, Series D, Vol. 91, June, 1969.
30. Wormley, D.N. and H.H. Richardson, "A Design Basis for Vortex-Type Fluid Amplifiers Operating in the Incompressible Flow Regime", Journal of Basic Engineering, Trans. ASME, Series D, Vol. 92, June, 1970.
- 311 Systems/360 Scientific Subroutine Package, (360A-CM-03X) Version III, Programmer's Manual, IBM, Technical Publications Department, White Plains, N.Y., No. H20-0205-2.

BIOGRAPHY

The author was born on January 5, 1944 in Webster City, Iowa. After graduating from Stratford Community School in Stratford, Iowa, he entered Iowa State University, Ames, Iowa in September, 1962. In 1966 he received the B.S. degree in Mechanical Engineering, graduating with honors.

In September, 1966 he entered M.I.T. as a National Science Foundation Trainee. He received the S.M. degree in June, 1968. He has been a research assistant in the Design and Control Division of the Mechanical Engineering Department at M.I.T. for the past three years, and has been associated with the laboratory portion of a course in Fluid Power Control. He is a member of Sigma Xi, Pi Tau Sigma, Tau Beta Pi, and ASME.